91602
new 82-10

LEGAL NOTICE

This report was prepared by Ontario Hydro and, while effort has been made to assure the accuracy and applicability of the material contained herein, neither Ontario Hydro nor any person acting on its behalf:

(a) makes any warranty, express or implied with respect to the use of any information, apparatus, method or process disclosed in this report or that such use may not infringe privately owned rights; or

(b) assumes any liabilities with respect to the use of, or for damages resulting from the use of, any information, apparatus, method or process disclosed in this report.

ontario hydro
research division

COMPLIMENTARY COPY
Please Credit Ontario Hydro Research if Reproduced in Whole or in Part

ASSESSMENT OF THE IRON-BASED, STRESSED-SHELL CONTAINER

Report No. 89-214-K

B. Teper, S.A. Reid
Engineers
Applied Mechanics Section
Mechanical Research Departmnent

ABSTRACT

The Iron-Based, Stressed-Shell (IBSS) container concept is being studied as an alternative design option for the immobilization and disposal of used fuel bundles from CANDU Nuclear Power Generating Stations, in a deep underground vault. The container design provides for the bundles to be placed in a basket, which is then placed in a steel cask covered by a thin titanium shell. The steel cask forms the structural component of the container and the titanium shell is used for corrosion protection. A good fit between the steel cask and the titanium shell is obtained through a carefully planned manufacturing process. An alternative design is proposed having a thick steel shell that includes a corrosion allowance. A press-fit, self-locking closure is being developed to facilitate easy and reliable remote assembly. Performance of the design was assessed through finite element analysis of stresses, buckling deformations and the long term creep. The analysis was supported by test programs on closure strength, sealing capability and on creep in steel at up to 150°C. Material testing and analysis are continuing.

job	file	date	report no.
21-292-461	825.123	October 6, 1989	89-214-K

91602
new 82-10

90-03534/

ontario hydro
research division

EXECUTIVE SUMMARY

ASSESSMENT OF IRON-BASED, STRESSED-SHELL CONTAINER

B. Teper, S.A. Reid
Applied Mechanics Section
Mechanical Research Department

An Iron-Based, Stressed-Shell (IBSS) container is proposed for the immobilization and disposal of used CANDU fuel bundles in an up-to 1000-m deep underground vault. The container is designed to hold 72 used-fuel bundles. Its components include a 19-tube basket, a steel cask that provides the required structural strength and a thin titanium shell placed over the steel cask for corrosion protection.

The design is based on standard 24-inch Schedule 80 pipe. This will support an external pressure of up to 10 MPa, as shown by finite element analysis and tests. The analysis showed that stress level in the container will be below specified stress limits under all postulated loads and that the cylindrical shell of the container will not buckle, even after 500 years of creep deformations. Information on creep was obtained from published data and from a test program. If larger pressures are anticipated, thickness of the container could be increased (to 38 mm for 13 MPa pressure).

An alternative design is proposed having a thick steel shell which includes a 25-mm corrosion allowance. This design and its corrosion allowance are based on the developments in similar U.S. and European programs.

A press-fit closure is proposed for the steel cask. A 6° taper at the contacting surfaces provides a high strength self-locking connection that can support high internal pressure. The closure is intended to eliminate the need for welding thick steel components after fuel is inside the container. The closure will have a partial, 12.7-mm seal weld. The closure concept was tested using 6-inch pipe specimens.

Several alternative bundle packing configurations are considered, including a 96-bundle capacity version.

JC

job	file	date	report no.
21-292-461	825.123	October 6, 1989	89-214-K

TABLE OF CONTENTS

		Page
LIST OF TABLES		iii
LIST OF FIGURES		iv
NOMENCLATURE		v
1.0	INTRODUCTION	1
2.0	CONTAINER DESCRIPTION	1
3.0	THICK-SHELL CONTAINER	2
4.0	DESIGN CONDITIONS	3
4.1	Loading Conditions	3
4.2	Design Criteria	3
5.0	EVALUATION OF STRESSES	4
5.1	Numerical Model	4
5.2	Assumptions	4
5.3	Results	4
6.0	BUCKLING ANALYSIS	4
6.1	Numerical Model	4
6.2	Results	5
7.0	CREEP STUDIES	5
7.1	Test Program	5
7.2	Creep-Buckling Analysis	5
7.3	Results	5
8.0	CLOSURE SYSTEM	6
8.1	Closure Design	6
8.2	Closure Model Tests	6
8.3	Closure Analysis	6
8.4	Results	6
8.5	Seal Weld Analysis	7
9.0	TITANIUM SHELL	7
9.1	Manufacturing Tolerances	7
9.2	Analysis of Top Head	7
9.3	Analysis of Bottom Head	8
10.0	THINER TITANIUM SHELL	8
10.1	Effect of Corrosion	8
10.2	Top Head Area	8
10.3	Bottom Head Area	8

Table of Contents (cont'd)

		Page
11.0	ALTERNATIVE DESIGNS	8
12.0	FUTURE ACTIVITIES	9
13.0	CONCLUSIONS	10
14.0	ACKNOWLEDGMENTS	11
REFERENCES		12
APPENDIX A	MANUFACTURING	A1
APPENDIX B	ALLOWABLE STRESSES	B1
APPENDIX C	STRESS DISTRIBUTION	C1
APPENDIX D	BUCKLING IN SHELLS	D1
APPENDIX E	CREEP IN STEEL	E1
APPENDIX F	SELF-LOCKING CLOSURE	F1
APPENDIX G	TITANIUM SHELL ANALYSIS	G1
APPENDIX H	NON-UNIFORM LOADING	H1
APPENDIX I	ACCIDENTAL DROP	I1
APPENDIX J	ALTERNATIVE DESIGNS	J1
DISTRIBUTION		last page

LIST OF TABLES

Table I Container Weight

Table II Material Properties

Table III Alternative Container Designs

LIST OF FIGURES

Figure 1 Conceptual Disposal Vault
Figure 2 Container Layout
Figure 3 Basket Arrangement
Figure 4 Steel Cask
Figure 5 Titanium Shell
Figure 6 Bottom Head Area
Figure 7 Top Head Area
Figure 8 Lifting Clamp Concept
Figure 9 Layout of Monolithic Container
Figure 10 Stresses in Monolithic Container
Figure 11 Finite Element Model of Top Head Area
Figure 12 Finite Element Model of Bottom Head Area
Figure 13 Stresses Intensities in Top Head at 10 MPa
Figure 14 Stresses Intensities in Bottom Head at 10 MPa
Figure 15 Through Thickness Stress Intensity Distribution
Figure 16 Geometry Used for Buckling Model
Figure 17 Stress-Strain Curve for Non-Linear Analysis
Figure 18 Bending Moment in Buckling Model
Figure 19 Displacement in Buckling Model
Figure 20 Post-Buckling Shape
Figure 21 500-Year Extrapolated Test Results
Figure 22 Creep Test Results
Figure 23 Steel Stress-Strain Curve with Creep
Figure 24 Displacement in Buckling Model with Creep
Figure 25 Seal-Welded Closure
Figure 26 Model Used for Top Closure Analysis
Figure 27 Stresses in Top Closure Area, No External Pressure
Figure 28 Tresca's Stresses in Closure Area at 10 MPa
Figure 29 Diagram of Lid-Closure Separation
Figure 30 Stresses in Seal Weld Area, No Pressure
Figure 31 Stresses in Seal Weld Area With 10 MPa Pressure
Figure 32 Alternative Basket Layouts

NOMENCLATURE

AECB	- Atomic Energy Control Board
AECL	- Atomic Energy of Canada Limited
Container	- A receptacle for immobilizing nuclear fuel waste
Disposal Facility	- A facility used to permanently emplace radioactive waste materials (for example an underground disposal vault and its supporting facilities)
Disposal System	- A disposal facility and the transportation facilities needed to bring the nuclear fuel waste from interim storage sites
e or ε	- Strain
IBSS	- Iron-Based, Stressed-Shell Container
Overpack	- A receptacle placed over a container for additional protection against corrosion
OHRD	- Ontario Hydro Research Division
S	- Calculated stress
Sm	- an allowable stress limit
Used fuel	- Fuel extracted from a reactor at the end of its useful life
WNRE	- Whiteshell Nuclear Research Establishment

ontario hydro
research division

To Mr. P.D. Stevens-Guille
Radioactive Materials Management
Nuclear Engineering Department

ASSESSMENT OF THE IRON-BASED, STRESSED-SHELL CONTAINER

1.0 INTRODUCTION

The concept of the Iron-Based, Stressed-Shell (IBSS) Container has been developed as part of an Integrated System Development Program pursued by Ontario Hydro/1/. The container, as presently proposed, is intended for the immobilization and disposal of used fuel bundles from CANDU nuclear generating stations, in an up-to 1000-m deep underground vault (see Figure 1). Some possibilities for other applications of the IBSS container including transportation and storage were considered/2/. The IBSS container design is one of several designs currently being investigated. It is the most recently introduced design and much of the assessment program is still incomplete. This program forms part of the Ontario Hydro's Technical Assistance Program (TAP) to AECL.

The container design was originally proposed in References /2/ and /3/. The design has evolved since then. The new reference design is described here in detail. All relevant information contained in reference /3/ is included here for completeness.

Two versions of the container are considered. The first version (shown in Figure 2) has a thick steel cask providing structural support and a thin external titanium shell providing corrosion protection (bimetallic design). The cylindrical shell of the cask is made of 24-inch, schedule 80 pipe and is suitable for external pressures up to 11.2 MPa, as shown in Subsection 6.3. If a higher pressure is postulated, a non standard, larger thickness shell may be required. One of the alternative designs included in Subsection 11.0 has a 38-mm thick wall, adequate for 13 MPa pressure.

The second version lacks the titanium outer shell, but has extra thick steel walls to provide 500-year corrosion allowance (monolithic design). This version is presented in Section 3.0.

This report presents the current state of development, together with the planned work programs.

2.0 CONTAINER DESCRIPTION

The Iron-Based, Stressed-Shell (IBSS) container has three main components: a fuel basket, a steel cask and a corrosion-resistant titanium shell. The container is expected to weigh 32.8 kN when loaded with used fuel bundles (see Table I).

The fuel basket consists of nineteen 4-inch mild steel pipes, 0.125-inch thick, arranged concentrically as shown in Figure 3. Each pipe (except for the center one) can contain four used fuel bundles allowing for up to 72 bundles to be placed in a container. The pipes are closed at the bottom with an 25.4-mm thick flat plate.

The steel cask is shown in Figure 4. A 24-inch Schedule 80 pipe forms the basis for the cylindrical shell. The bottom head is 76-mm thick and is welded to the cylindrical shell with a full penetration weld. The 40-mm radius at the bottom rim (see Figure 6) is for easy fitting of the bottom titanium head. The top of the cylindrical shell is designed to accept a press-fit closure or a full penetration weld. The top closure head is a 76-mm thick steel plate (see Figure 7). The 6° taper at the perimeter is for the self-locking effect. After the used fuel is loaded, the top head is pressed in place and seal-welded.

The titanium overpack is made of 4.76-mm thick, B265 Grade 2 titanium plate, rolled to a 610-mm cylinder, to fit over the steel cask (see Figure 5).

The container would likely be handled in both horizontal and vertical positions. Horizontal handling may be preferred during fuel loading and during transportation to and inside the vault. Most assembly processes and emplacement in a borehole will require vertical handling. For vertical handling, the container can be lifted using the top lifting ring, shown in Figure 5. Ring gripping could be provided by three clamps positioned 120° apart, in a jig. A conceptual clamp design is shown in Figure 8. In the horizontal position, the container could be supported on a bed-like frame. This bed could be used to rotate the vessel between horizontal and vertical positions. Alternatively, electromagnetic pick-ups could be designed for both vertical and horizontal handling.

Based on our discussions with prospective manufacturers, a method for manufacturing and assembling the container is proposed in Appendix A. The container can be produced and assembled economically using existing technology.

3.0 THICK-SHELL CONTAINER

A monolithic, thick wall version of the container is proposed as an alternative to the design outlined above. For this version, the shells and plates will be thicker to provide a 500-year corrosion allowance. The container would be made of cast steel or cast iron and would accommodate the same basket. The thickness required for structural support is assumed to be equal to that of the steel shells of the bimetallic design. Similar container designs are being developed in several U.S. and European programs. A proposed design of a monolithic container is shown in Figure 9a. Its cylindrical shell is 56-mm thick and flat plates are 100 mm (and has 25 mm corrosion allowance used in some foreign programs).

Stresses in the container were calculated using the finite element method. A 25-mm corrosion allowance was assumed. For the 10 MPa uniform external pressure, the largest stress at the head to cylindrical shell discontinuity is 107 MPa or 53% yield (see Figure 10). Should the external pressure increase to 13 MPa (see Subsection 4.2), the peak stress would still be 67% yield. Buckling or creep of the container need not be considered for the 500-year planned life of the container, because its thickness is larger than the thickness of the bimetallic container and the bimetallic container is not expected to buckle, as shown below.

4.0 DESIGN CONDITIONS

4.1 Loading Conditions

The container is designed to meet the following conditions:

1. It must not perforate by corrosion for at least 500 years.

2. It must be able to support an external pressure of up to 10 MPa that would occur when the vault re-saturates with ground water.

3. The container outer shell temperature will not exceed 100°C.

4. The container must be able to support an internal pressure of 0.1 MPa, due to an increase in temperature of up to 90°C.

Several other performance criteria (welding, corrosion, geology etc.) are studied by other AECL and Ontario Hydro investigators within the program. Their findings may effect the container design (see Section 12.0).

Several other loading conditions are also considered including: an additional pressure of up to 3 MPa due to the bentonite swelling (see Section 12.0); non-uniform external pressure due to a non-uniform, gradual water ingress (see Appendix H); accidental drop of the container in a borehole (see Appendix I).

4.2 Design Criteria

There are no codes or standards directly applicable to disposal containers that would provide the guideline for stress limits. The steel shell of the container is a pressure-retaining boundary. As such it can be designed using the ASME Boiler and Pressure Vessel Code. Since the container is used for handling of nuclear materials, Section III, Subsection NE (for MC components) will be used. A general discussion of the requirements of Subsection NE of the Code is presented in Appendix B.

The thin titanium shell of the bimetallic design is not capable of supporting an external load and will deform under external pressure until it is fully supported by the steel cask. The shell is considered to fail if large strains cause it to breach or if the shell buckles. Compressive stresses are assumed not to cause failure, except if buckling occurs. The shell will not breach if the sum of two mutually orthogonal local tensile strains is below 5.3% (see Appendix B).

The Code does not require creep analysis for low temperature applications. Because of the 500-year postulated container life, an additional condition including the effect of creep is postulated: the steel shell design is considered acceptable if in its worst possible configuration, it will not buckle below 10 MPa after the effect of 500-year creep is considered.

5.0 EVALUATION OF STRESSES

5.1 Numerical Model

Stress distribution in the bimetallic IBSS container was evaluated with two finite element models. The first model includes the top head area while the second model is of the bottom head area. The two finite element models were developed using four-noded axisymmetric elements. The models do not consider the effects of the press-fit closure and of the small weld at the top head. The heads and shell are assumed to form uniform continuous structure. The models are shown in Figures 11 and 12.

5.2 Assumptions

The following assumptions were made to simplify the analysis:

1. The container is axisymmetric.
2. Material is linear-elastic even beyond yield stress (except for a few special cases where plasticity and large deformation theory are included).
3. Nominal pipe and plate thicknesses are used in both models.
4. External pressure is uniform.
5. Deformations in the top and bottom heads are independent of each other.

Properties of steel used in the analysis are listed in Table II.

5.3 Results

An external pressure of 10 MPa was applied to both models. The stress intensity distribution in both models is shown in Figures 13 and 14. The stresses in the cask have been evaluated at five sections, shown in Figure 11. The average through-thickness stress intensities for all five sections ranged from 25 to 41% yield (an average stress of up to 67% yield is allowable). The average plus bending stress intensities reach 57% yield. They are below the material yield value of 200 MPa. Typical through-thickness stress distributions are shown in Figure 15.

The largest peak principal stress of 280 MPa occurred on the inner wall just above the bottom head. In this analysis, no limit is placed on local peak stresses because they effect fatigue life only, as postulated in the Code. Fatigue need not be considered for the container. A more complete discussion of this analysis appears in Appendix C.

6.0 BUCKLING ANALYSIS

6.1 Numerical Model

Cylinders under external pressure may buckle. If buckling initiates, large deformations may occur with no increase in load.

To investigate the possibility of buckling, a non-linear stress analysis was performed. This analysis used large deformation theory and included the effects of worst pipe configuration and material nonlinearities (see Appendix D).

Because of symmetry of the cask, only one quarter was modeled. Four-noded shell elements were used. The elements were assigned varying thicknesses around the circumference to simulate the greatest possible thickness variation allowed by 24-inch Schedule 80 pipe tolerances. Two orientations of pipe eccentricity were analyzed. Only the results from the more conservative orientation are presented here. The finite element model is shown in Figure 16.

A piecewise-linear approximation of the stress strain relationship of 1020 steel at 100°C was used for this analysis, as shown in Figure 17 and in Table II.

6.2 Results

The model was analyzed assuming a 10 MPa uniform external pressure on the heads and the shell. The allowable pressure below which buckling will not occur is given in the ASME Code (NE-3228 and Appendix II-1430(b)), see Appendix B. Plots of reaction moments and displacements versus external pressure at the two points that buckled first are shown in Figures 18 and 19. Locations 1 and 2 are shown in Figure 16. The buckled shape of the container is shown in Figure 20. Buckling occurs when large increase in deformation occurs without increase in load (at constant pressure). Internal moments opposing deformation drop as the radius of curvature increases. The calculated external pressure at which buckling is likely to initiate is 16.8 MPa. The allowable external pressure is 66.7% of 16.8 MPa or 11.2 MPa. Appendix D contains a more detailed discussion of this analysis.

7.0 CREEP STUDIES

7.1 Test Program

We were unable to find adequate data for creep of steel at low (100°C) temperature. Extrapolation of the available high temperature, low-stress test results indicates (see Appendix E) that creep may occur in steel at postulated vault temperature and at stress above 70% yield, see Figure 21. Many assumptions were made in this extrapolation. The accuracy of the graph was confirmed in a test program on 10-foot long steel rods subjected to tensile loads ranging from 70% to 100% yield. Five tests have been completed (see Figure 22). The results of 2,500 to 7,000-hour tests were extrapolated to 500 years and plotted on the graph in Figure 21.

7.2 Creep-Buckling Analysis

To evaluate the effect of creep on the container's ability to resist buckling, the steel stress-strain curve was modified to include the anticipated 500-year creep strain. The creep strain from Figure 21 was added to the material short-term stress-strain relationship, as shown in Figure 23. The finite element model used here is identical to that used in Section 5.2. Material properties used in analysis are listed in Table II.

7.3 Results

The change in the material stress-strain relationship has a significant effect on the container's ability to resist buckling.

Buckling again initiated at locations 1 and 2, shown in Figure 16. The container may buckle at an external pressure of 11.3 MPa as shown by the displacements at location 1 and 2, plotted against external pressure in Figure 24. A detailed discussion of creep and creep induced buckling appears in Appendix E.

8.0 CLOSURE SYSTEM

8.1 Closure Design

Several closure designs for sealing the bimetallic and monolithic IBSS containers by a remote operation have been considered, from full penetration weld to a loose fitting seal welded. A full penetration weld between the top lid and the cylindrical shell would be 31 to 100-mm thick. The difficulty in making, inspecting and repairing such a weld may make it unattractive. As an alternative, a closure system with a small seal weld is proposed.

A sketch of the closure is shown in Figure 25. A lid with a 6° taper (for self-locking) is press-fit into a similar taper at the top of the steel cask. Our preliminary tests indicate that such a closure has adequate strength, but its leak rate, although low, is unacceptable for disposal. Therefore, a small seal weld is proposed. A stress analysis of the closure showed that although yield stress is introduced at the contact surfaces, Code allowable stresses are not exceeded.

8.2 Closure Model Tests

Several tests were conducted on specimens made of 6" pipes, Schedules 10, 40, 60, and 160. The thickness of the closure plate ranged from 25 mm (for schedule 10 and 40 specimens) to 63 mm for the schedule 160-pipe specimens. In all tests, the 6° angle of contact was maintained. The lid was pressed in until the circumferential stresses in the shell reached yield. Test results varied widely. The helium leak test results ranged from below 10^{-9} Atm.cc/sec to rates too high to measure. An internal pressure required to open the closure increased as thicknesses increased and frequently exceeded 2 MPa, as discussed in Appendix F.

8.3 Closure Analysis

Stresses of the closure area were evaluated by the finite element method using solid, four-noded axisymmetric elements (see Figure 26). The 6° taper was included in the analysis. An interference fit of 0.7 mm was imposed in the closure causing plastic strains between 0.10% and 0.15%. Gap elements were introduced between the wall and lid to evaluate forces and deformations along the interfering surfaces. A uniform external pressure of 10 MPa was then applied and the behavior of the closure was monitored.

8.4 Results

The first analysis did not include a weld. Before external pressure is applied, the entire length of the closure is in contact. Stresses in the closure area are shown in Figure 27. When 10 MPa external pressure is applied, stresses in the closure area do not change significantly (see Figure 28). Only localized plastic deformations can be anticipated at this pressure. As external pressure increases, the shell and lid deform inwards, pivoting about the inner corner of their contact. This tends to open a gap. Under 10 MPa, the closure has opened along approximately

67% of its depth. At the outer surface this gap is 1.5×10^{-3} mm wide (see Figure 29). A small seal weld is required at the outer surface of the lid closure to prevent separation of the lid and shell. A more detailed description of this analysis appears in Appendix F.

8.5 Seal Weld Analysis

The lid closure model was refined to include a seal weld. Within a weld, the existing stress distribution is complex and depends on a number of factors including: welding procedure, cooling rates and post welding heat treatment. A complete discussion of assumptions introduced in the analysis is presented in Appendix G. This second analysis was aimed at quantifying changes in the weld area stress state due to the external pressure. The analysis was carried out in three steps: (1) an interference fit was imposed, (2) elements representing the seal weld were added, and (3) 10 MPa of external pressure was applied.

Figure 30 shows the Tresca's stresses in the weld area of the closure. It shows that the weld material is at yield before any pressure is applied. High stresses are caused by an introduction of new elements into an already deformed area and should be neglected. Figure 31 shows stresses in the same area after an external pressure of 10 MPa is applied. Comparison of the two figures shows only a marginal change in the stress magnitude or distribution. Thus, any change in external pressure or deformation of the lid/wall interface is insignificant compared to the stresses due to the interference fit and welding.

9.0 TITANIUM SHELL

9.1 Manufacturing Tolerances

The titanium shell will be made by forming and welding 4.76-mm and 6.35 mm plates (see Section 2.0). The manufacturing process must ensure that a gap between the steel canister and the shell is not greater than 1.0 mm at the cylindrical shell and at the top head to ensure a proper support.

9.2 Analysis of Top Head Area

Two finite element models of the top head area were created. The first model has a triangular reinforcing ring filling the gap between the steel head and the titanium lid (see Figure 5a), while in the second model this area is empty. The finite element models use axisymmetric two-noded shell elements for the titanium shell and four-noded axisymmetric solid elements for the cask. The material properties of titanium are shown in Table II. The elements forming the reinforcing ring were continuous with the cask and had properties of 1020 steel. Between the steel cask and the shell, 1.0 mm gap elements were defined to represent the size of space between the titanium shell and the steel. Both analyses used large displacement theory and isotropic material hardening (described in Table II).

At 10 MPa, the titanium shell is supported by the cask everywhere except in the corner region of the top head. The corner region is distorted, but plastic strains are only 0.3%. Plastic strain in the cylindrical shell did not exceed 0.12%. The removal of the support ring from the model had no significant effect. The highest stressed areas are in the top corner region. The calculated plastic strains were of the same order whether the support ring was present or not.

A more complete description of this analysis is presented in Appendix G.

9.3 Analysis of Bottom Head

The strain in the titanium shell in the bottom head region was evaluated with an axisymmetric finite element model. As before, 1.0 mm thick gap elements were defined between the steel cask body and the shell.

Under 10 MPa of external pressure the largest plastic strains occur at the corner radius and they are less than 0.3%.

A detailed description of this analysis appears in Appendix G.

10.0 THINER TITANIUM SHELL

10.1 Effect of Corrosion

The titanium shell will be made of 4.76-mm thick plate. A uniform, 500-year corrosion will result in a locally reduced thickness. For this analysis, uniform corrosion was postulated, which may reduce the shell thickness to 2 mm. The analysis has been conducted to show that even a 2-mm thick shell is structurally adequate.

10.2 Top Head Area

The finite element models with the 4.76-mm thick titanium overpack (discussed in Section 9.2) were modified to have a 2-mm thick titanium shell.

Under 10 MPa external pressure, the 2-mm shell model with a support ring has plastic strains in the corner of up to 0.29%.

If the support ring is not used, large deformations are anticipated. At 7 MPa external pressure, the unsupported corner region has been compressed until the wall and the lid contact. Plastic strains reached 2%. The analysis was not continued past 7 MPa because the rate of deformation increased, making analysis unstable - excessive strains are anticipated. Plastic strain in the cylinder walls remains below 0.2%. A more complete description of this analysis, including the location and magnitude of plastic strains, appears in Appendix G.

10.3 Bottom Head Area

At 10 MPa pressure the 2 mm thick titanium is supported everywhere by the underlying steel cask. Plastic strains in titanium reach a maximum of 0.21% at the corner. This value is below the maximum level of acceptable plastic strain proposed in Section 4.3. Further details on this analysis appear in Appendix G.

11.0 ALTERNATIVE DESIGNS

Only the reference design was considered so far. Several alternative container designs are proposed within the IBSS project in consideration of (see Appendix J):

- design for a 13 MPa overpressure
- alternative bundle capacity: 72 or 96

- alternative container diameters
- alternative cask material: steel, cast iron or a corrosion resistant metal.
- alternative overpack material: titanium, copper, other metal or ceramic.

The largest hydrostatic pressure considered above is equal to the 1000-m water head that may occur in a fully re-saturated repository. The backfill material used to support the container in a borehole contains bentonite. As the bentonite absorbs water it may expand and exert additional pressure. D.A. Dixon and M.N.Gray/4/ postulate that the swelling pressure can reach 3 MPa, for the total maximum repository pressure of 13 MPa.

The proposed reference design is suitable for pressures of up to 11.3 MPa, as discussed in Subsection 7.3, because of the possibility of creep induced buckling. Buckling is highly sensitive to imperfections, such as out-of-roundness in the shell. If tighter tolerances were imposed on the container's shell, it could support much higher pressures without buckling. Alternatively, a thicker container shell could be used without any need for tight out-of-roundness tolerances. The analysis of Sections 6.0 and 7.0 were repeated using 41.3-mm thick steel shell. The largest allowable external pressure is 13.5 MPa when creep effects are included in the analysis. Buckling is not expected to occur below 16.0 MPa external pressure, according to the Pressure Vessel Code criteria. A 41.3-mm pipe having an outside diameter of 622 mm can be manufactured as a non-standard pipe or by centrifugal casting. The thickness of heads would not change in this case.

Used fuel will be transferred to containers from modules holding 96 bundles. Disposal containers having capacity of 96 bundles may be considered (see Figure 32). The dimensions and configurations of several alternative container designs are illustrated in Table III.

The structurally weakest area of the container is in the titanium shell at the top corner where diffusion bonding is used. This area could be modified by providing a radius at the top of the cask identical to that at the bottom corner. The top titanium head would be identical to the bottom head. Gas-tangsten-arc welding could be used to close the container. Handling of the container would be provided by magnetic pick-ups because of the thick steel head.

A granular material can be introduced inside the container (without compaction) to reduce the void space which will form when containers fail (following their minimum 500-year useful life).

The alternative designs are considered further in Appendix J.

12.0 FUTURE ACTIVITIES

The IBSS container concept was introduced recently to the TAP program. Although we feel confident that the design is viable, much work remains to demonstrate its effectiveness. Some of the remaining questions are discussed here. Several activities are proposed to resolve them. The program should continue for several more years.

Corrosion of the steel cask may result in a high rate of hydrogen formation. This rate will have to be assessed together with the methods and consequences of hydrogen flow out of the repository.

Manufacturing process for the container is proposed based on preliminary discussions with prospective fabricators. More discussions are needed to ensure that the proposed process is suitable. Building of a prototype would provide the best demonstration of the manufacturing viability.

The finite element analysis discussed here, although quite comprehensive, is incomplete. Outstanding items include closure weld analysis, a consideration of the largest allowable flaw and the possibility that the overpressure might not build uniformly on the container surface. The 'threshold' impact height should be evaluated to determine the ability of the container to survive a minor handling accident. Our ability to do such analysis has been demonstrated as shown in Appendix H. The effect of tolerance on the buckling pressure should also be evaluated. A simplification was introduced in the analysis by replacing actual creep laws with artificial material properties (which includes the effect of the 500-year creep). The effect of this simplification has been shown to be small (see Appendix E).

Many assumptions were made during the stress analyses. A hydrostatic test program of a limited scope could provide good verification of analytical results.

Creep tests of steel at low temperature have finished. The tests are continuing and will include a creep study in titanium and copper. The study also includes the evaluation of the effect of tension and bending moment on creep of the steel cask in the discontinuity areas (see Appendix E).

We have only a limited understanding of the performance of the proposed closure. The test program on the closure should continue.

AISI 1020 L steel has been selected for the reference design. This may not be the most suitable selection. A metallurgical evaluation should be conducted to determine if steel or cast iron would be more suitable. Various types of steels and cast irons should be examined to ensure the best selection.

The alternative designs have only been mentioned in this report. Much work remains before we can establish any preferences.

The design offers some favorable features:

1. Retrievability (not required in the Canadian program/5/) may offer some advantages and may be facilitated by this design.

2. The thick steel shell will reduce radiation on the outside of the container which may simplify container handling and reduce radiolysis in the vault.

An investigation should be considered to determine their importance to the Canadian program.

13.0 CONCLUSIONS

The program is well defined including its scope and objectives. The work completed to date indicates that the concept may be viable. The reference containers meet the postulated criteria. No performance characteristics were identified which could make the container unsuitable. Development of the concept, however, is in its early stages and we recommend that the program should continue.

14.0 ACKNOWLEDGMENTS

The experimental work described here was done by Messrs. A.C. Fallis, N.N. Shah and R.M. Zane including testing of the closure system. Many design features of the IBSS container were taken from the Thin-Walled, Particulate-Packed Container which was developed jointly by Mechanical Design and Mechanical Research Departments of Ontario Hydro. Dr. G. Bellamy, Dr. M. D. Moles and Mr. P. Y. Maak are providing the metallurgical evaluation of the container. Mr. J.L. Crosthwaite of AECL provides a technical review of the program. The authors acknowledge and thank them for their input.

Approved by:

G.J. Clarke
Manager
Mechanical Research Department

Recommended by:

J.A. Chadha
Area Coordinator
Container and Immobilization
Studies of Nuclear Waste
Nuclear Waste Management

Submitted by:

B. Teper
Engineer
Applied Mechanics Section

per S.A Reid
Engineer
Applied Mechanics Section

Reviewed by:

J.D. Tulk
Unit Head-Special Projects & Computing
Applied Mechanics Section

BT/SAR:cm

REFERENCES

1. P. Pearson, *"Integrated Irradiated Fuel Management Systems - Metallic Container Development Program, 1983 Program Plan"*, Ontario Hydro Design and Development Division report number 83094, dated January 1983.

2. B. Teper, *"Development of Integrated Metallic Container - Project Status"*, Ontario Hydro Research Division report 84-416-K, issued January 23, 1985.

3. B. Teper, *"Evaluation of Iron-Based Stressed-Shell Container Concept"*, Ontario Hydro Research Division Report 86-98-K, dated August 5, 1986.

4. D.A. Dixon, M.N. Gray, P. Baumgartner, G.L. Rigby, *"Pressure Acting on Waste Containers in Bentonite-Based Materials"*, Second International Conference on Radioactive Waste Management, September 7-11, 1986, Winnipeg, Manitoba.

5. *"The AECL Public Consultation Program Workshop on the Canadian Nuclear Fuel Management Program, 1988 March 25-27"*, AECL Technical Report TR-472, prepared by Pat Delbridge Associates Inc., issued January 1989.

TABLE I

CONTAINER WEIGHT

ITEM	VOLUME (L)	MASS (kg)	WEIGHT	
			kN	lbs
STEEL CASK	163	1272	12.49	2804
TI SHELL	25.1	114	1.12	251
BASKET	33	262	2.60	578
BUNDLES	162	1698	16.60	3743
TOTAL		3346	32.81	7376

TABLE II

MATERIAL PROPERTIES

MATERIAL	TEMPERATURE °C	PROPERTY	STRESS MPa	PLASTIC STRAIN (%)	OTHER
STEEL	100	YOUNG"S MODULUS	200,000		
		POISSON"S RATIO			0.29
		ULTIMATE STRENGTH	413		
		YIELD STRENGTH	201		
		PLASTICITY	201	0.0	
			202	0.5	
			295	5.0	
		PLASTICITY WITH 500-YEAR CREEP*	150	0.0	
			200	0.46	
			202	0.99	
TITANIUM	100		300	7.19	
		YOUNG'S MODULUS	100,000		
		POISSON'S RATIO			0.34
		ULTIMATE STRENGTH	345		
		YIELD STRENGTH	216		
		PLASTICITY	216	0.0	
			325	0.02	
			345	0.20	

* TO INCLUDE CREEP STRAIN IN ANALYSIS, THE EXTRAPOLATED 500-YEAR CREEP IS COMBINED WITH THE PLASTIC STRAIN

TABLE III
ALTERNATIVE CONTAINER DESIGNS

ALTER NO	NO OF BUNDLES	NO OF LAYERS	CONTAINER DIMENSIONS (mm)			
			DIAMETER		HEIGHT	
			INSIDE	OUTSIDE	INSIDE	OUTSIDE
1	72	4	547.7	620.3	2014	2250
2	72	4	540.0	652.0	2012	2212
3	96	6	547.4	620.3	3005	3241
4	96	4	720.0	842.5	2014	2250
5	72	4	547.7	620.3	2014	2120
6	72	4	547.7	641.0	2014	2250

NOTES

1. ALTERNATIVE NUMBER 1 REPRESENTS REFERENCE DESIGN FROM FIGURES 2 THROUGH 5.
2. ALTERNATIVE NUMBER 2 REPRESENTS THE MONOLYTHIC CONTAINER FROM FIGURE 3.
3. ALL ALTERNATIVE CONFIGURATIONS (EXCEPT 2) ARE BASED ON BIMETALIC CONCEPT ALTHOUGH THEY CAN BE ADOPTED FOR MONOLYTHIC CONCEPTS.
4. ALTERNATIVE DESIGNS 4 AND 5 ARE INTENDED FOR USE WITH 96-BUNDLE BASKETS (see FIGURE 32)
5. ALTERNATIVE DESIGN NUMBER 5 REPRESENTS A CONTAINER WITH BOTH HEADS IDENTICAL.
6. ALTERNATIVE 6 IS INTENDED TO SUPPORT 13 MPa EXTERNAL PRESSURE.

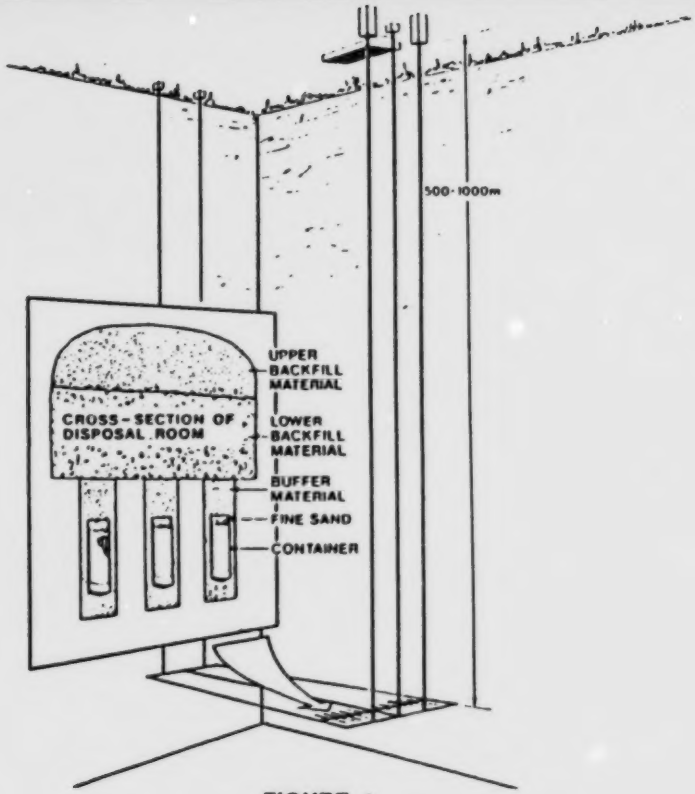

FIGURE 1
CONCEPTUAL DISPOSAL VAULT

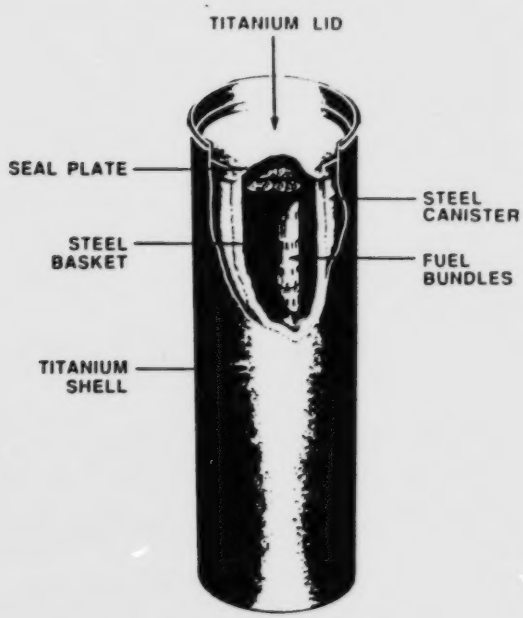

IRON-BASED STRESSED-SHELL CONTAINER

FIGURE 2
CONTAINER LAYOUT

190374 G6 RD RD
89-214-K

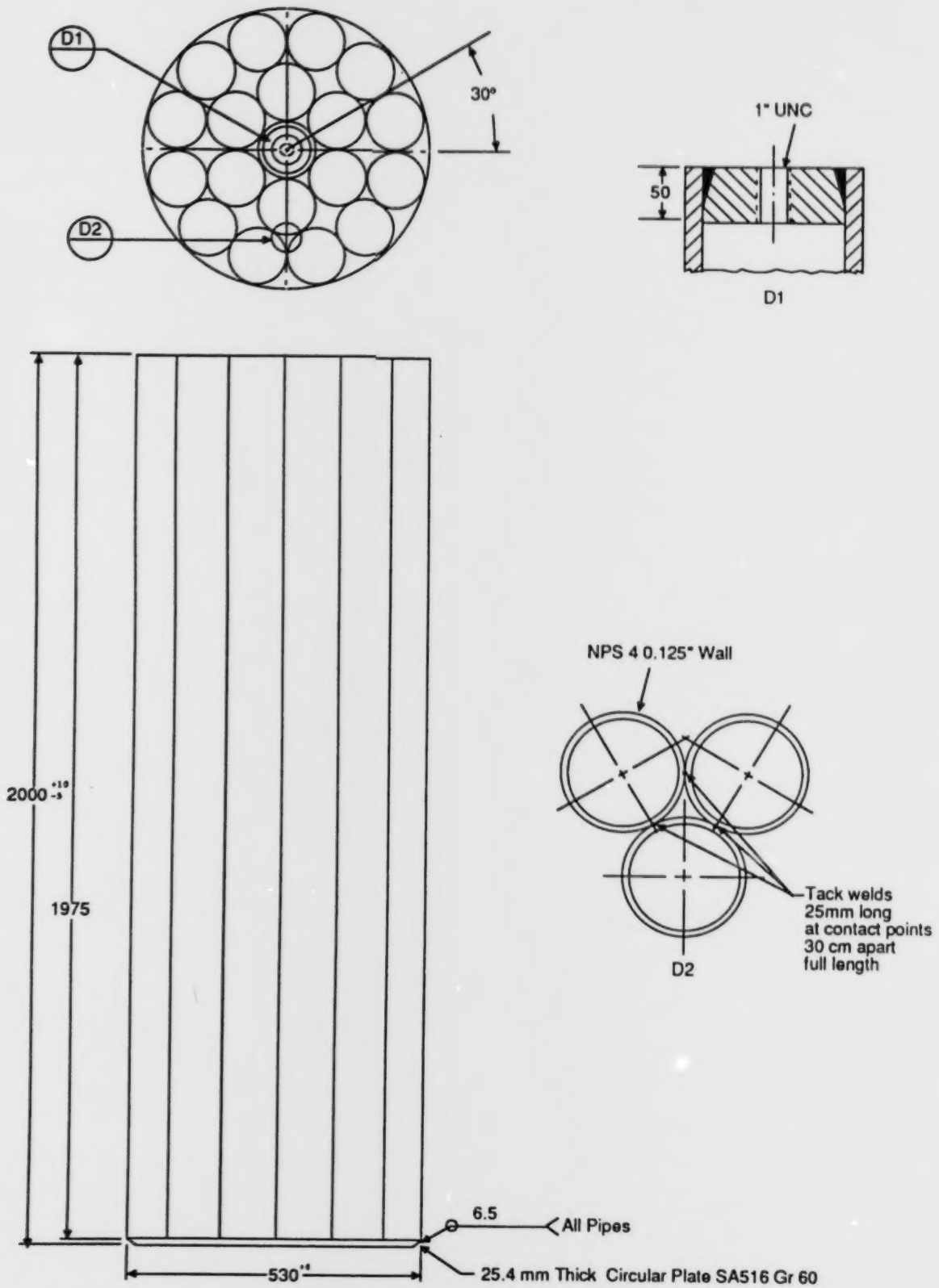

FIGURE 3
BASKET ARRANGEMENT

89-214-K
177553-G6-RD

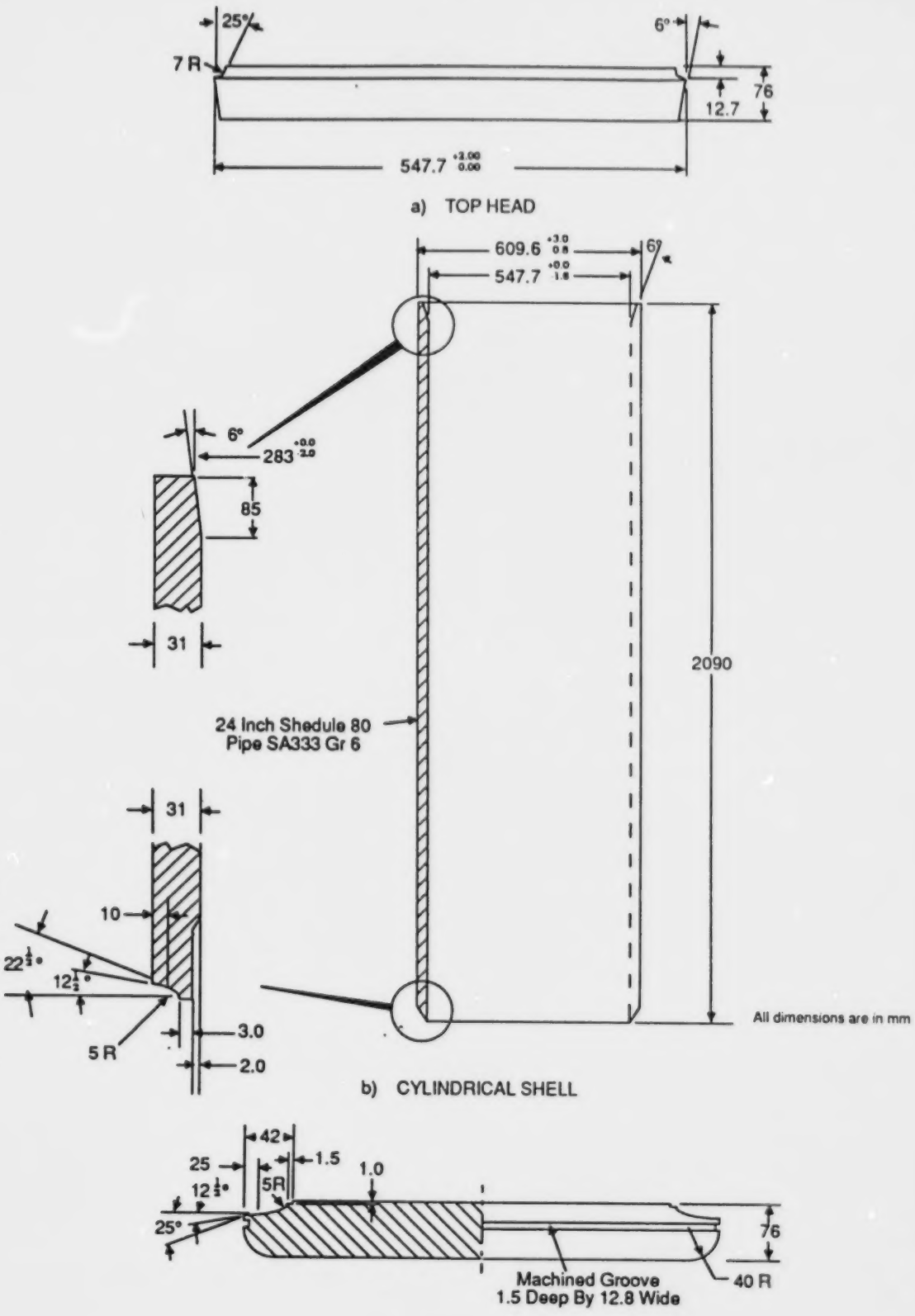

FIGURE 4
STEEL CASK

89-214-K
177546-G8-RE

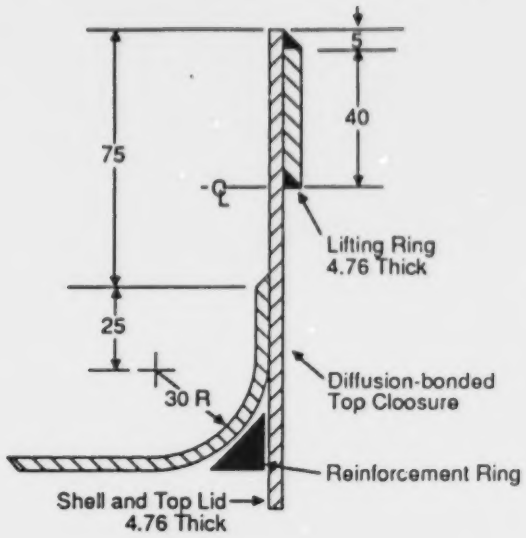

a) TOP LID WELD

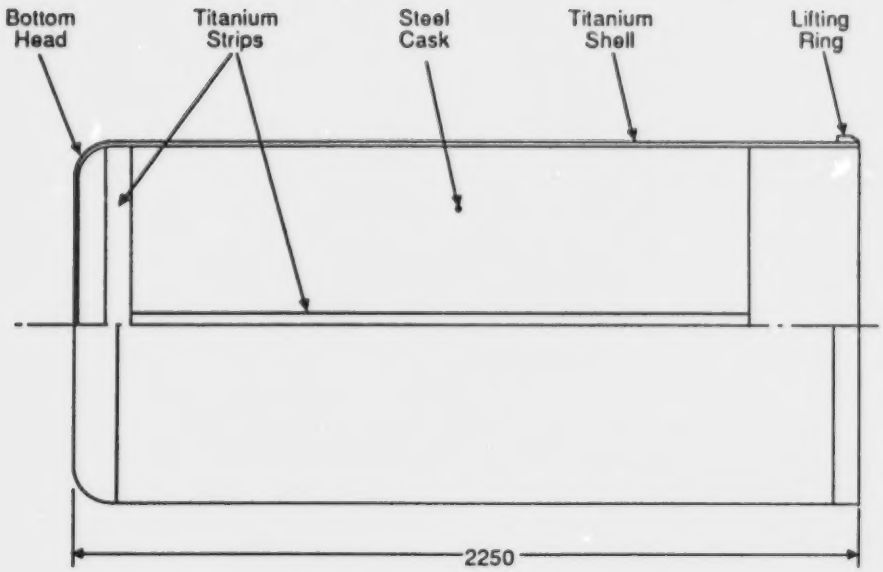

b) SHELL ASSEMBLY

FIGURE 5
TITANIUM SHELL

89-214-K
177536-G6-RD

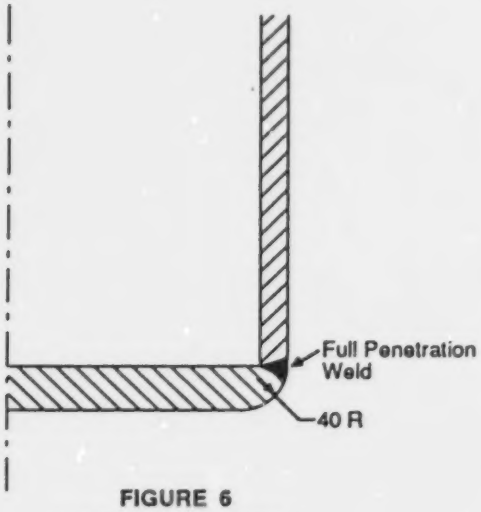

FIGURE 6
BOTTOM HEAD AREA

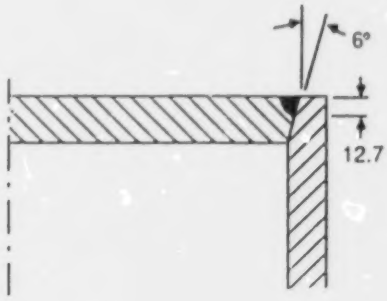

FIGURE 7
TOP HEAD AREA

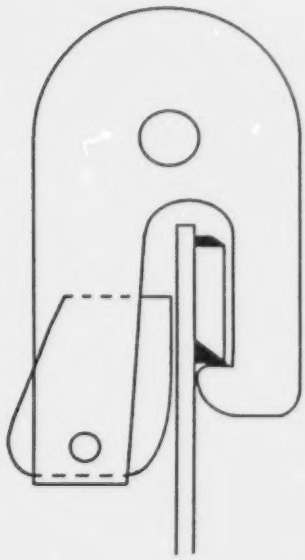

FIGURE 8
LIFTING CLAMP CONCEPT

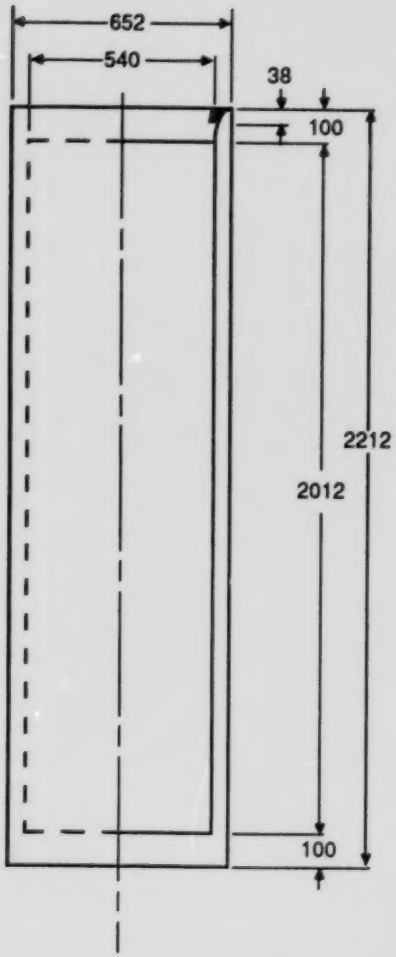

a) GEOMETRY

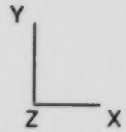

b) FINITE ELEMENT MODEL

FIGURE 9
LAYOUT OF MONOLYTHIC CONTAINER

a) AT 10 MPa PRESSURE

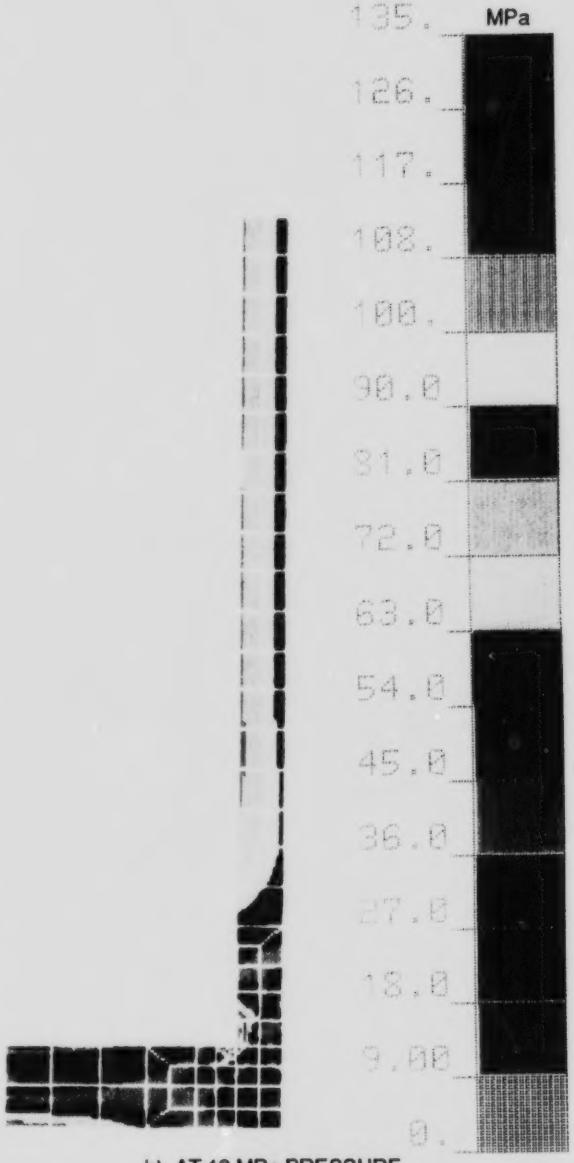

b) AT 13 MPa PRESSURE

FIGURE 10
STRESSES IN MONOLITHIC CONTAINER

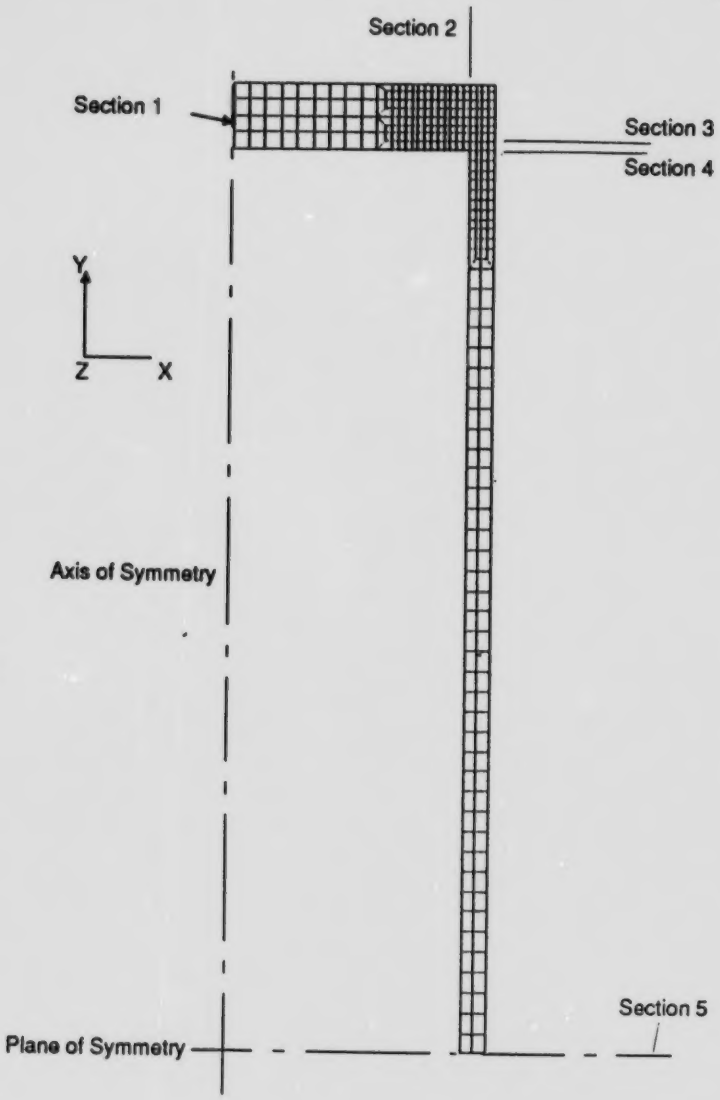

FIGURE 11
FINITE ELEMENT MODEL OF TOP HEAD AREA

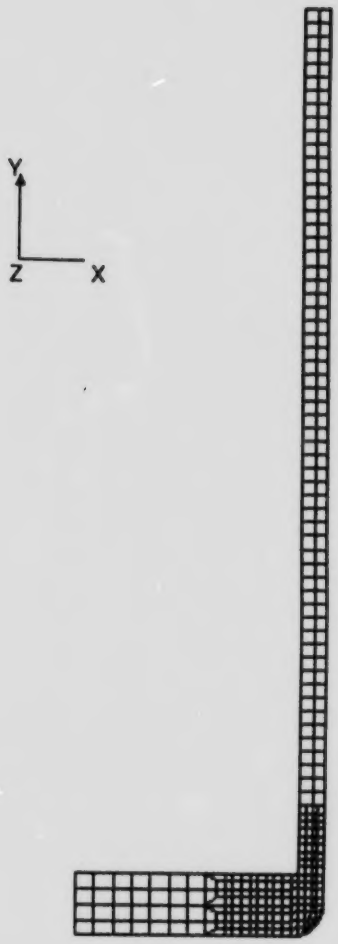

FIGURE 12
FINITE ELEMENT MODEL OF BOTTOM HEAD AREA

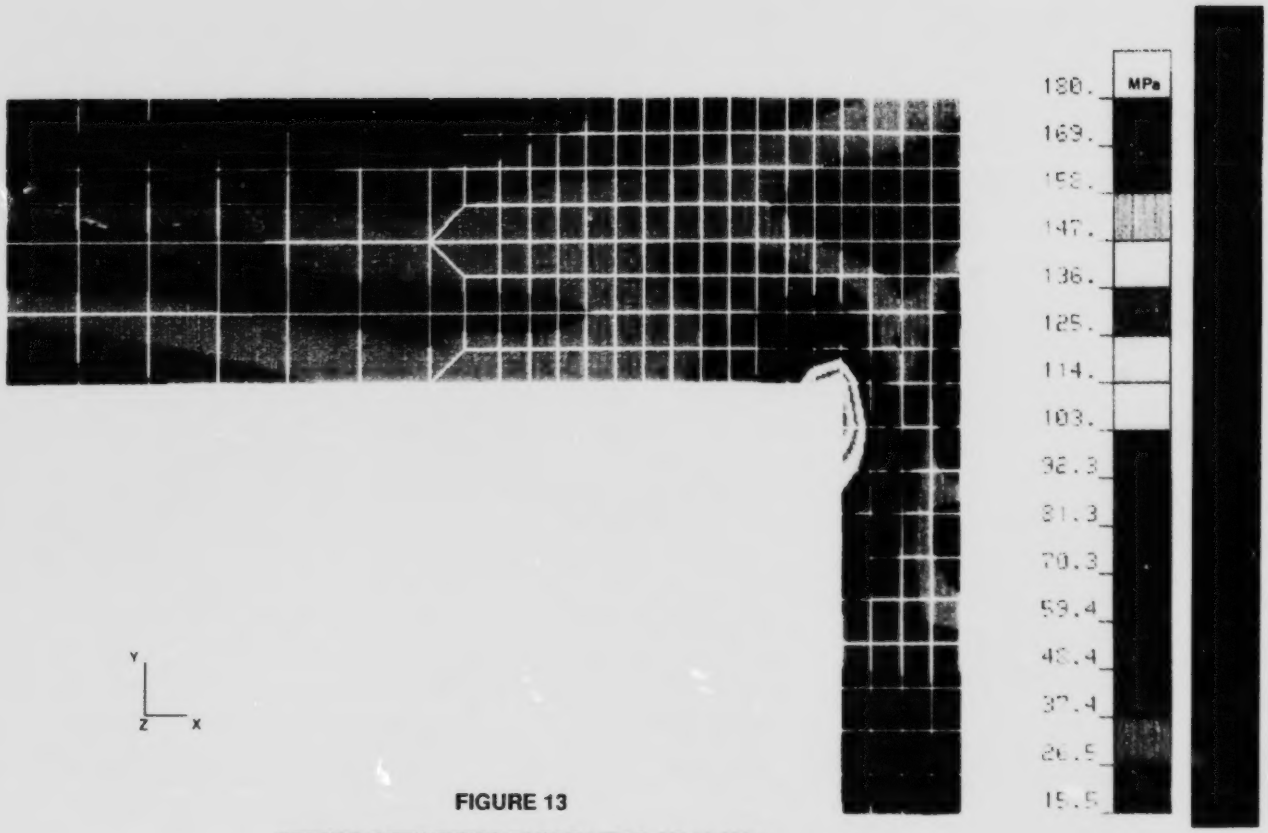

FIGURE 13

STRESS INTENSITIES IN TOP HEAD AT 10 MPa

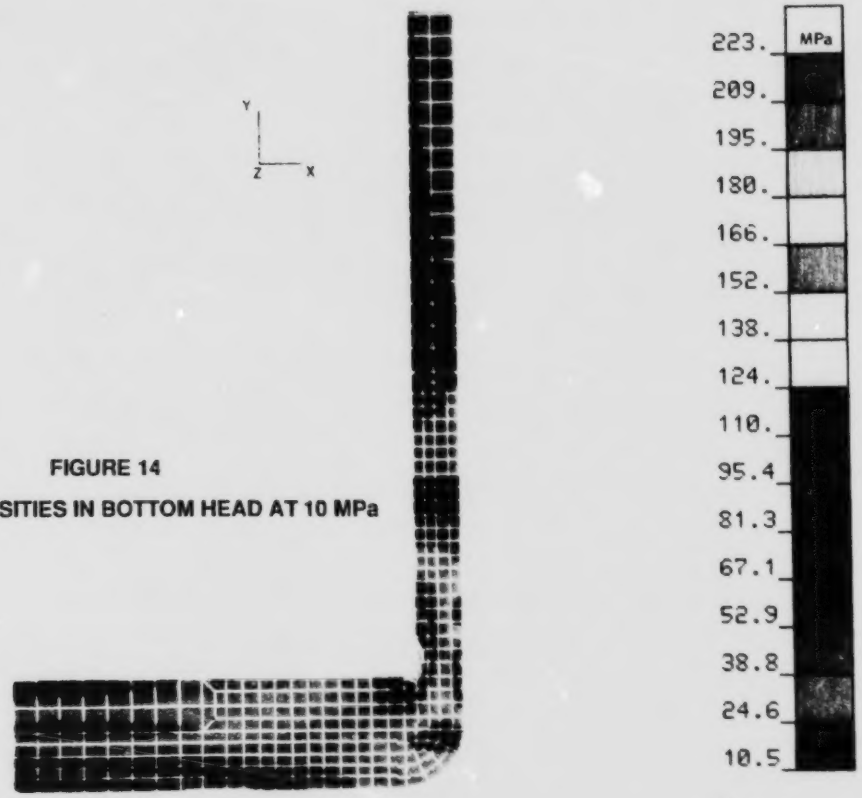

FIGURE 14

STRESS INTENSITIES IN BOTTOM HEAD AT 10 MPa

89-214-K
180387.RD

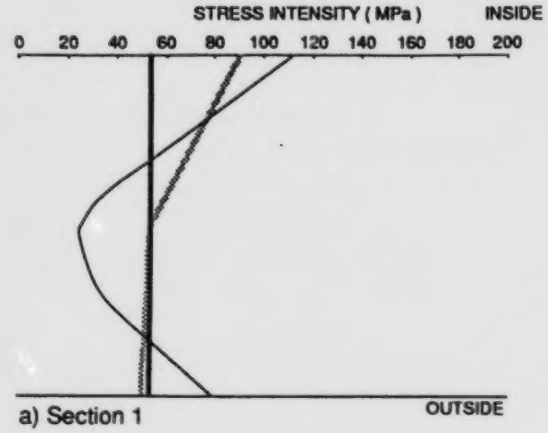

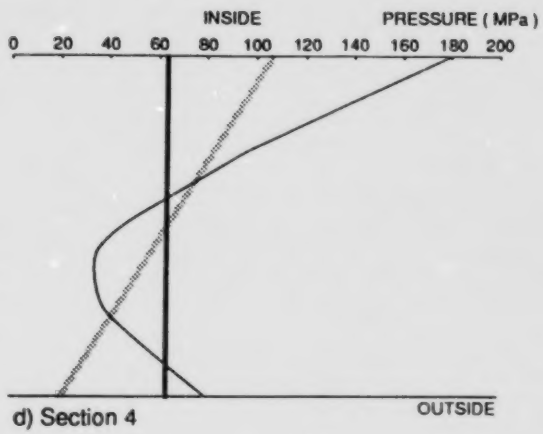

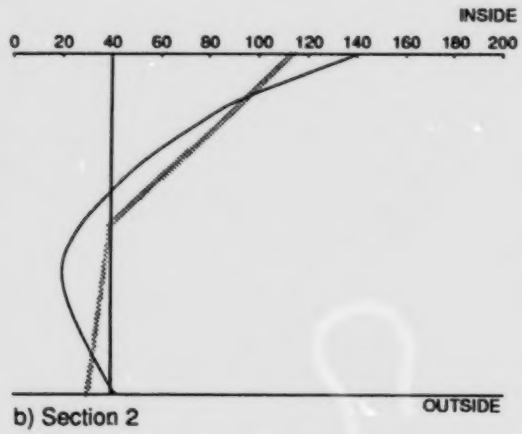

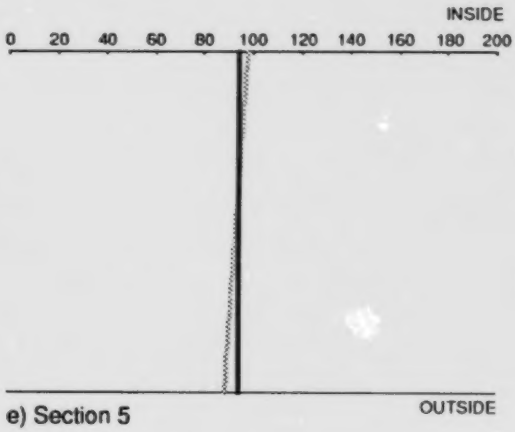

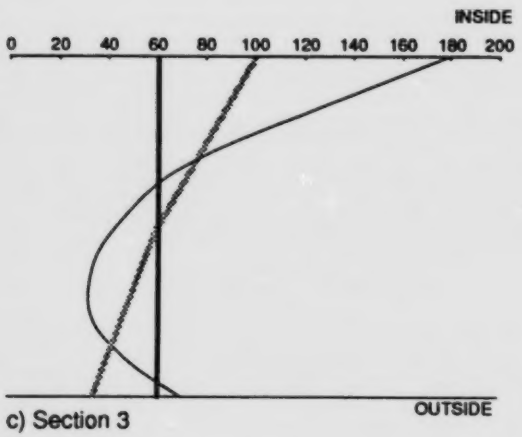

Results of Analysis
Membrane
Membrane plus Bending

Note:
Location of sections is shown in Figure 11

FIGURE 15
THROUGH THICKNESS STRESS INTENSITY DISTRIBUTION, TOP HEAD AREA

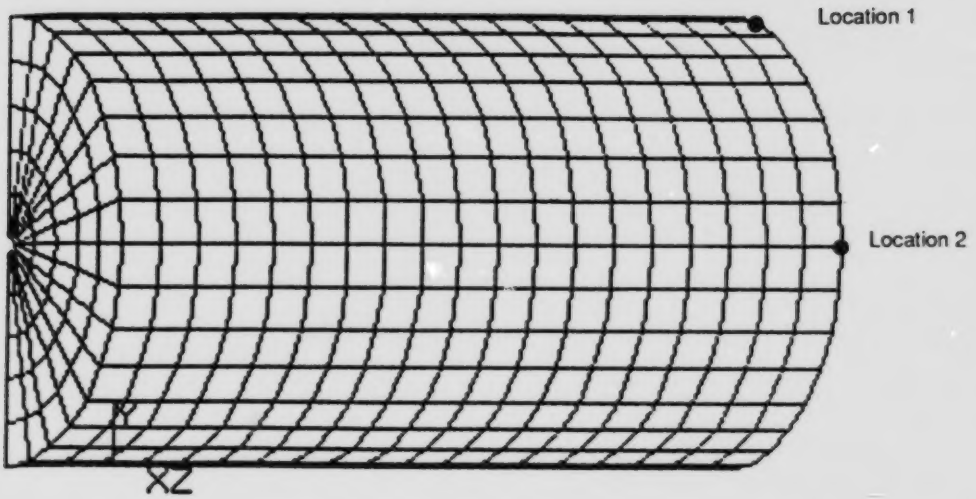

a) FINITE ELEMENT MODEL

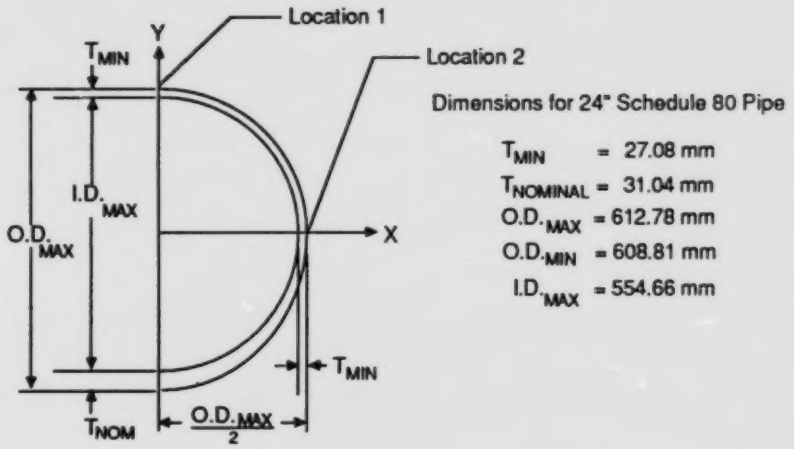

b) MODEL DIMENSIONS

FIGURE 16
GEOMETRY USED FOR BUCKLING MODEL

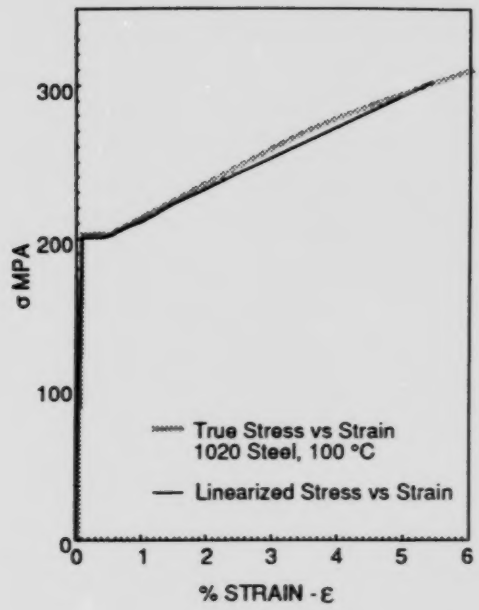

FIGURE 17
STRESS-STRAIN CURVE FOR NON-LINEAR ANALYSIS

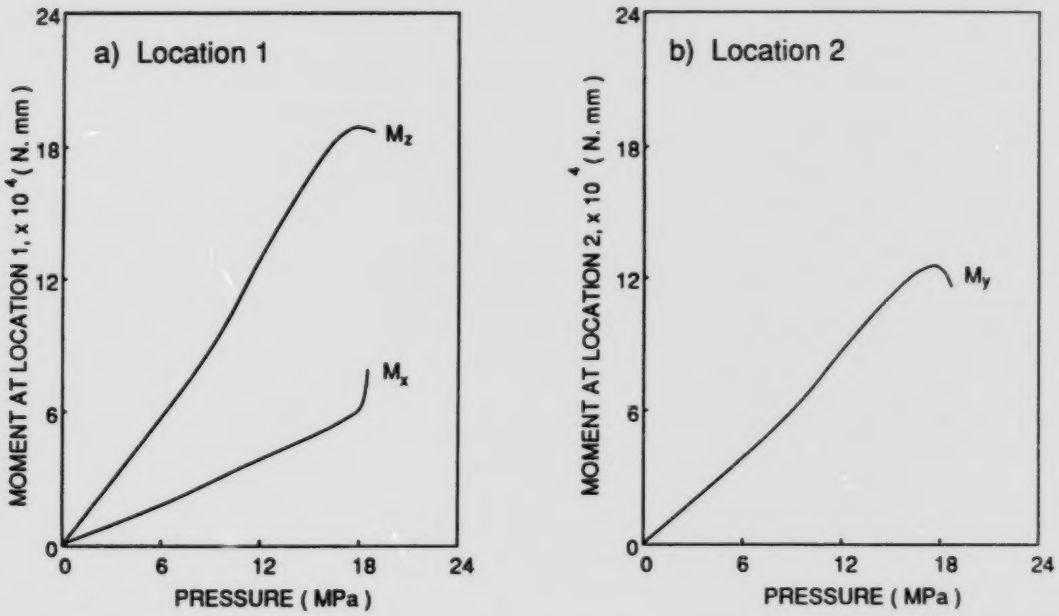
a) Location 1
MOMENT AT LOCATION 1, x 10 4 (N. mm)
M z
M x
0 6 12 18 24
PRESSURE (MPa)
b) Location 2
MOMENT AT LOCATION 2, x 10 4 (N. mm)
M y
0 6 12 18 24
PRESSURE (MPa)

Locations are defined in Figure 16

FIGURE 18
BENDING MOMENT IN BUCKLING MODEL

89-214-K
177579-G6-RD

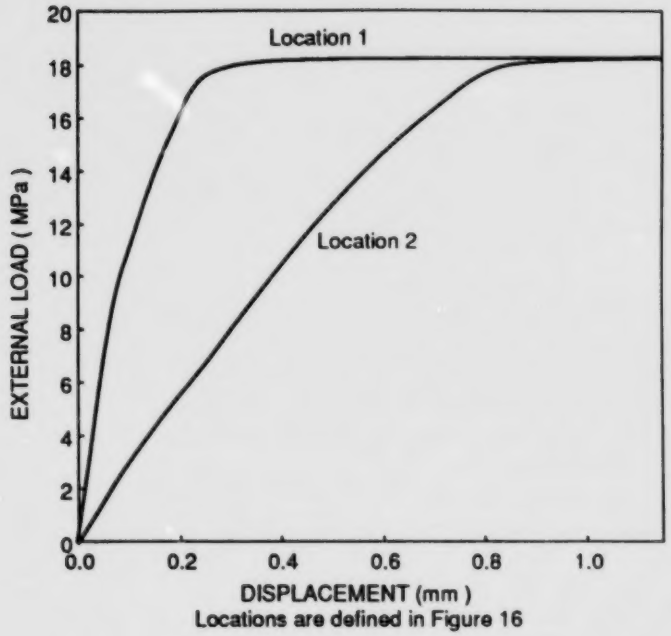

Locations are defined in Figure 16

FIGURE 19

DISPLACEMENT IN BUCKLING MODEL

Displacement amplified 100 times - max displacement is 0.3 mm

FIGURE 20

POST - BUCKLING SHAPE

89-214-K
177580-06-R0

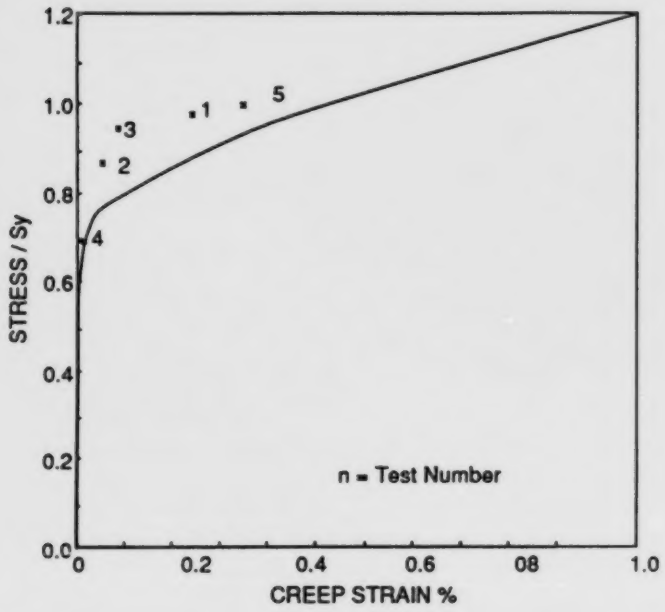

FIGURE 21
500- YEAR EXTRAPOLATED TEST RESULTS

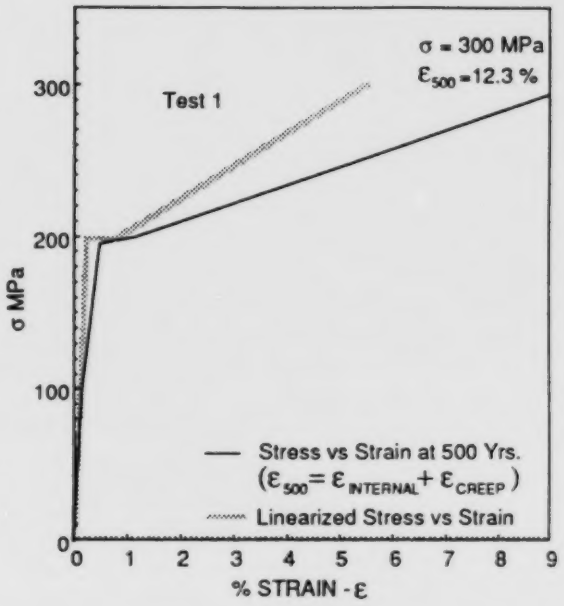

FIGURE 23
STEEL STRESS - STRAIN CURVE WITH CREEP

1020 Steel was used in Tests

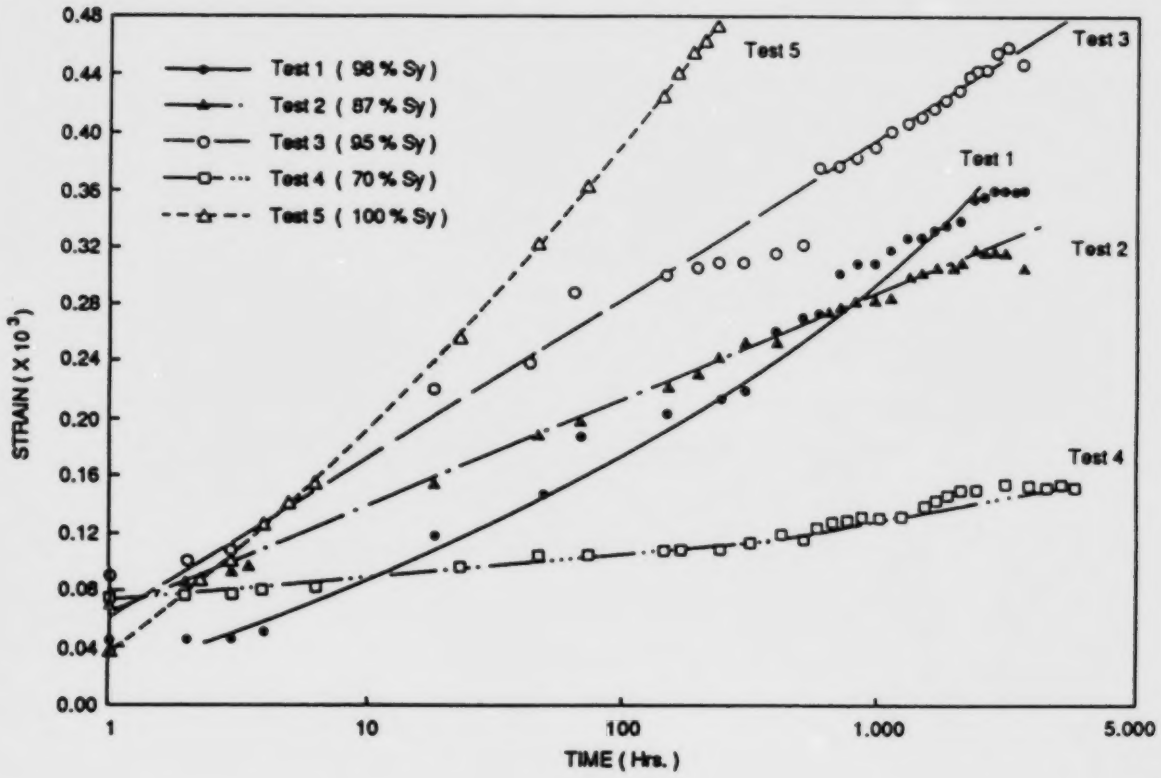

FIGURE 22
CREEP TEST RESULTS

89-214-K
180388-G4- RD

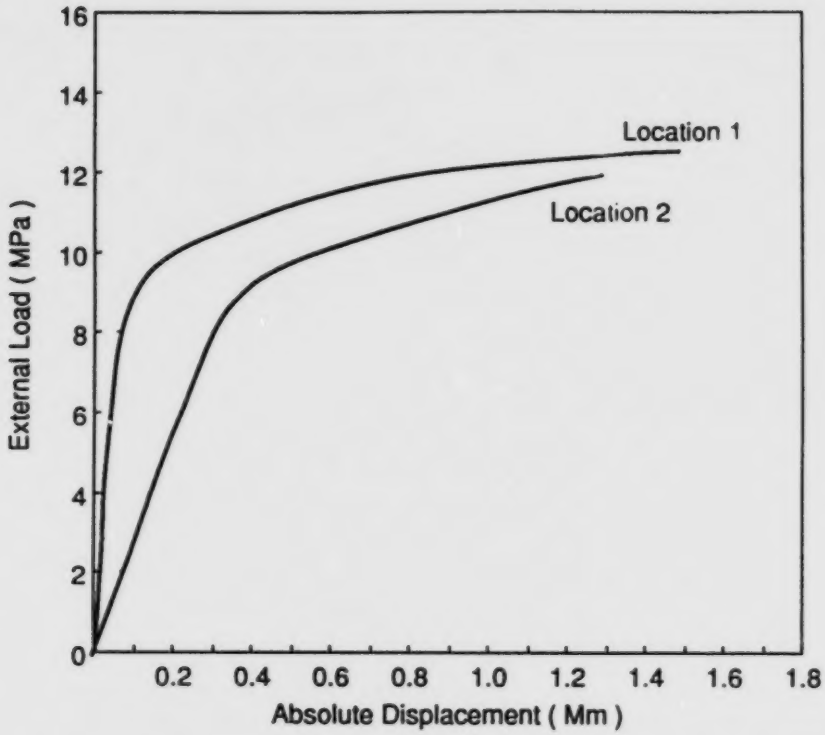

FIGURE 24

DISPLACEMENT IN BUCKLING MODEL WITH CREEP

89-214-K

177581-GG8-RD

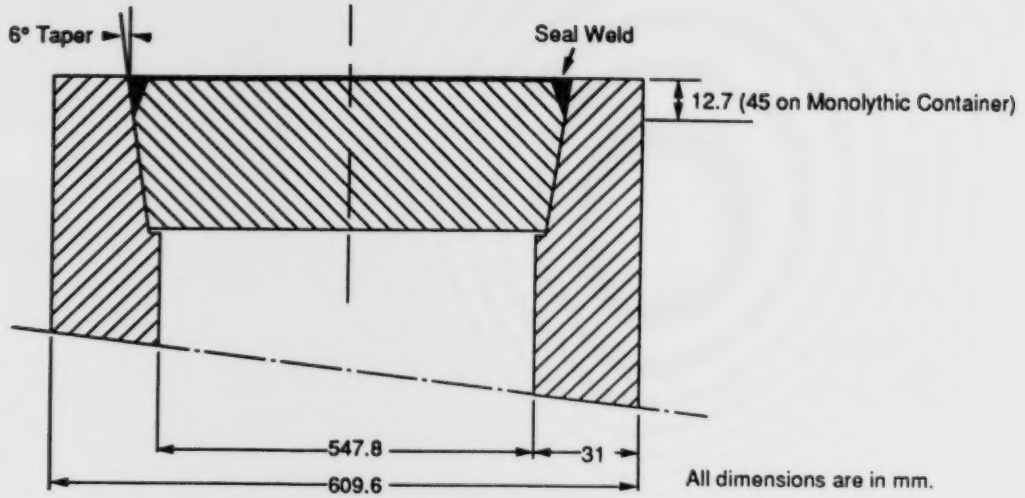

FIGURE 25
SEAL - WELDED CLOSURE

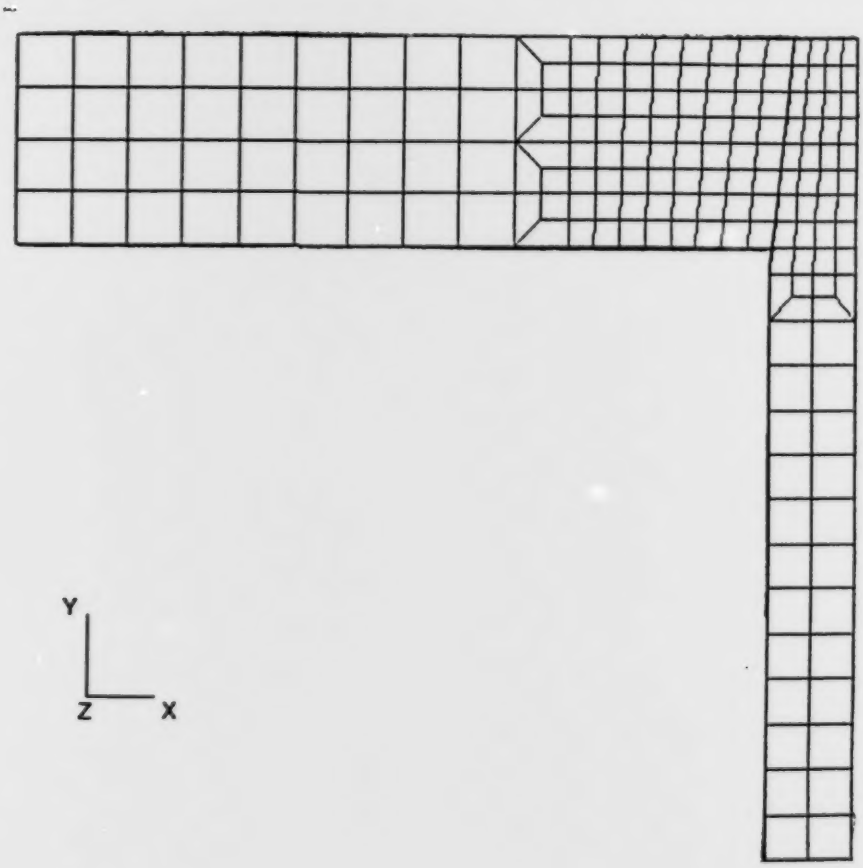

FIGURE 26
MODEL USED FOR TOP CLOSURE ANALYSIS

89-214-K
177520-006-RD

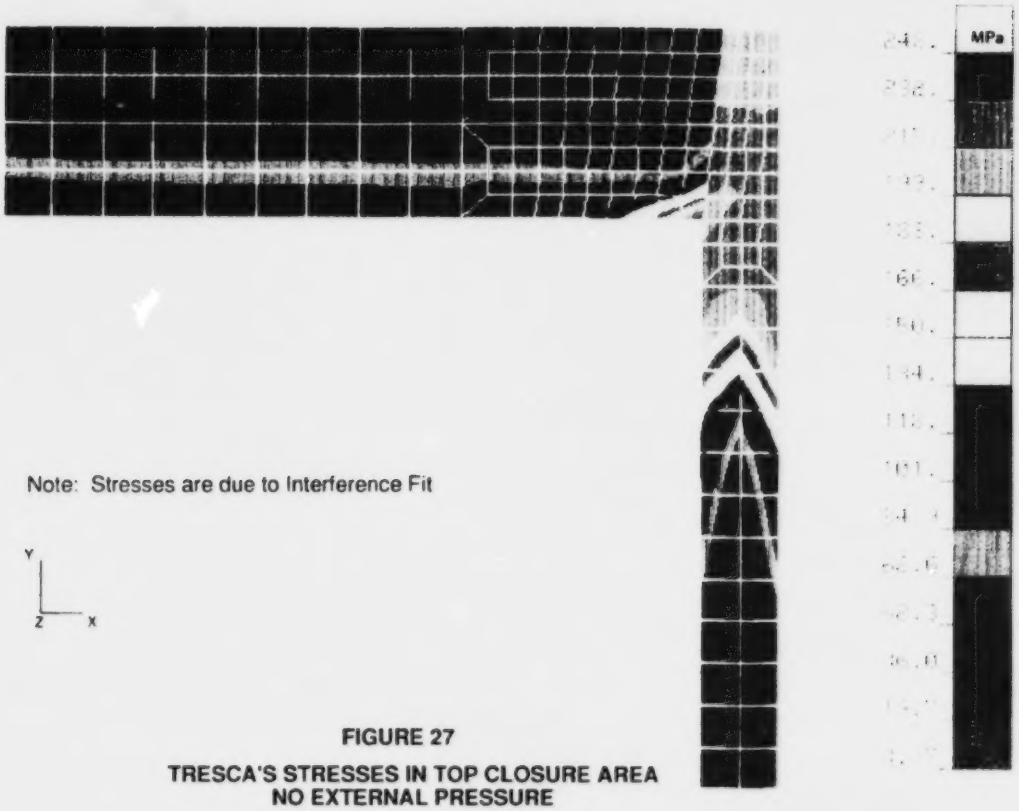

FIGURE 27

TRESCA'S STRESSES IN TOP CLOSURE AREA NO EXTERNAL PRESSURE

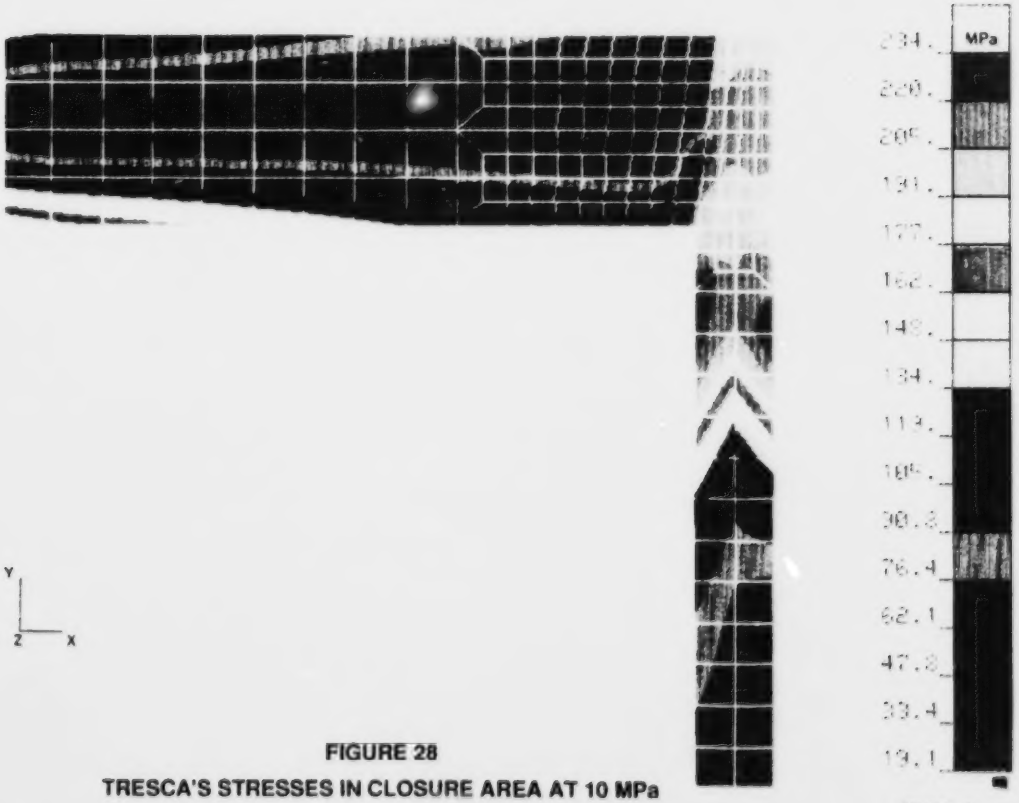

FIGURE 28

TRESCA'S STRESSES IN CLOSURE AREA AT 10 MPa

89-214-K

180388-RD

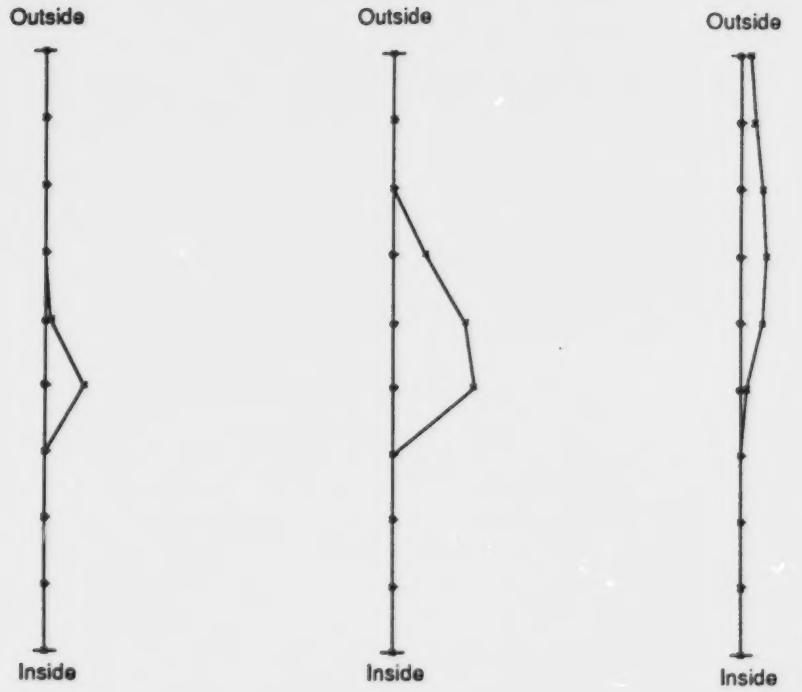

a) 0.7 mm INTERFERANCE
0 MPa PRESSURE

b) 0.7 mm INTERFERANCE
6 MPa PRESSURE

c) 0.7 mm INTERFERANCE
10 MPa PRESSURE

Notes:

1. Dot Indicates Nodal Deflection In The Lid
2. Cross Indicates Nodal Deflection In The Cylindrical Shell
3. Scales:

Horizontal Scale
= 1×10^{-3} mm in (a) and (b)
1×10^{-2} mm in (c)

Vertical Scale
= 9.5 mm

FIGURE 29
DIAGRAM OF LID - CLOSURE SEPARATION

89-214-K

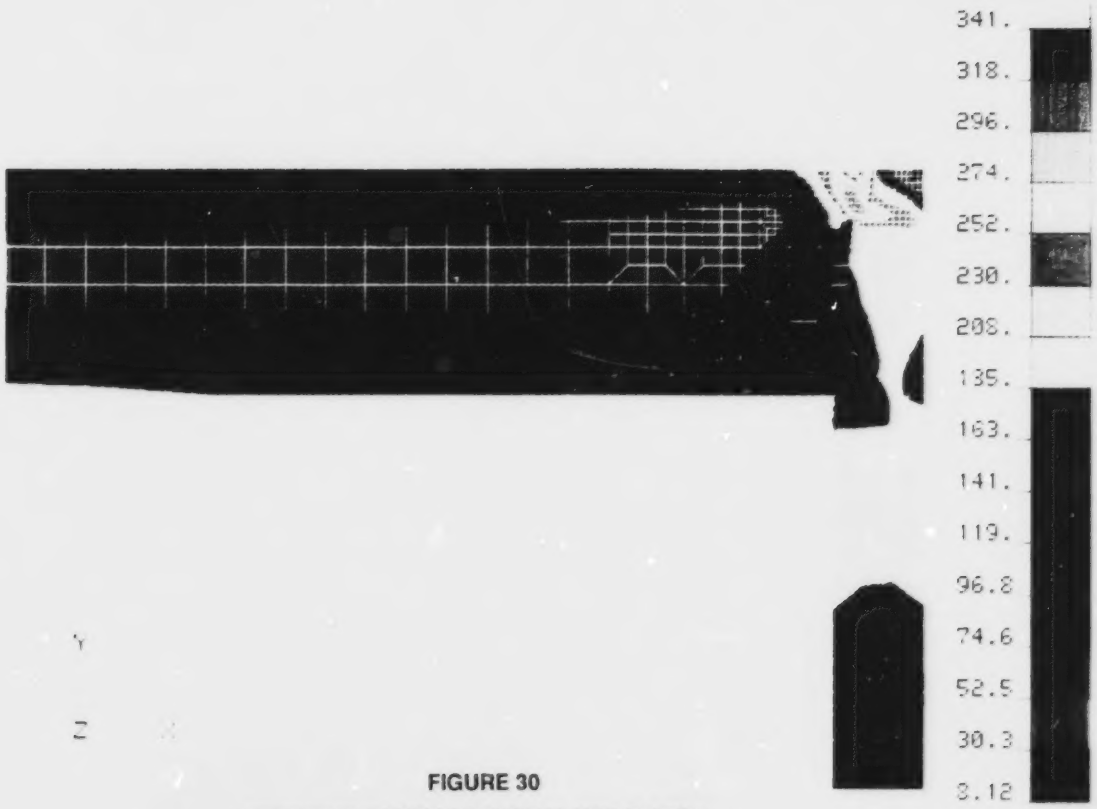

FIGURE 30

TRESCA'S STRESSES IN SEAL WELD AREA, NO PRESSURE

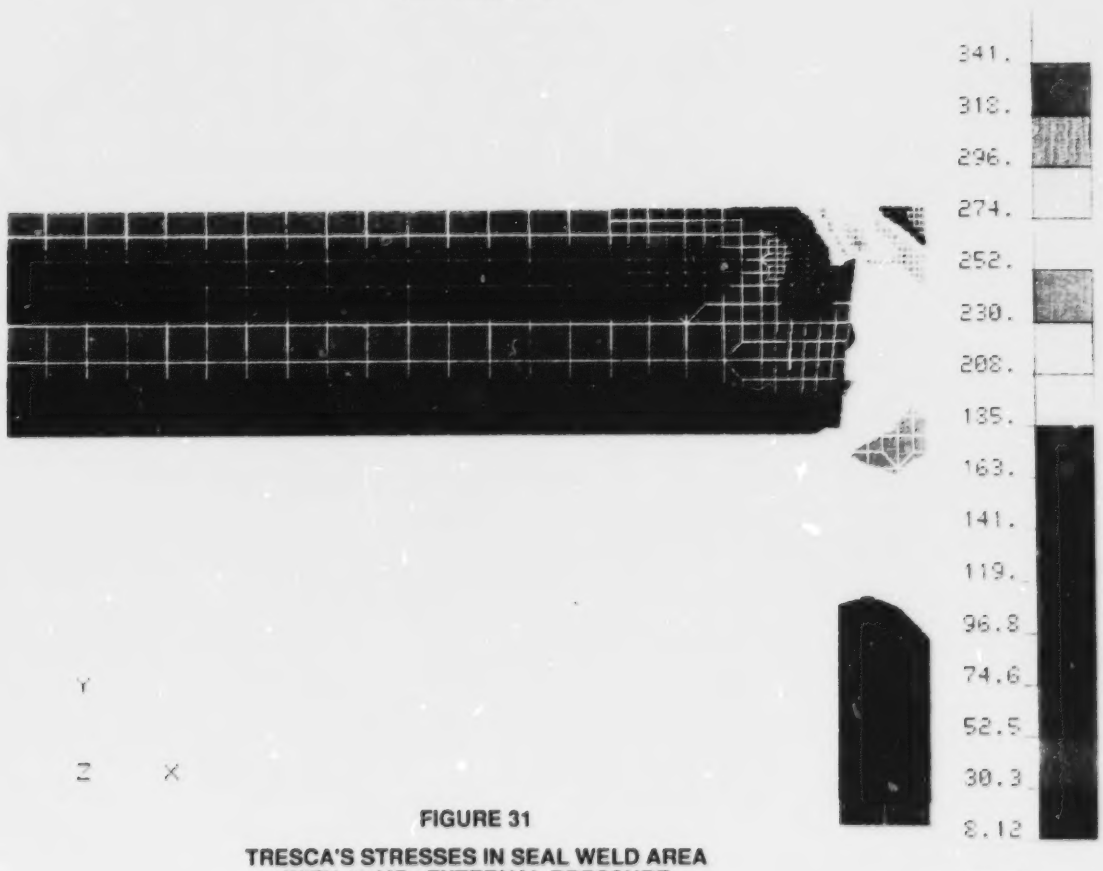

FIGURE 31

TRESCA'S STRESSES IN SEAL WELD AREA WITH 10 MPa EXTERNAL PRESSURE

89-214-K

180384 RD

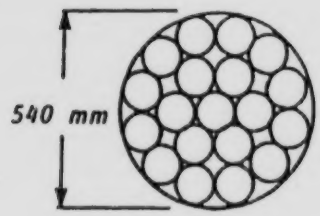

a) 72-Bundle Basket Arrangement

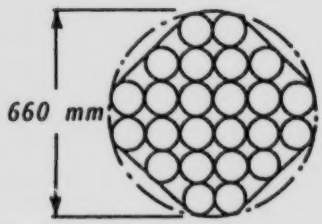

4-layer design

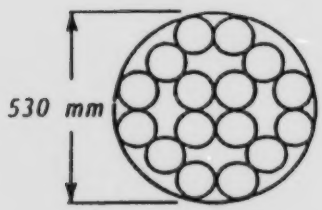

5-layer design

b) 96-Bundle Basket Arrangement

See Table III for Container Dimensions

FIGURE 32

ALTERNATIVE BASKET LAYOUTS

APPENDIX A

MANUFACTURING

Table of Contents

A.1 Introduction

A.2 Steel Cask

A.3 Titanium Shell

A.4 Steel Basket

A.5 Steel Ring

A.1 Introduction

The reference design of the container was presented in Section 2.0, and it is shown in Figure A-1. Manufacturing of the container was discussed with several prospective manufacturers to ensure viability and effectiveness of the proposed methods.

A.2 Steel Cask

The cylindrical shell of the steel cask will be made of a segment of a 24-inch, Schedule 80 pipe. The top area of the pipe will be machined to the dimensions in Figure 4 to allow for the self-locking closure and for seal-welding. The bottom area will be machined to prepare it for a full penetration weld. The pipe must meet all tolerances of Standard ASTM A530, including out-of-roundness. A groove 12.7 mm wide and 1.5 mm deep will be machined axially over the full length of the shell to accomodate a backing strip for the weld.

The bottom head will be machined from a 76-mm thick plate or forged to the dimensions in Figure 4c to allow for the full penetration weld and for overpacking with a titanium shell. A groove, 12.8 mm wide and 1.5 mm deep will be cut circumferentially and axially, as shown in Figure 4c. A full penetration weld will be made. The weld will be stress relieved, examined and qualified to the ASME Boiler and Pressure Vessel Code, Section III, for MC Components. The weld will be machined smooth and the axial groove will be remachined in the weld area.

The top lid will be machined out of a 76-mm thick plate or forged. The dimensions of the finished plate are shown in Figure 4a.

A.3 Titanium Shell

A titanium strip 12.5-mm wide and 1.4-mm thick will be inserted into the grooves of the prepared steel cask. The strips will be used as backing for welding of the titanium shell.

The cylindrical titanium shell will be made by rolling a 1910 mm by 2286 mm, 4.76-mm thick plate into a cylindrical shell (maintaining the 2286-mm edge straight during rolling). A lifting ring, 40-mm high and 4.76-mm thick, will be welded in place before rolling (see Figure A-2). After the shell is placed over the steel cask, it will be welded in place using standard plate fitting techniques, as shown in Figure A-3. The bottom head, formed to the dimensions in Figure A-4, will then be welded in place (see Figure A-3). The top titanium head will be formed to the dimensions in Figure A-5 and installed in the cylindrical shell in the hot cell after fuel is loaded into the container.

A.4 Basket

The basket will be made of nineteen tubes having 110-mm outside diameter and 3 mm thick walls. The tubes will be 1975 mm long. The center pipe is used for handling the basket and will not contain bundles. It will be made of 4-inch Schedule 40 pipe. The pipes will be fillet welded to the 1-inch bottom plate and spot welded to each other. The center pipe will have a 2 inch plate welded on top with a tapped hole for handling in the vertical position and for insertion into the steel cask.

The basket should be inserted and welded inside the steel cask at the manufacturing facility and delivered to the fuel loading facility fully assembled to avoid possible problems with interference between the two components. Alternatively, the basket can be first loaded with fuel then inserted into the cask. The following additional inspections are recommended to facilitate smooth assembly in the hot-cell:

- a basket and a steel cask could be pre-matched at a manufacturing facility to ensure their good fit, or
- the smallest inside diameter of the cask must be 543.0 mm, including any warping or axial distortions (reference inside diameter is 547.7 mm)
- the basket is largest outside diameter must be below 540.0 mm including warping and other axial distortions (reference outside diameter is 533 mm).

The detailed drawings discussed in this section are preliminary. They will be finalized after manufacturing techniques proposed here are re-evaluated.

The viability of the proposed manufacturing technique could be confirmed in a test program. Some of the features which should be tested are:

- operation of the lifting system (see Figure A-2)
- welding with titanium strip backing

A.5 Steel Ring

A steel spacer ring having geometry shown in Figure A-6 is required during container assembly. The ring is placed on top of steel cask before the top lid is inserted. This ring fills a gap between the steel and titanium lids and reduces stresses in the titanium shell under hydrostatic pressure.

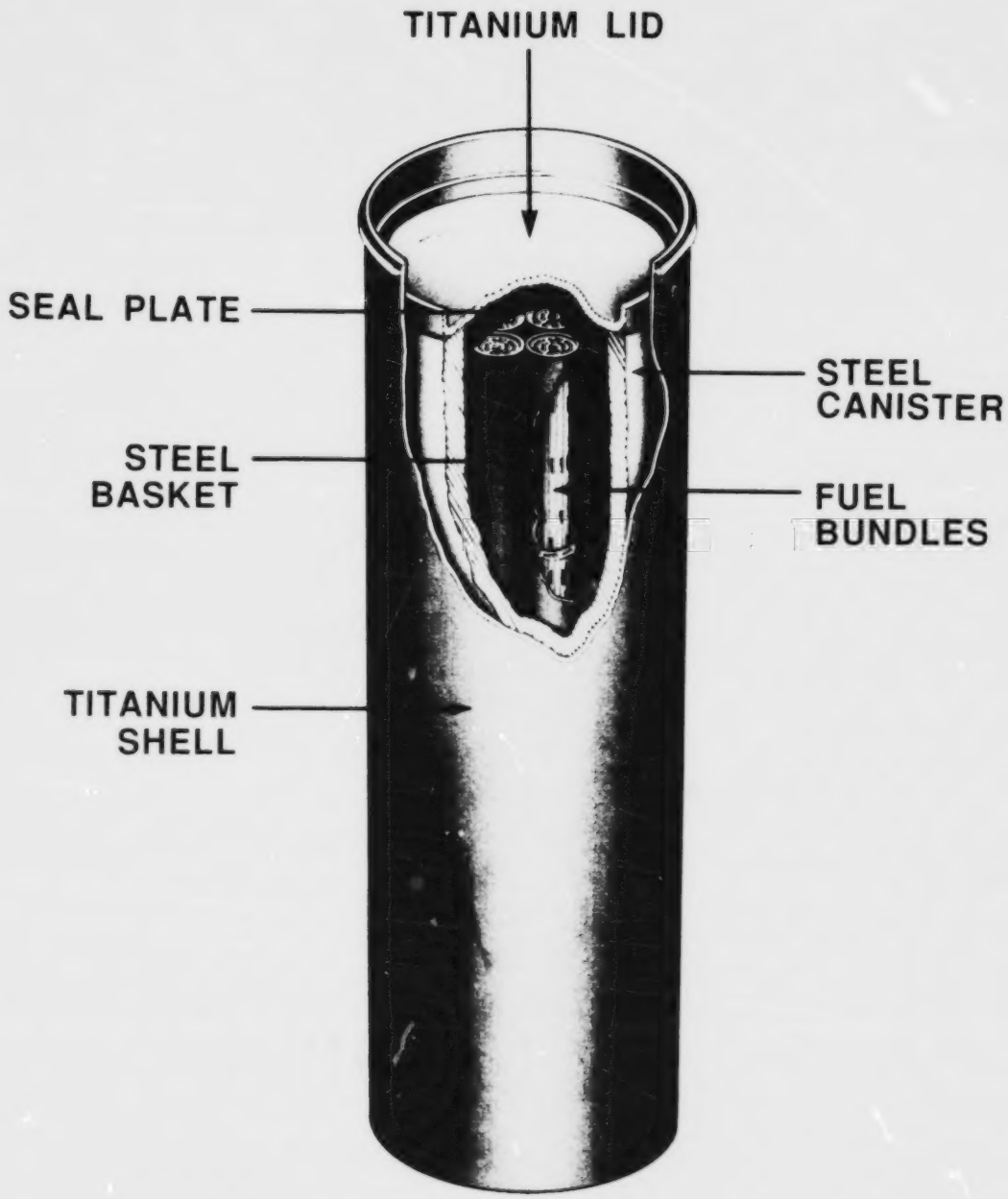

IRON-BASED STRESSED-SHELL CONTAINER

FIGURE A-1

89-214-K

177625 RD
GG7

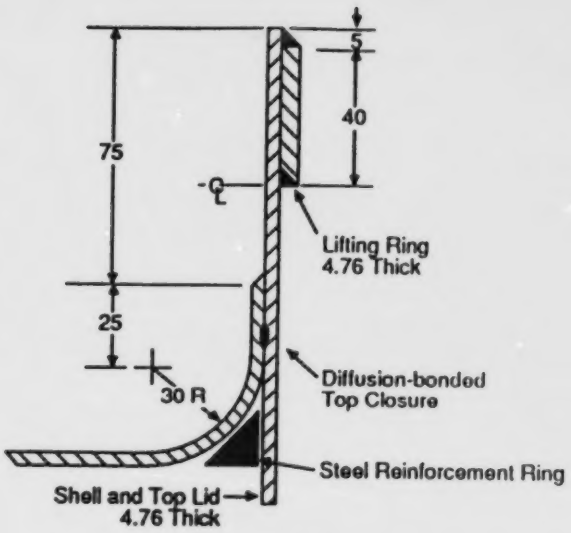

FIGURE A-2
LIFTING ARRANGEMENT

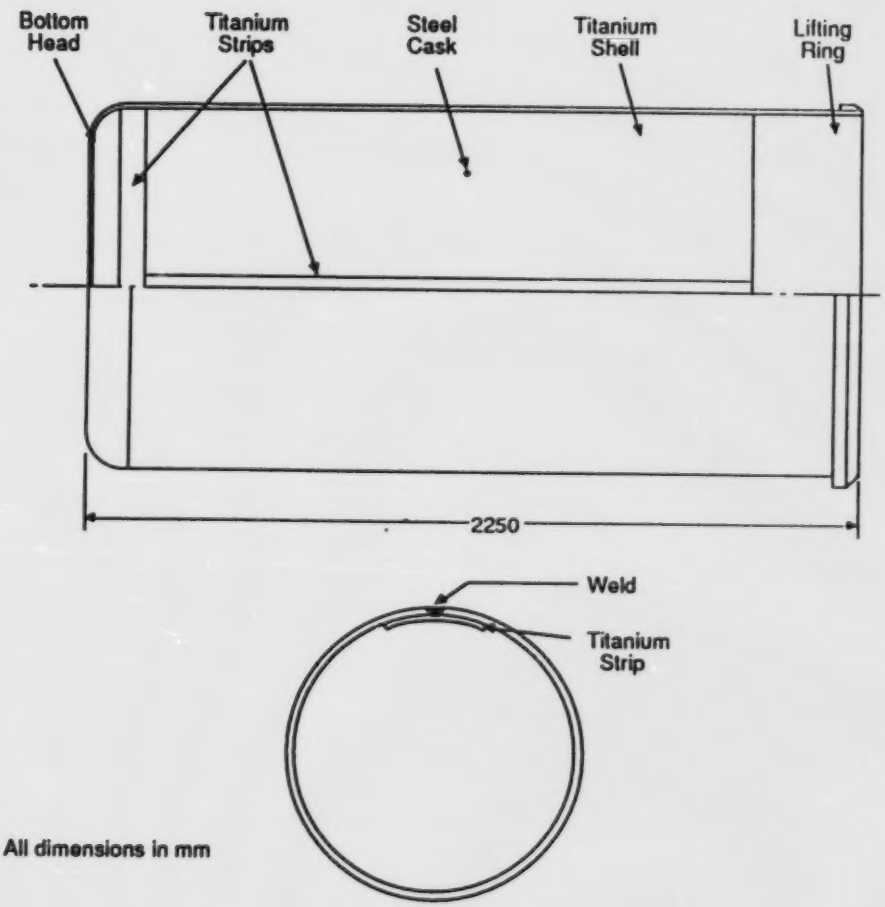

NOTE: All dimensions in mm

FIGURE A-3
ASSEMBLY OF TITANIUM SHELL

177622 RD
007
89-214-K

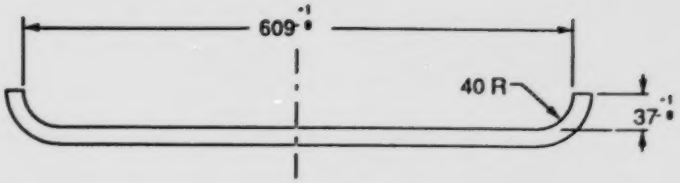

FIGURE A-4
BOTTOM

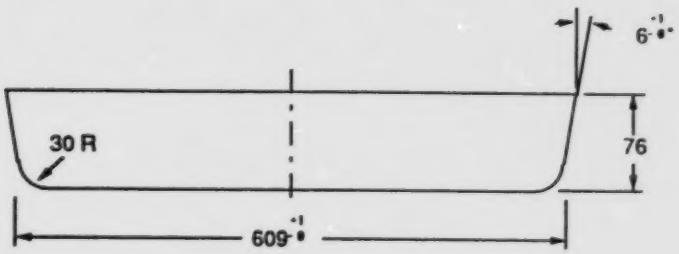

FIGURE A-5
TOP HEAD

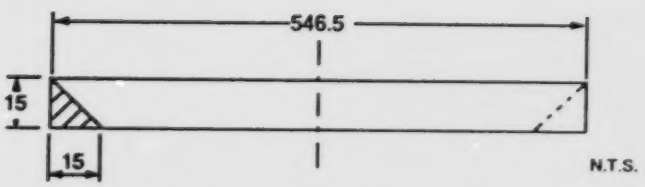

NOTE: All dimmensions in mm

FIGURE A-6
STEEL RING

89-214-K
177627-G7-RD

APPENDIX B

ALLOWABLE STRESSES

Table of Contents

B.1 Applicable Standards

B.2 Stress Limits

B.3 Buckling Consideration

B.4 Creep Consideration

B.5 Strain Limits

B.1 Applicable Standards

There are no codes or standards directly applicable to nuclear waste disposal containers that provide full guidelines for stress limits. Several countries (including U.S.) are now in the process of preparing such guidelines. A set of guidelines is proposed here for comparison with the calculated stresses, loads or deformations. The comparison is used to show the adequacy of the container for the proposed loading conditions. The proposed criteria are based on existing codes or on the anticipated level of conservatism.

B.2 Stress Limits

The steel shell of the container is a pressure-retaining boundary. As such, we propose to use the ASME Boiler and Pressure Vessel Code criteria for stress limits. Since the container is used for handling of nuclear materials, Section III, Subsection NE (for MC components) will be used. The description of stress limits provided in the Code is detailed and lengthy. Only a brief and highly simplified summary of the limits are presented here.

The Code divides stresses in a cross-section into three components shown in Figure B-1: an average through section stress Pm, bending stress component Pb, and peak stress Pa. The Code does not provide limits for principal stresses (except for areas of local stress concentration). The stress limits are imposed on the largest difference between principal stresses (Tresca's stress). An averaged through-thickness stress away from any discontinuity is limited to 66.7% yield or 0.33% of ultimate strength (stress intensity Sm). At a discontinuity, local membrane stress P_L is limited to yield (1.5 Sm). The averaged plus bending stress components is also limited to yield (1.5 Sm) near or at a discontinuity. The peak stress component is only limited by fatigue (number of loading cycles). Fatigue need not be considered for the intended operation.

B.3 Buckling Consideration

The Code allows plastic analysis of local instabilities. This provision is used to show the adequacy of the titanium shell and cylindrical shell of the steel cask.

The titanium shell cannot support an external load and would deform under the external pressure until it is fully supported by the steel cask. The steel cask is considered to fail if large strains cause it to breach or the cask buckles. Compressive stresses are assumed not to cause failure. The steel or titanium shell will not breach if the sum of two mutually orthogonal local tensile strains is below 5.3%.

The cask is considered not to buckle if conditions listed in paragraph Appendix II-1430 of Section III of the Code are met. It describes how to construct the graph in Figure B-2. The actual load-deformation curve is obtained from the non-linear finite element analysis. Angle θ is measured from the graph. Angle ϕ is calculated as $\phi = \tan^{-1}(2 \tan \theta)$. The critical load is read on the vertical axis corresponding to the point of intersection (A). This critical load is multiplied by 0.67. The product must be higher that the specified external load for a Code acceptable design. The IBSS container is designed to support 10 MPa external pressure. We must show that buckling will not occur at pressures below 15 MPa.

B.4 Creep Consideration

The Code is designed for components with a life that would not normally exceed 30 years. The Code does not require creep analysis for low temperature applications. Because of the required 500-year container life, an additional condition including the effect of creep is specified: the steel shell design is considered acceptable if in its worst possible configuration, it will not buckle below the postulated external pressure after the effect of the 500-year creep is considered in material properties (see Subsection 7.2).

This is conservative because:

- the worst possible geometrical configuration is assumed.
- relaxation of the highest stressed areas due to creep is not considered in the analysis - the conservatism of this assumption is currently under consideration.

B.5 Strain Limits

Large deformations and strains (beyond yield) are calculated in the finite element analyses of the titanium shell. The large deformations in the titanium shell are necessary to transfer the external pressure through the shell onto the steel cask. Such deformations are considered acceptable provided that the shell does not stretch until it tears. Plastic deformations are better characterized by strain than stress because small changes in stress result in large strain variations. Furthermore, it can be shown (assuming constant volume of material) that:

$$\varepsilon_x + \varepsilon_y + \varepsilon_z = 0$$

To gain a better understanding of what constitutes an acceptable strains in the titanium shell, a small square region of a shell (flat plate shown in Figure B-3) was analyzed using the finite element model in Figure B-4. For large deformations, the true stress-strain curve must be used. The engineering curve (in Figure B-5) is recalculated into the true curve using relationships:

$$\text{True strain} \quad \varepsilon = \ln(1 + \varepsilon')$$
$$\text{True stress} \quad \sigma = (1 + \varepsilon')\,\sigma'$$

where (') designates engineering values of stress and strain. Figure B-5 shows the true stress-strain curve. The finite element analysis shows that both compressive strains reach about 8% as stress approaches ultimate. Reduction of the shell thickness also approaches 8% (see Figure B-6).

The same finite element model was used to evaluate the effect of uniform biaxial tension. The through-thickness strain increased faster here than in uniaxial case and reached 8% at about 90% ultimate strength (see Figure B-7). Thickness of the plate reduced by the same amount of 8% at 90% ultimate strength. Both in-plane strain components were equal and reached 4%, or $\varepsilon_x + \varepsilon_z = 8\%$. Strains increased too rapidly above 90% ultimate strength to be considered acceptable. Based on the above analysis of a flat plate, titanium shell is not expected to fail by tearing until its thickness is reduced by over 8%. This thickness reduction occurs when in-plane tensile strains total 8%.

$$-\varepsilon_y = \varepsilon_x + \varepsilon_z < 8\% \qquad \text{(failure condition)}$$

Strains will be considered acceptable if $\varepsilon_x + \varepsilon_z <$ (2/3) of 8%, or 5.3%.

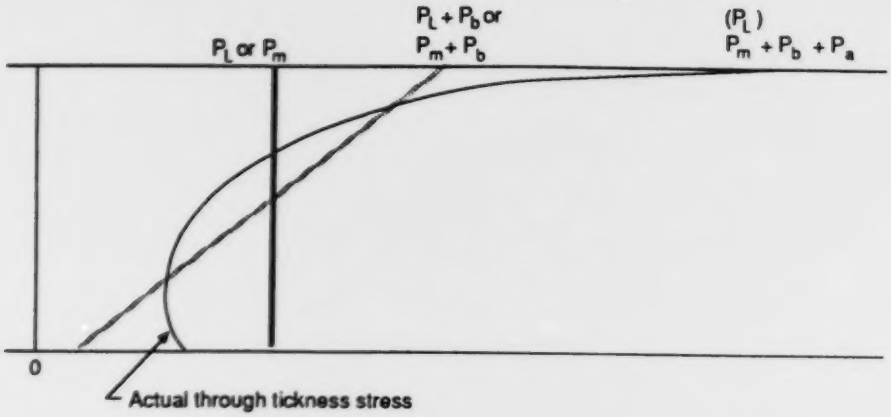

FIGURE B-1
TYPICAL ARBITRARY THROUGH - SECTION STRESS DISTRIBUTION

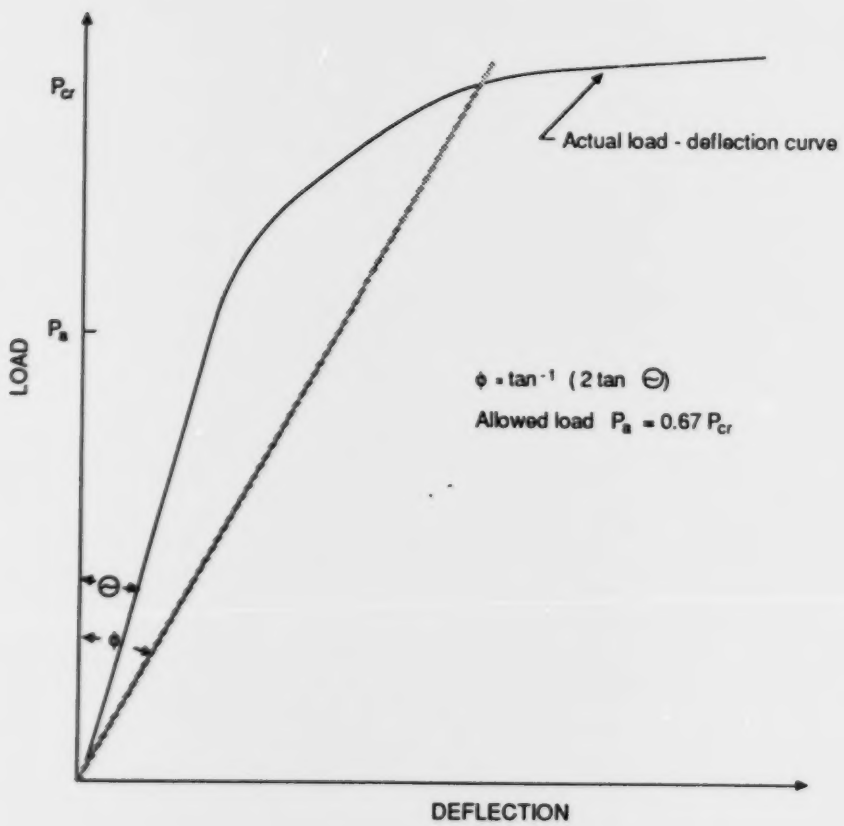

FIGURE B-2
EVALUATION OF CRITICAL LOAD

89-214-K
177633 RD
GG 7

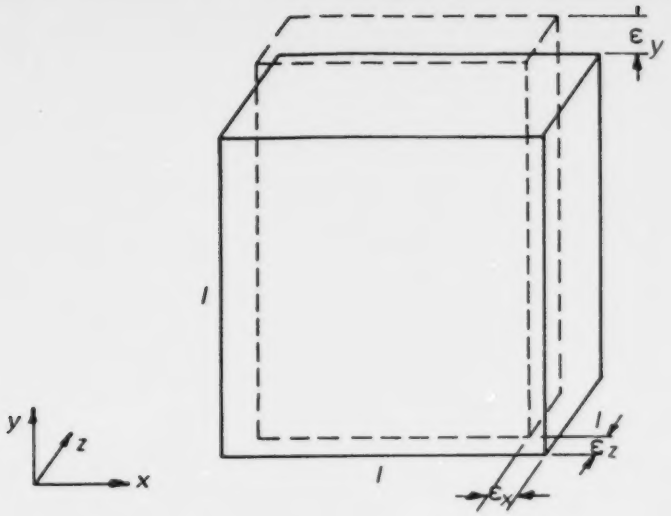

FIGURE B-3
DEFORMATION OF A CUBE

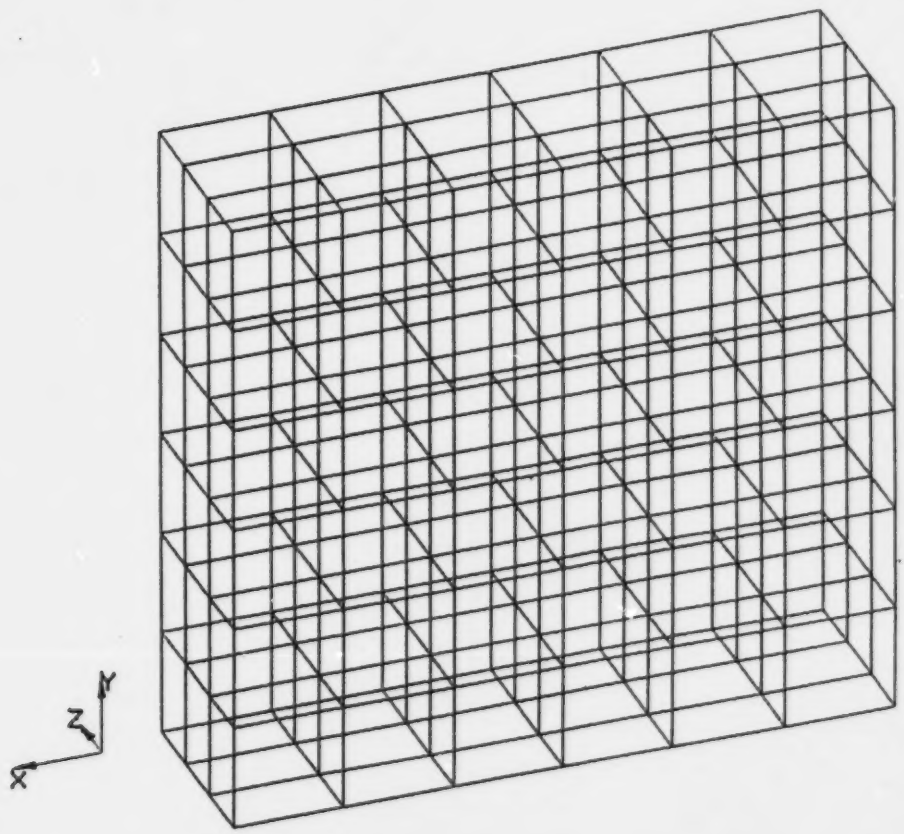

FIGURE B-4
FINITE ELEMENT MODEL OF SHELL

89-214-K
177695 RD
GG7

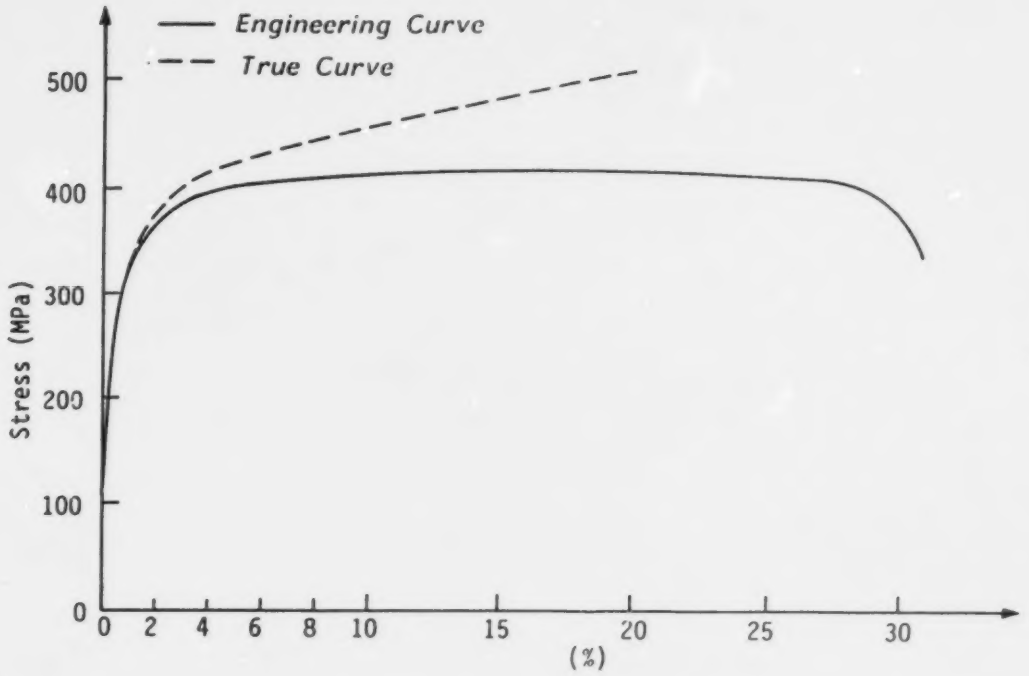

FIGURE B-5
ENGINEERING AND TRUE STRESS - STRAIN CURVES

89-214-K
177696 RD
GG7

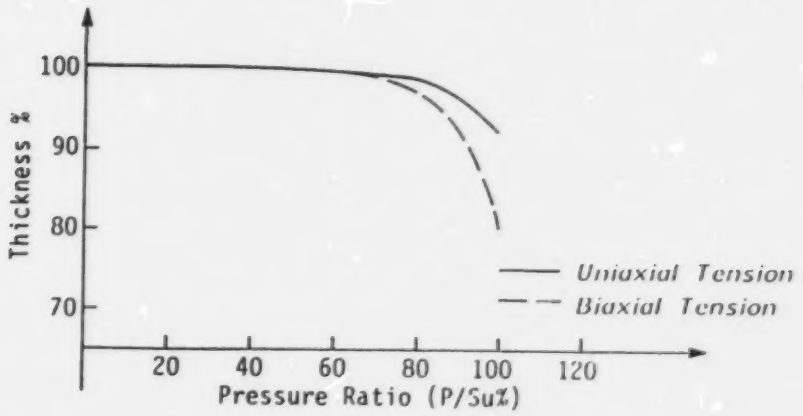

FIGURE B-6
STRAINS AT PLATE CENTER

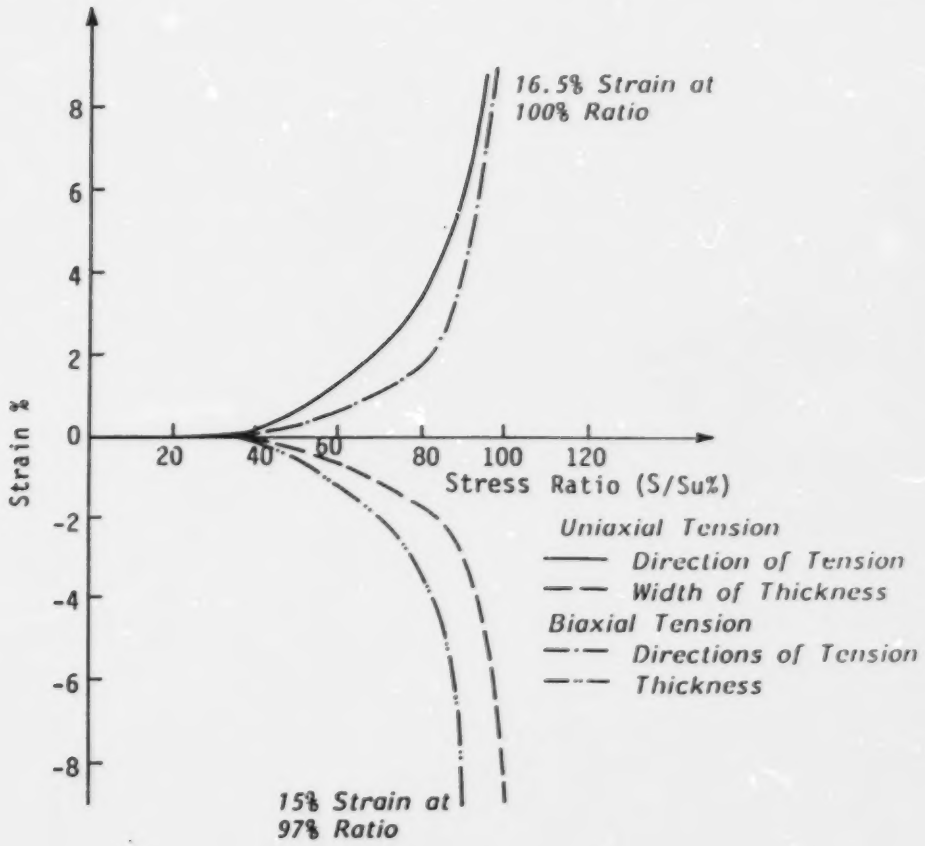

FIGURE B-7

PLATE THICKNESS REDUCTION DUE TO
TENSION IN PLATE

89-214-K
177692 RD
QG 7

APPENDIX C

STRESSES IN SHELL

Table of Contents

C.1 Description of Finite Element Models

C.2 Model Assumptions

C.3 Results - Stress Distribution

C.1 Description of Finite Element Models

Overall stress distribution and corresponding deflections in the container were analyzed with two general models. Regions and conditions of special concern were analysed separately in greater detail and are discussed in subsequent appendices.

The IBSS container can be described in cylindrical co-ordinates with the geometry, material properties, external loads and boundary conditions independent of theta, see Figure C-1. Two models, one of the top head and wall, and a second of the bottom head geometry and wall were developed using approximately 400 linear elastic axisymmetric elements. The element mesh was refined (approximately 5 mm x 5 mm) in the region adjacent to the wall/head junction. All models were analysed using ABAQUS version 4.5. Pre- and post- processing was performed using PATRAN. The models are axisymmetric about Y (the vertical axis) and symmetric in the X - O plane. The axis and plane of symmetry are defined in Figure C-1.

C.2 Model Assumptions

The following assumptions were made in the idealization of the top and bottom head models:

1. Heads and cylinder walls are axisymmetric about the Y axis.

2. Material properties are linear elastic.

3. Wall thickness is uniform and equal to the nominal thickness of Schedule 80 pipe.

4. External surface pressure is uniform and equal to 10 MPa.

5. The stress distribution in a head to shell junction does not effect the other junction.

C.3 Results - Stress Distribution

Deflections of the top and bottom heads are shown in Figures C-2(a) and C-2(b). The top head has been depressed inwards 0.32 mm while the bottom head moved inwards 0.47 mm. The deflection of the heads falls between the extreme cases of a fully constrained flat disk (lower bound deflection) and a simply-supported disk (upper bound deflection). The top head behaves as if 61% constrained (39% simply supported) while the bottom head with the 40 mm radius behaves as if 54% constrained and 46% simply supported. In both models, the cylinder wall has moved inwards by approximately 0.12 mm and reaches this uniform deflection approximately 300 mm away from the heads. This distance is 1/8 the total height of the container. Nodal average values were used to indicate peak Tresca's stresses. Figure C-3 shows nodal Tresca's stresses in the model of the top head while nodal Tresca's stresses for the bottom head are shown in Figure C-4. The highest values (up to 223 MPa) occur on the inside of the cylindrical wall adjacent to both heads.

To meet the acceptability standard defined in Appendix B, average Tresca's stress through a section must be less than 67% yield in section 5 (see Figure C-5) and 100% yield in remaining sections. Nodal Tresca's stresses through the container at five sections (shown in Figure C-5) have been plotted in Figures C-6 and C-7. The sections are:

Section 1: through the center of the head
Section 2: through the head at the wall
Section 3: through the wall at the head
Section 4: through the wall adjacent to the head (11.4 mm away)
Section 5: through the wall at the mid-height of the container.

A summary of Tresca's stresses through the five sections of the model with the top head geometry appears in Table B.1. Table B.2 summarizes the same information for the model with the geometry of the bottom head. The stresses are within the Code allowable values. The local peak stress at the bottom head to shell junction exceeds yield. This is acceptable because the sum of bending stress P_b and average local P_L stress is below yield.

TABLE C.1

SUMMARY OF TRESCA'S STRESSES IN TOP HEAD AREA

Section #	Tresca's Stresses				Shown in Figure
	Range		Avg. Value		
	MPa	(% Yield)	MPa	(% Yield)	
1	23 - 109	(12 - 55 %)	65	(33 %)	Figure C-6 (a)
2	19 - 157	(10 - 79 %)	104	(52 %)	Figure C-6 (b)
3	35 - 157	(18 - 79 %)	81	(40 %)	Figure C-6 (c)
4	39 - 180	(20 - 70 %)	90	(44 %)	Figure C-6 (d)
5	88 - 98	(40 - 49 %)	93	(47 %)	Figure C-6 (e)

TABLE C.2

SUMMARY OF TRESCA'S STRESSES IN BOTTOM HEAD AREA

Section #	Tresca's Stresses				Shown in Figure
	Range		Avg. Value		
	MPa	(% Yield)	MPa	(% Yield)	
1	20 - 127	(10 - 63 %)	71	(35 %)	Figure C-7 (a)
2	22 - 185	(11 - 92 %)	65	(32 %)	Figure C-7 (b)
3	42 - 185	(21 - 92 %)	93	(46 %)	Figure C-7 (c)
4	45 - 223	(22 - 110 %)	106	(53 %)	Figure C-7 (d)
5	88 - 98	(44 - 48 %)	93	(46 %)	Figure C-7 (e)

89-214-K
177647 RD
GG7

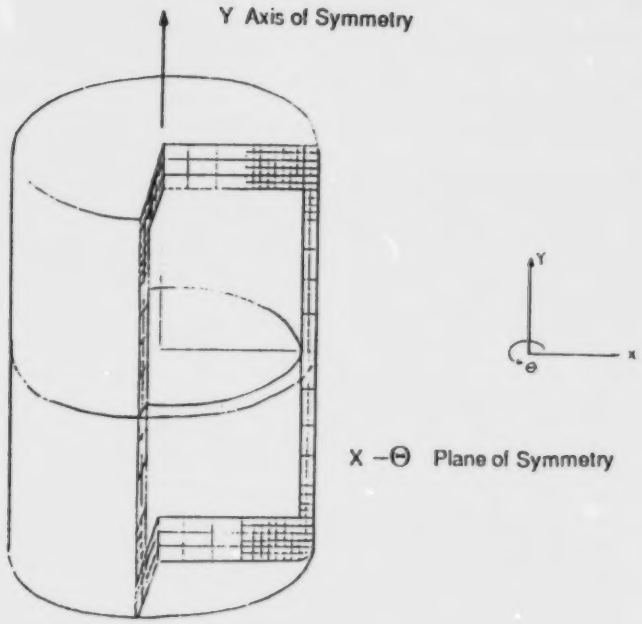

FIGURE C-1
AXIS AND PLANE OF SYMMETRY IN FINITE ELEMENT MODELS

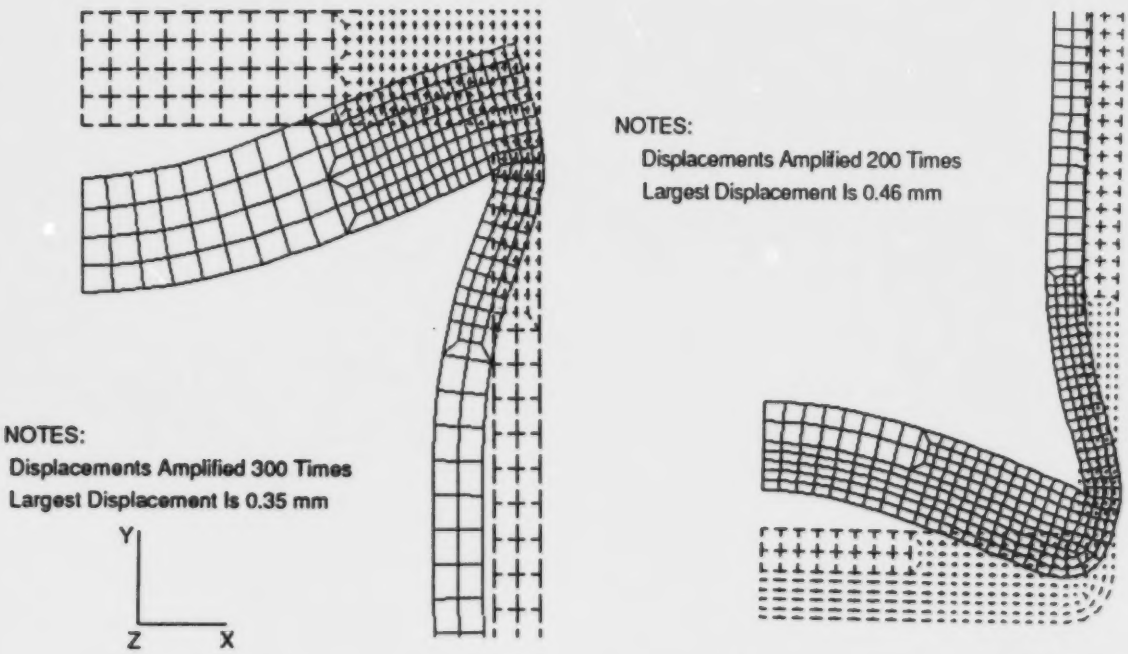

a) Displacements in Top Head b) Displacements in Bottom Head

FIGURE C-2
DEFORMATIONS IN THE IBSS CONTAINER AT 10 MPa PRESSURE

89-214-K
127647 RD
GG-7

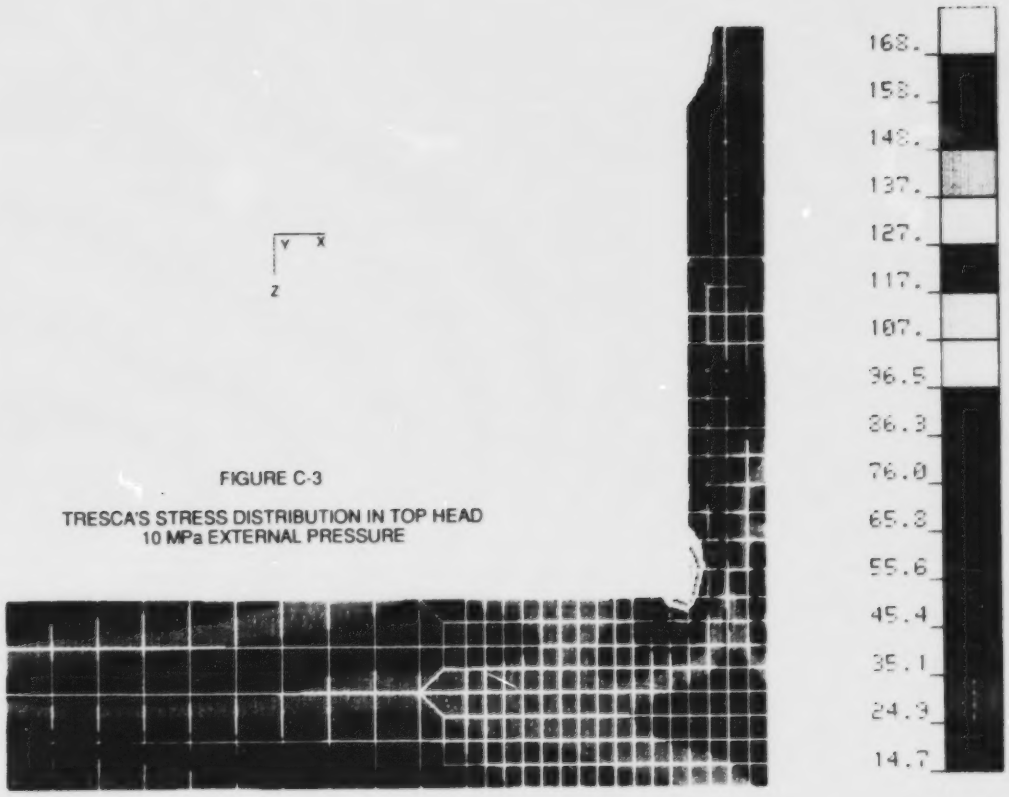

FIGURE C-3

TRESCA'S STRESS DISTRIBUTION IN TOP HEAD
10 MPa EXTERNAL PRESSURE

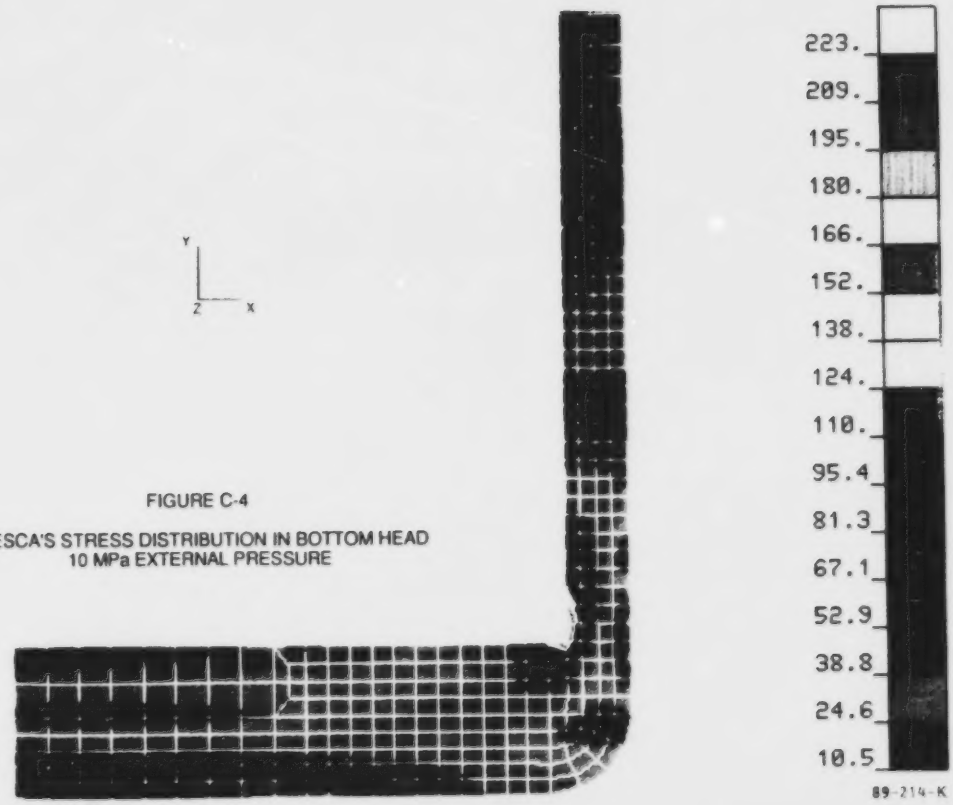

FIGURE C-4

TRESCA'S STRESS DISTRIBUTION IN BOTTOM HEAD
10 MPa EXTERNAL PRESSURE

89-214-K

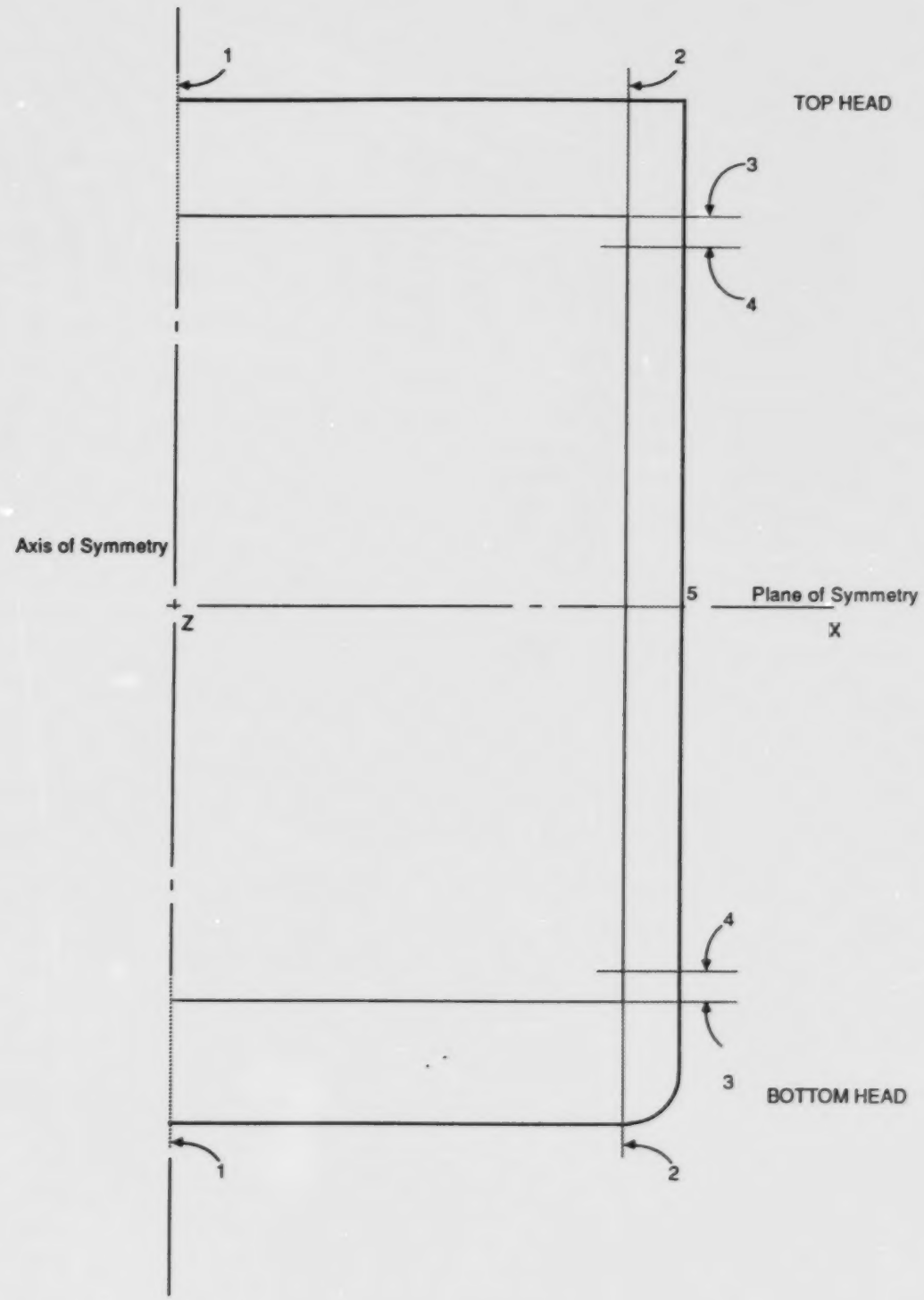

FIGURE C-5
LOCATION OF PLOTTED SECTIONS

89-214-K
177649 RD
0G7

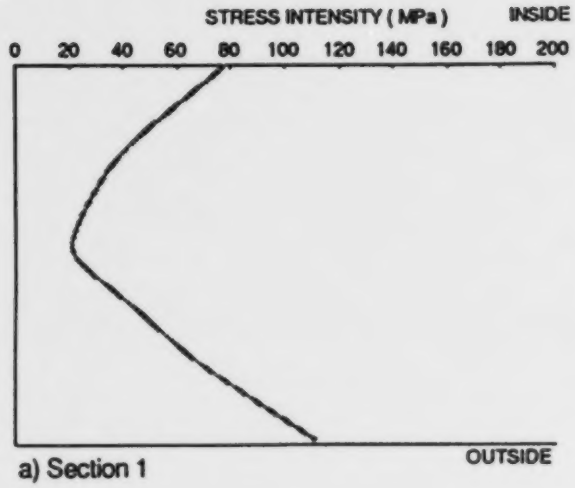

a) Section 1

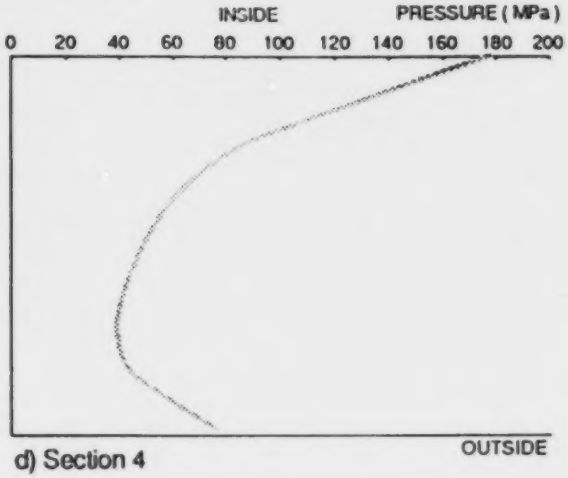

d) Section 4

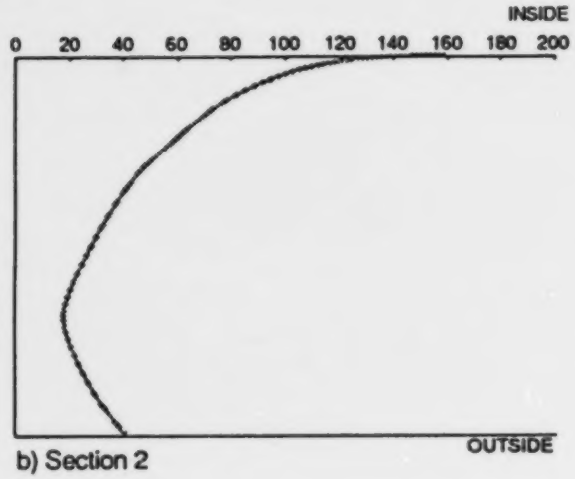

b) Section 2

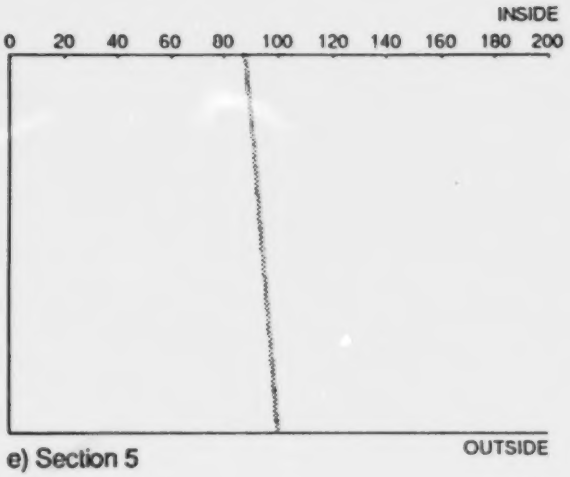

e) Section 5

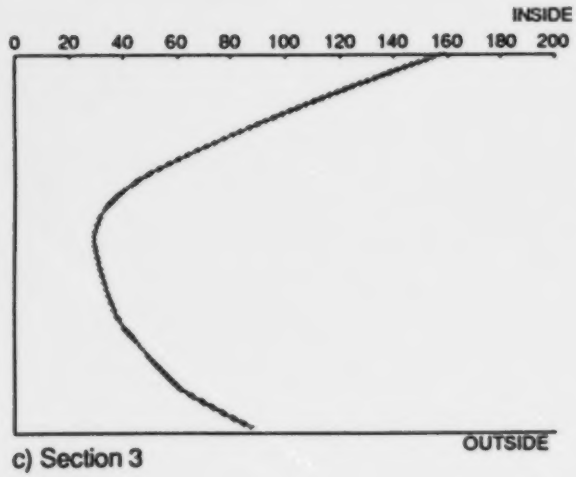

c) Section 3

FIGURE C-6
TRESCA'S STRESS DISTRIBUTION THROUGH TOP HEAD SECTIONS

89-214-K
177648 RD
00 7

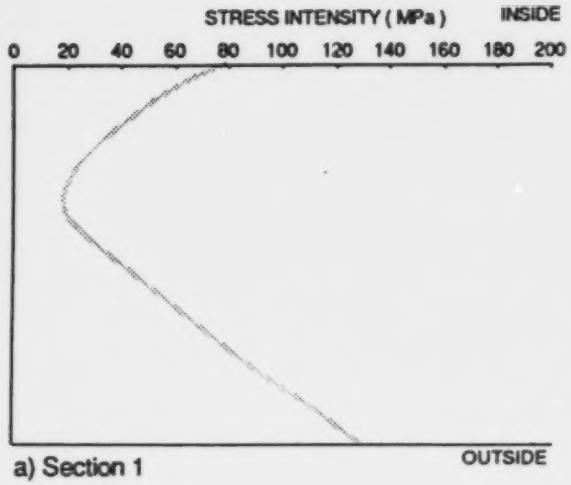

a) Section 1

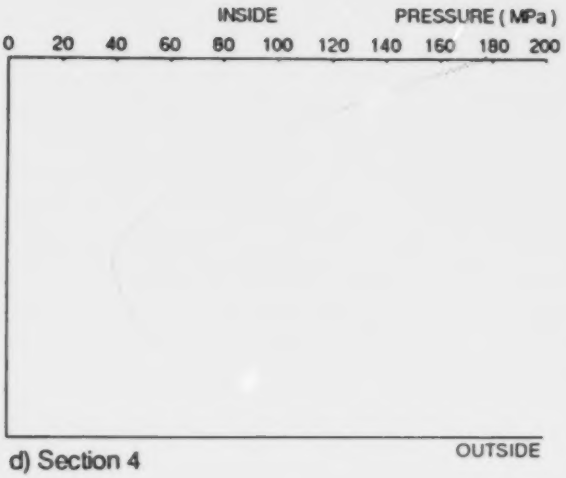

d) Section 4

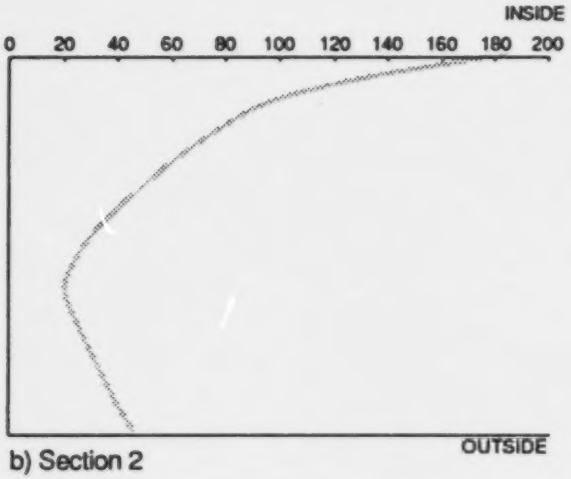

b) Section 2

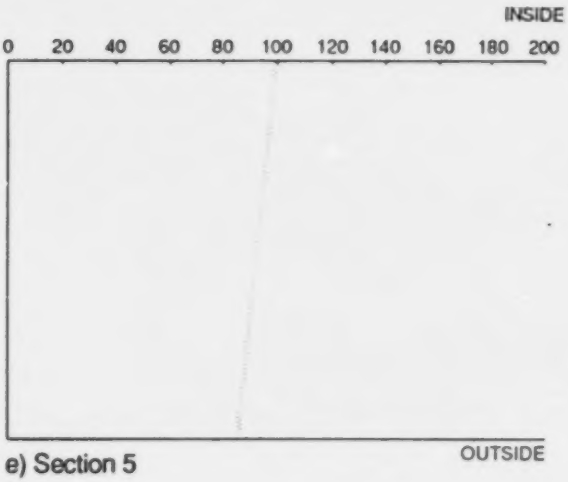

e) Section 5

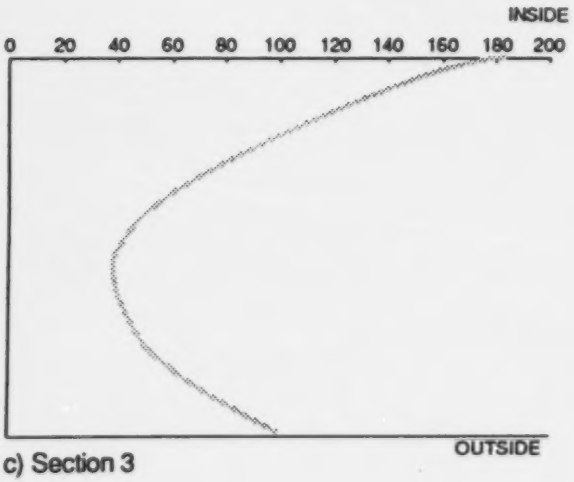

c) Section 3

FIGURE C-7

TRESCA'S STRESS DISTRIBUTION THROUGH BOTTOM HEAD SECTIONS

89-214-K
177641 RD
GG 7

APPENDIX D

BUCKLING IN SHELLS

Table of Contents

D.1 Nomenclature

D.2 Buckling in Shells

D.3 Analysis of Axisymmetric Shell

D.4 Analysis of Imperfect Shell

D.1 Nomenclature

a - path in linear-elastic equilibrum zone

A - bifurcation point shown in Figures D-1 through D-4

b - path of unstable equilibrum before buckling

B - point of largest force

c - deformation in buckled condition

CL - critical load evaluated using classical techniques

CR - critical load determined experimentally on a component which may contain a flaw

E - Young's modulus of elasticity

I - moment of inertia

L - length of a column

P - generalized load such as force linear pressure or surface pressure

S - stress

S_y - yield strength

S_1 - stress at 0.5% strain used for elastic-plastic analysis

S_2 - stress at 5.0% strain used for elastic-plastic analysis

u - deformation in the x direction

w - deformation in the direction perpendicular to column axis or shell surface

x - axis along a column or a shell surface

δ - deflection

ε - "effective" strain in the x direction indicating an overall reduction in length

μ - imperfection ratio

∂ - partial derivative

D.2 Buckling in Shells

In the small deformation theory of elasticity, it is assumed that the deformations are such that:

- external forces and moments in plates and shells are balanced by bending moments alone (uniform tension is neglected)
- rotations are very small so that $(dw/dx)^2 << du/dx$) and the derivative square can be neglected in the analyses.

In this case, the strain is approximated by $\varepsilon = du/dx$ /D1/.

In the buckling theory, slightly larger deformations are considered and the second term describing the angular rotation is included in the strain equation/D2/:

$$\varepsilon = (du/dx) + (dw/dx)^2/2$$

This equation has a trivial solution: $w = 0$ indicating that buckling may not occur in a "perfect" component (having no defects). Multiple non zero solutions usually exist for different and discrete values of external load (called eigenvalues). The lowest eigenvalue indicates the critical load. At the critical load, two equilibrium positions usually exist showing two possible directions of deformation, as signified by the two diverging lines c in Figure D-1. Line c shows that when buckling starts, large deformations occur without an increase in load. Path b indicates an unstable path. A point where the two lines separate is called the bifurcation point. The lines shown in Figure D-1 are for mathematically "perfect" columns or shells. For real components, which have flaws, out of roundness, and are not perfectly straight, buckling starts at much lower loads and the bifurcation point is much more difficult to establish (see Figure D-2). For example, if a cylindrical shell has an axisymmetric flaw, the critical load reduces rapidly as the size of the flaw increases (see Figure D-3).

In structures with imperfections, buckling starts at significantly lower loads then indicated by the eigenvalue solutions. However, the shell behavior quickly approaches the theoretical post-buckling curve (see Figure D-2). If the path drops downward, equilibrium is unstable, buckling is abrupt, and the buckling load of the imperfect structure is reduced, as shown in Figure D-2 for a thin, cylindrical shell. If the path curves upward, the structure may have a considerable post buckling strength/D3/, as seen in flat plates, illustrated in Figure D-4.

Our analysis of the cylindrical shell and the flat plates consider "imperfections": out of roundness of the shell and variation in wall thickness. Standard pipes are manufactured to close tolerances. However, the largest allowed imperfections reduce the critical pressure from above 20 MPa to below 16 MPa, as shown below.

D.3 Analysis of Axisymmetric Shell

To quantify the effects of geometric "imperfections" on the ability of the IBSS container design to withstand external pressures, it is useful to analyze a perfectly uniform container. This provides a condition indicating the optimum performance of the cask. Thus the severity of "imperfections" can be judged by their effect on this optimum performance.

Description of Model

Utilizing the horizontal and vertical planes of symmetry, one quarter of the cask was modeled with 4 noded linear displacement shell elements. Elements were assigned a constant thickness about the circumference of 30.96 mm, which is the nominal manufacturing wall thickness. The manufacture's dimensional tolerances are shown in Figure D-5. A relatively coarse model is used in the analysis because changes in stress and deformation patterns are gradual over the distance. There is no area that would require refinement for buckling analysis.

Boundary conditions were assigned such that nodes on planes of symmetry could not move into or out of that plane.

The material stress-strain curve and the linearized approximation used in this analysis are shown in Figure 17. Table D.1 shows steel material properties used in the non-linear buckling analysis.

Results

Figure D-6 is a plot of reaction moments versus external pressure at mid height of the cask. It shows that at 20 MPa we are not near a buckling condition. The analyses was stopped at 20 MPa because the instability point 'A' is too far away. According to the Donnell's solution /D4/, the instability pressure should be about 120 MPa.

D.4 Analysis of a Imperfect Shell

Description of Model

As discussed previously in Section D.1, the ability of a structure to withstand buckling is greatly affected by the presence of defects. To evaluate the buckling behavior of an imperfect IBSS container, a non-linear stress analysis was performed.

For a model similar to that described in Section D.2, elements were assigned varying thicknesses about the circumference to simulate the least favorable variation. The minimum allowable wall thickness in this type of pipe was assigned to one half the circumference of the model. Additionally, the worst orientation of inside diameter eccentricity (allowed by manufacturing tolerances) was included to generate the greatest degree of pipe out-of-roundness. Both orientations of internal eccentricity were analyzed. Only the results from the more conservative orientation (first to buckle) are presented. Boundary conditions were assigned using planes of symmetry.

The model's geometry and dimensions are shown in Figure D-6.
The material stress-strain curve and the linearized approximation used in this analysis are shown in Figure 17. Table D.1 shows the steel material property definitions used in the non-linear buckling analysis.

Results

Buckling in the model is marked by a rapid decrease in the reaction moment M_x, M_y or M_z. One half the circumference has the minimum allowable thickness and the model begins to buckle at the midpoint of this area. This point is designated as location 1, while location 2 is 90° about the circumference at the point where the wall thickness begins to increase. Reaction moments versus external pressure are plotted in Figure 18 (a) and 18 (b) for both locations.

Plastic buckling starts at approximately 17 MPa external pressure when both bending moments, M_x and M_y, begin to collapse. This calculated resistance to buckling exceeds the stated acceptable minimum of 15 MPa (see Subsection B.3 of Appendix B).

REFERENCES

D1. Theory of Elasticity, SP Timoshenko, Third Edition, McGraw-Hill Publication, 1970, page 247.

D2. Buckling of Bars, Plates and Shells, DO Brush and BO Almroth, McGraw-Hill Publication, 1975, page 5.

D3. Ibid, page 235.

D4. Ibid, page 165.

TABLE D.1

STEEL MATERIAL PROPERTIES AT 100 ° C

Property	Value Assigned	Percent Plastic Strain
E	200000.0 MPa	-
μ	0.29	-
S_y	201.0 MPa	0.0
S_1	202.0 MPa	0.5
S_2	195.0 MPa	5.0

89-214-K
177648 RD
GG7

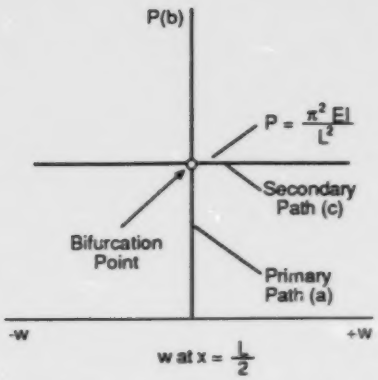

Equilibrium Paths for Initially Straight Column

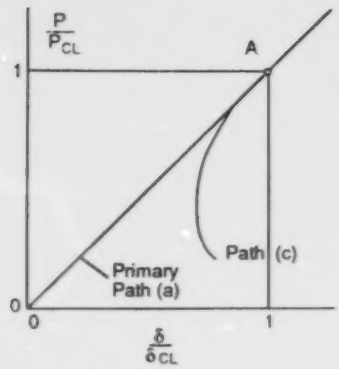

Equilibrium Path for Axially Compressed Cylindrical Shell

FIGURE D-1

EQUILIBRUM PATHS - MATHEMATICAL SOLUTION

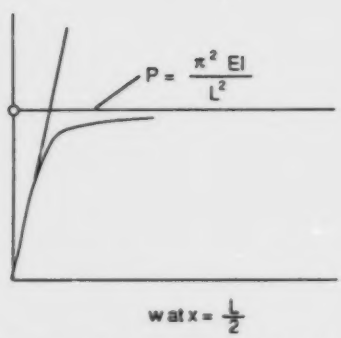

Equilibrium Paths for Slightly Crooked Column

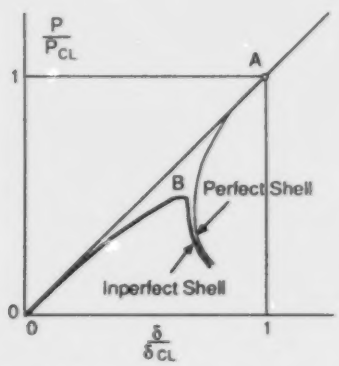

Equilibrium Path for Imperfect Cylindrical Shell

FIGURE D-2

EQUiLIBRUM PATHS - REAL COMPONENTS

$\mu = \frac{\text{Imperfection Size}}{\text{Wall Thicknes}}$

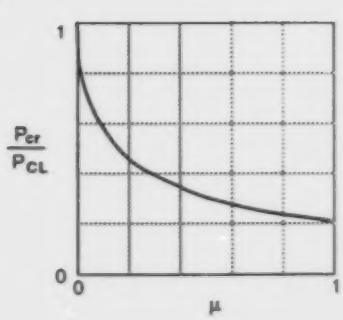

FIGURE D-3

INFLUENCE OF IMPERFECTION MAGNITUDE (Axially Loaded Cylindrical Shell)

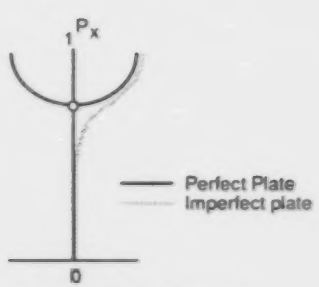

Notes: 1. All Edges Simbly Supported
2. Loading: In-Plane Compression

FIGURE D-4

LATERAL DISPLACEMENTS IN A FLAT PLATE

Figures D-1 Through D-4 Reprinted from Reference 2

89-214-K

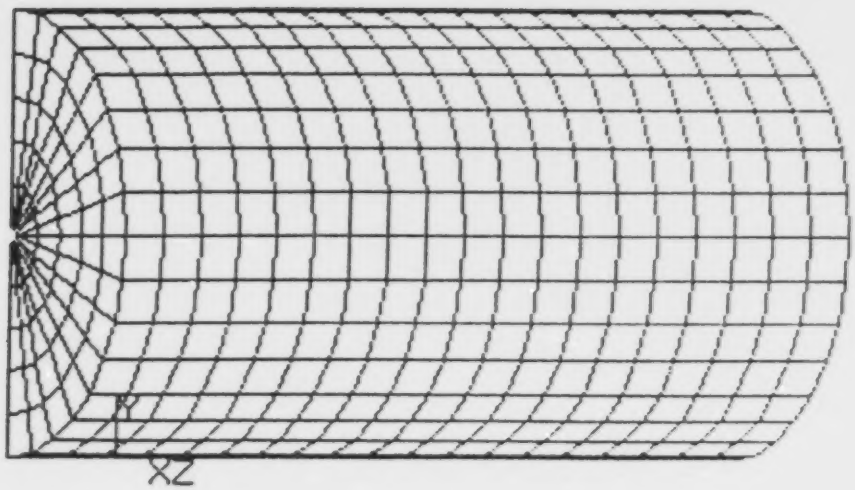

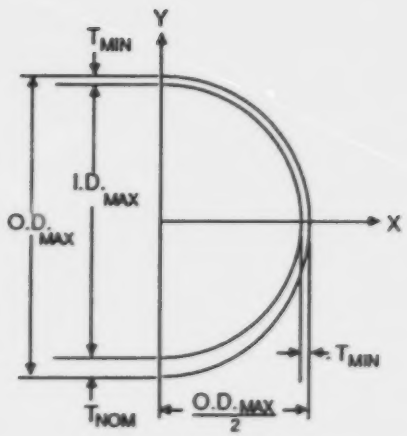

Tolerances for Schedule 80 Pipe

T_{MIN} = 27.08 mm
$T_{NOMINAL}$ = 31.04 mm
O.D.$_{MAX}$ = 612.78 mm
O.D.$_{MIN}$ = 608.81 mm
I.D.$_{MAX}$ = 554.66 mm

FIGURE D-5
MODEL GEOMETRY AND DIMENSIONS FOR THE NON - LINEAR BUCKLING ANALYSIS

89-214-K
177638 RD
GG:7

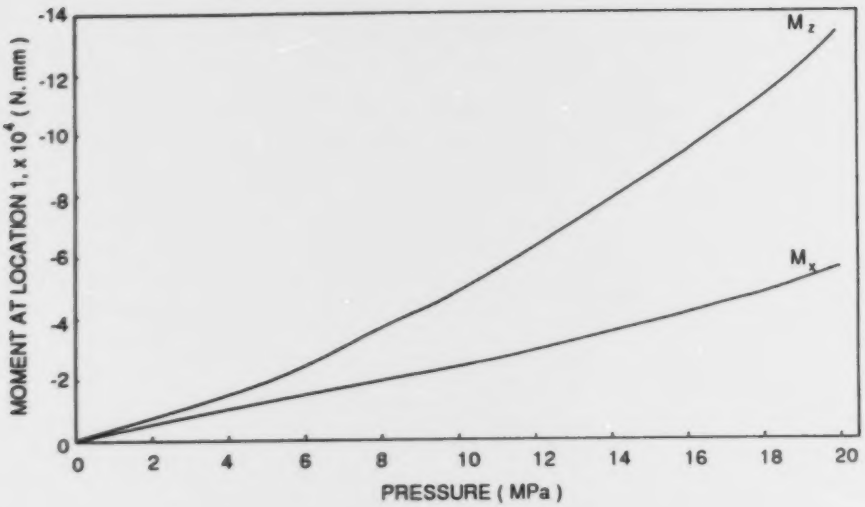

FIGURE D-6

BENDING MOMENTS IN THE AXISYMMETRIC MODEL

89-214-K

177687 RD
00.7

APPENDIX E

CREEP IN STEEL

Table of Contents

E.1 Creep in Metals

E.2 Creep in Steel at Low Temperature

E.3 Stress Relaxation

E.4 Summary of Assumptions

E.5 Test Program

E.6 Creep Induced Buckling

E.7 Finite Element Analysis

E.8 Stress-Strain Curve Modification

E.1 Creep in Metals

Description of Creep

Creep is a property of metal involving time-dependent deformations. The rate of creep depends on temperature and stress. High temperature creep deformation is usually divided into three consecutive stages, shown in Figure E-1:

- Primary or logarithmic creep starts as soon as temperature and load are applied and is characterized by creep rates which decrease with time.

- Secondary creep has a constant creep rate.

- In tertiary creep, the creep rate increases again until failure occurs. This stage can only be anticipated under tensile loading when a reduction of cross section area occurs.

The three stages of creep may exist in metals at temperatures above 0.3 Tm (where Tm is the melting temperature in degrees Kelvin or Rankin). Secondary creep is not anticipated below 0.3 Tm. The tertiary creep may occur at low temperatures under tensile stress near yield/E1/.

Creep Equations

The first two stages are frequently described by a creep rate equation:

$$d\varepsilon/dt = A\, S^n\, t^m\, e^{-rT} \qquad (1)$$

Coefficients m, n, r and A are independent of time. Coefficient m is called the creep time exponent, n is called the creep stress exponent and r is the creep temperature exponent. Coefficient m is equal to zero for uniform, secondary creep and minus one (-1) for logarithmic creep. For tertiary creep, m is greater than 0. F. Garofalo /E1/ proposes that for face-centered cubic and body-centered cubic materials at temperatures between 5% and 30% of melting temperature, strain varies linearly with the logarithm of time:

$$\varepsilon = A' \ln t + \varepsilon^\circ \qquad (2)$$

where ε° is an initial elastic-plastic strain.

The above equations are approximate. When data for mild steel at 400° C from Reference /E2/ was substituted into equation 1, values of coefficients varied widely. For example, values for m ranged from -0.055 to -0.5. This variation is reflected by the change in the profile of the creep curves in Figure E-2. The creep temperature exponent varies from 0.04 to 0.06. The creep stress exponent n is nearly constant at 7.

The available creep test results are reviewed to:

- estimate the total 500-year creep strain in the steel cask,

- show that the steel cask will not buckle due to the long term creep.

E.2 Creep in Steel at Low Temperature

Introduction

The IBSS container will operate at about 373 K (22.5% of melting temperature Tm). Stresses in the steel cask due to the external pressure of 10 MPa, discussed in Appendix C, are considered.

The author was unable to find acceptable test results for creep in steel at temperatures below 0.3 Tm. The results available in literature are usually for temperatures above 400°C or 0.41 Tm. Two literature sources are used in the analysis /E2 and E3/, presenting results of up to 10,000-hour tests (1.14 years). In our analysis, these results are extrapolated to 500 years.

Stress levels considered in the literature are relatively low (below 120 MPa) for the 1-year tests. They are extrapolated to 225 MPa. The third extrapolation was used to estimate the creep properties of steel at the postulated cask temperature of 100°C.

Such multiple extrapolation is likely to cause inaccuracies.

Effect of Temperature

Results presented in reference /E2/ refer to 673 to 773 K temperatures (41% to 47% Tm) or above the Garofalo's proposed transition from primary to secondary creep. At these temperatures, secondary and tertiary creep dominate, as illustrated in Figure E-2 showing creep strain as a function of time. The creep rate exponent for 673 K (0.41 Tm) temperature and 130 MPa stress is near 0.0 indicating secondary creep. At 723 K and 75 MPa, the creep exponent is positive at 1.24 indicating the tertiary creep. At the 373 K temperature, expected in the steel cask, only primary (or logarithmic) creep is anticipated. However this extrapolation is achieved using secondary or tertiary creep results. The validity of the extrapolation is uncertain. A test program was conducted to verify the results of the extrapolation.

Extrapolation of Literature Data

The results of reference /E2/ were replotted to show the temperature - time dependency for various creep strains at constant stress of 75 and 130 MPa. By plotting various creep strains in the available time and temperature ranges, a straight line relationship was obtained which was used to extrapolate the results from the 10,000-hour tests to 500 years. Extrapolation for stress levels of 75 and 130 MPa is shown in Figure E-3.

The 500-year results from Figure E-3 are plotted to show the stress - temperature relationship after 500 years (see Figure E-4). Three points are obtained from Figure E-4 for creep strains of 0.1%, 0.5% and 1.0% for carbon steel at 100°C and are plotted in Figure E-5. The creep strain of above 0.2% follows nearly a straight line. The line is assumed to curve rapidly to zero strain at zero stress. This behavior suggests that there may be a threshold stress below which creep will not occur. Stress of 130 MPa is assumed to be this value since we could not measure creep rate at this stress in the subsequent test program.

The creep strain data from Figure E-4 can be used to estimate the creep rate coefficients from equation (1). By integrating the equation with respect to time and assuming logarithmic creep ($m = -1$), a relationship for creep strain is obtained in form:

$$d\varepsilon/dt = A\, S^n \ln(t) + D \qquad (4)$$

Coefficient D represents the initial, pre-creep strain. Taking two points from figure B-4 at 0.1% and 0.5% creep, the equation coefficients are:

$$A = 2.0 \times 10^{-20} \quad , \quad m = -1, \quad n = 7.0$$

Further confirmation of the above results was obtained from a short-term test program.

A more detailed discussion of the results obtained from literature is presented in Reference /4/.

E.3 Stress Relaxation

Creep deformation can cause stress relaxation, if deformation is not stress-controlled. Creep can be expected to continue in a location until stresses in this location drop below threshold value of 130 MPa. The stress distribution in the flat plates remains unchanged except near the pressed-fit closure where yield stress of 225 MPa will reduce to 130 MPa. In the IBSS bimetallic container, the circumferential stress in the cylindrical shell at the closure will also reduce to 130 MPa, because this is a displacement controlled deformation. The internal pressure required to open the closure is expected to drop from 8.4 MPa by the ratio of (130/200) or to 5.4 MPa.

E.4 Summary of Assumptions

Limited data are available on creep in carbon steel at 100°C. Several assumptions were made to facilitate the creep analysis at this temperature. They are summarized below:

1. Results from creep tests are scattered. Figures E-2 and E-3 show only average creep strains.

2. The available test results are for a relatively small temperature, stress and time ranges. They are extrapolated to range far from the original test results, which adds to the uncertainty of the extrapolated results.

3. Figure E-5 shows creep strain at stresses above yield. The effect of elastic-plastic transition on steel properties was neglected in the preparation of this figure, giving unconservative results.

4. A logarithmic creep law was assumed, based on limited information.

E.5 Test Program

To gain better confidence in Figure E-5, a uniaxial test program was conducted on 1/4-inch diameter steel rods. The rods were 10-feet long to obtain more accurate measurements of small changes in strain. The deformations were measured using two sets of instruments: LVDT's and dial indicators. The layout of the test station is shown in Figure E-6. The displacement indicating devices are shown in Figure E-7. The results of the tests are shown in Figure 22. An initial (first hour) deformation is not shown in this figure so that results from all tests can be plotted on one graph with good resolution. The initial strain is included in the calculation of the coefficients of the creep equations, listed in Table E-I. Logarithmic creep was obtained for stresses below yield. As the axial stress was increased to near yield, the deviation from the logarithmic curve became apparent, as shown in Figure 22 and in Table E-I.

At tensile stress below 70% yield, the 500-year creep strain is negligibly small at about 0.01%. It increases rapidly with increased stress. At stresses below 95% yield, the test results closely follow the logarithmic model. As stress approaches yield, an exponential law is more accurate, and the extrapolated 500-year creep strain is higher, exceeding 0.2% in all tested cases (see Table E-I). The results from the tests were extrapolated to 500 years and superimposed on Figure E-5 (see Figure 21).

E.6 Description of Creep Induced Buckling Models

As discussed in Appendix D, Section D.1, buckling strength largely depends on the size and nature of geometric "imperfections". The cumulative effects of creep in the IBSS container will tend to increase any existing imperfections. Creep strain introduces non-linear behavior of the material at stresses below yield.

The stress-strain curve of steel was modified to include the anticipated effect of 500 year creep in order to allow an evaluation of the effect of creep on the ability of the container to resist buckling. The estimated creep induced strain after 500 years at 100°C was added elastic-plastic strain from the original material stress-strain curve. This modified stress strain curve, shown in Figure 23, was used to define the material properties of the creep buckling model. The linearized stress strain curve used in the buckling analyses discussed in Appendix D has been included in this figure for comparison.

The model geometry was the same as that used in the buckling analysis (described in Appendix D, Section D.3). Material properties are listed in Table E.II.

E.7 Finite Element Analysis Results

The change in the material response over time has a significant effect on the ability of the design to withstand external pressure without buckling. In Figure E-8 (a) and (b), reaction moment plotted against external pressure shows buckling in the container wall at approximately 10 MPa pressure. At this point the largest deflection is 0.21 mm and occurs at mid height in the center of the thinnest section of wall. Figure 20 shows post buckling displacements of the model.

E.8 Stress-Strain Curve Modification

A brief analytical investigation was carried out to determine if the modification of the stress-strain curve to include the extrapolated 500-year creep strain is valid. Figure 23 shows a simplified stress-strain curve for the finite element analyses with increased strains.

To verify the creep analyses, a simple frame was modeled (see Figure E-9) and loaded in bending. Deflection of the frame was calculated twice. Once using the creep equation (2) above with coefficients from Table E.1 and basic stress-strain curve from Figure 17. Second time using the modified stress-strain curve from Figure 23. The difference in the results between the two models was within 4%.

REFERENCES

E1. Fundamentals of Creep and Creep-Rupture in Metals, Frank Garofalo, The McMillan Company, New York, 1965.

E2. High Temperature Design Data for Ferritic Pressure Vessel Steels, The Creep of Steel Working Party of the Institute of Mechanical Engineers, Mechanical Engineering publications Ltd, London, England, 1983.

E3. R.F. Miller, J.J. Heger, "Report on the Strength of Wrought Steels at Elevated Temperatures", Special Technical Publication Number 100, published by the American Society for Testing Materials, 1950.

TABLE E-I

CREEP TEST RESULTS

a) Equation Coefficients

Test	Temp °C	%S_y	A x 10^6	B x 10^6	C x 10^6	D x 10^6	m
1	100	98.0			44	38.3	0.27
2	125	87.0	60	32.8			
3	150	95.5	60	49.6			
4	125	70.0	10	6.4			
5	125	100.0			30	229.0	0.17

THE CREEP TEST RESULTS ARE APPROXIMATED BY EQUATIONS

$\varepsilon = A + B \ln t$ or $\varepsilon = C + D t^m$

ε - Creep Strain
t - Time in Hours

b) Extrapolated Results

Time		Creep Strain (x 10^6)				
Hours	Years	Test 1	Test 2	Test 3	Test 4	Test 5
1		82.3	60.0	60.0	10.2	259
100		176.9	211.2	288.2	39.5	534
1.000		291.4	286.8	402.4	54.2	777
5.0000		426.1	339.6	482.1	64.4	1,014
8.766	1	488.6	358.1	509.9	68.0	1,113
0.44 x 10^6	50	1.322	486.5	703.8	92.9	2,147
0.88 x 10^6	100	1.586	509.2	738.2	97.3	2,414
4.38 x 10^6	500	2.425	562.1	817.9	107.6	3,170
8.77 x 10^6	1.000	2.915	584.8	852.3	112.0	3,566

89-214-K
177659 RD
GG 7

TABLE E-II

STEEL MATERIAL PROPERTIES WITH 500 YEAR CREEP

Property	Value Assigned	% Plastic Strain
E	200,000.0 MPa	0.0
mu	0.29	-
S_{yield}	150.0 MPa	0.0
$S_{hard\ 1}$	200.0 MPa	0.46
$S_{hard\ 2}$	202.0 MPa	0.99
$S_{hard\ 3}$	300.0 MPa	7.19

89-214-K
177658 RD
GG 7

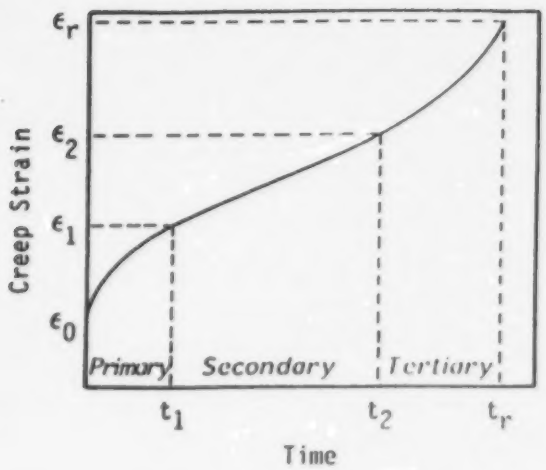

FIGURE E-1
SCHEMATIC REPRESENTATION OF A
CREEP- RUPTURE CURVE

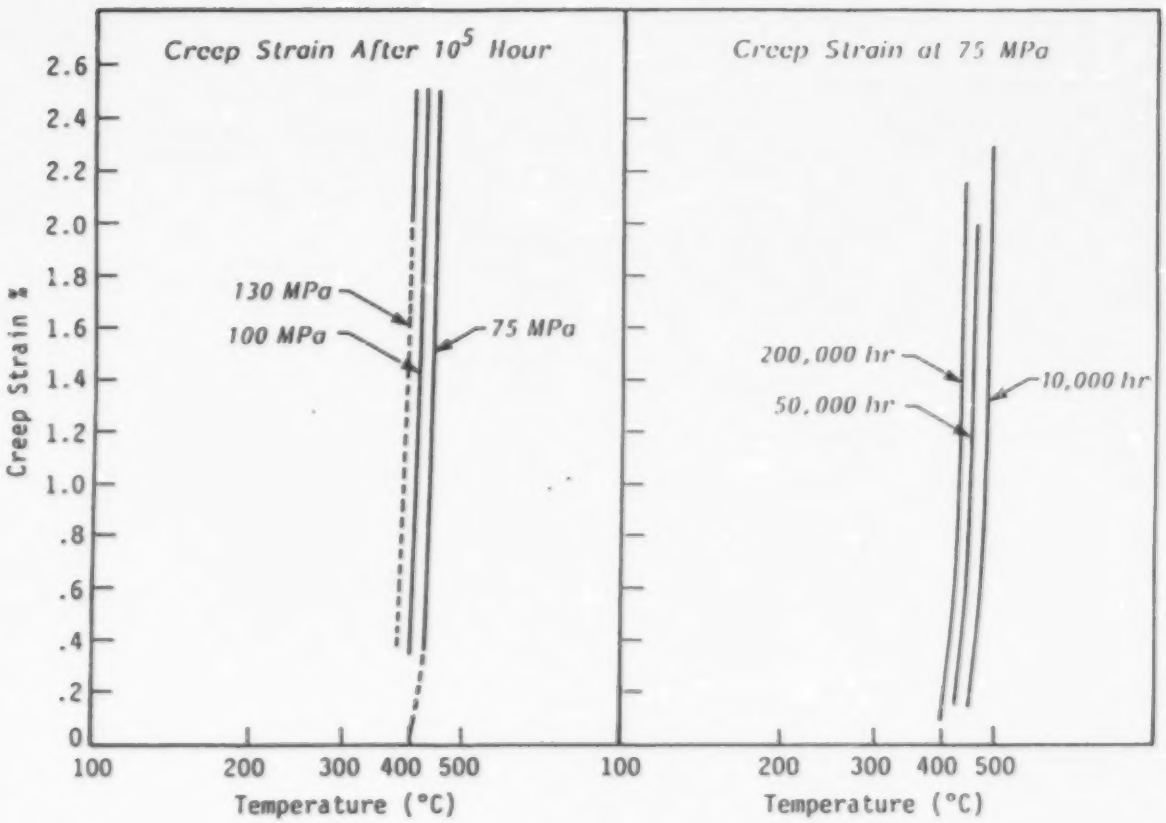

FIGURE E-2
CREEP - TEMPERATURE RELATIONSHIP

89-214-K
1776910
GG7

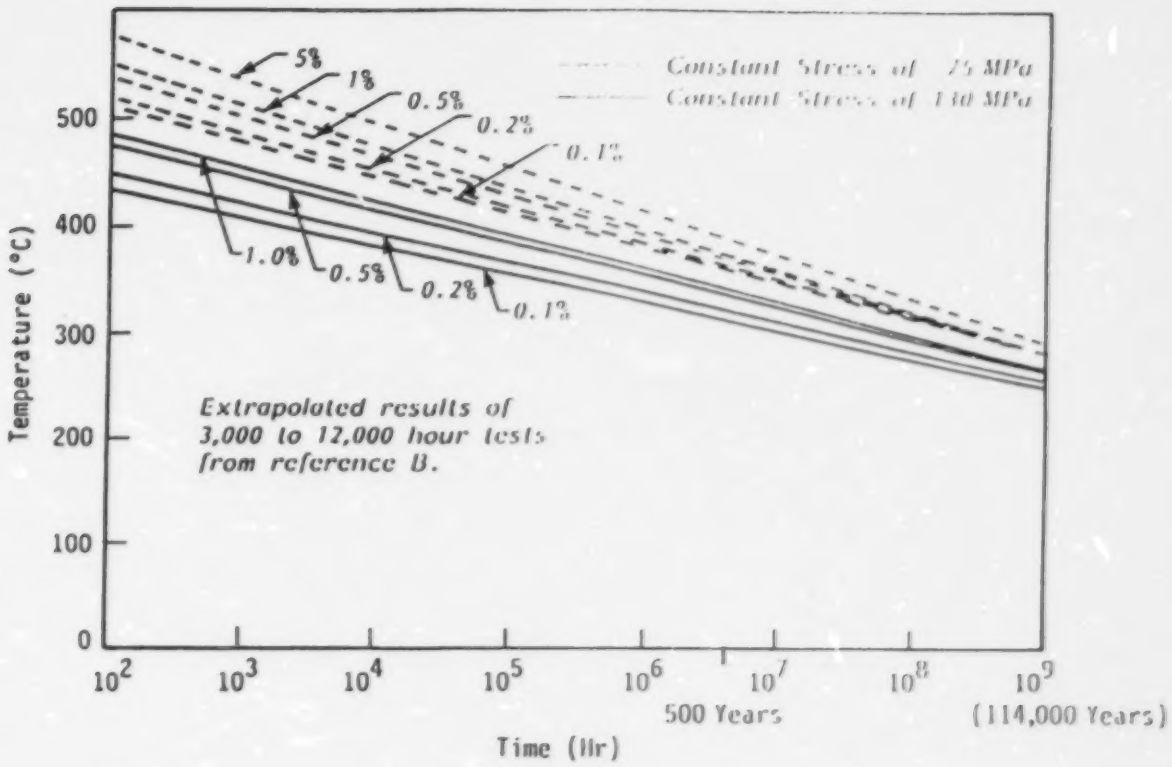

FIGURE E-3
EXTRAPOLATED LITERATURE RESULTS

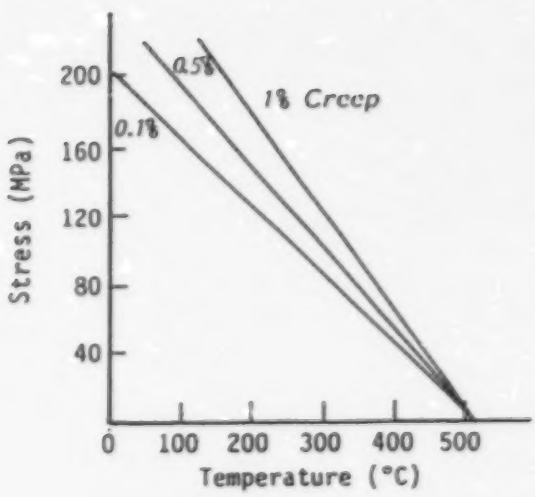

FIGURE E-4
200-YEAR CREEP STRAIN
AT VARIOUS TEMPERATURES

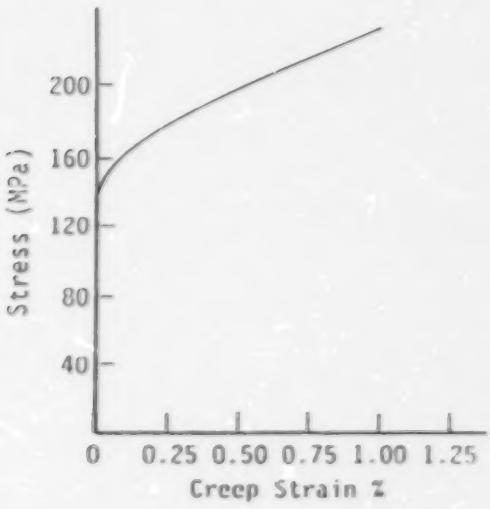

FIGURE E-5
500-YEAR CREEP STRAIN
AT 100 °C

89-214-K
17690 RD
GG 7

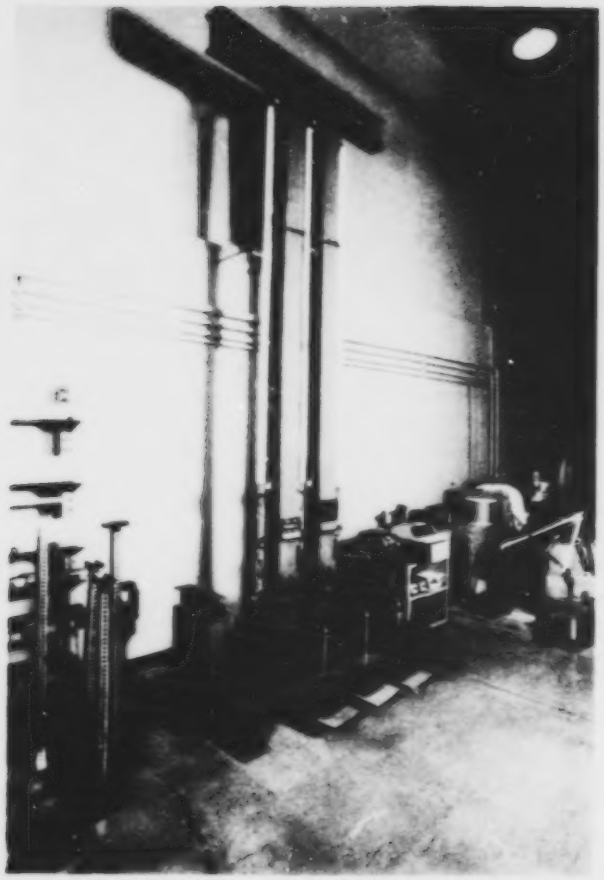

FIGURE E-6
CREEP TEST RIG

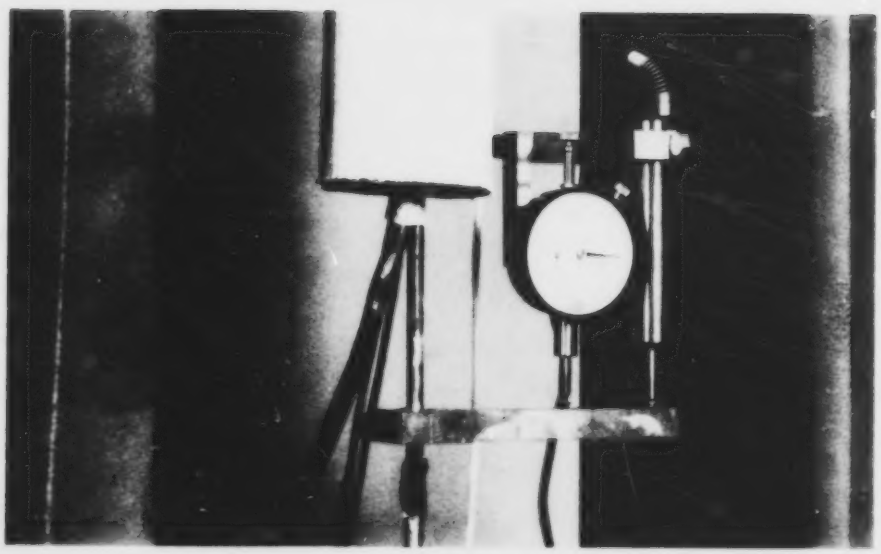

FIGURE E-7
DISPLACEMENT INSTRUMENTATION

89-214-K
177684 RD
QG7

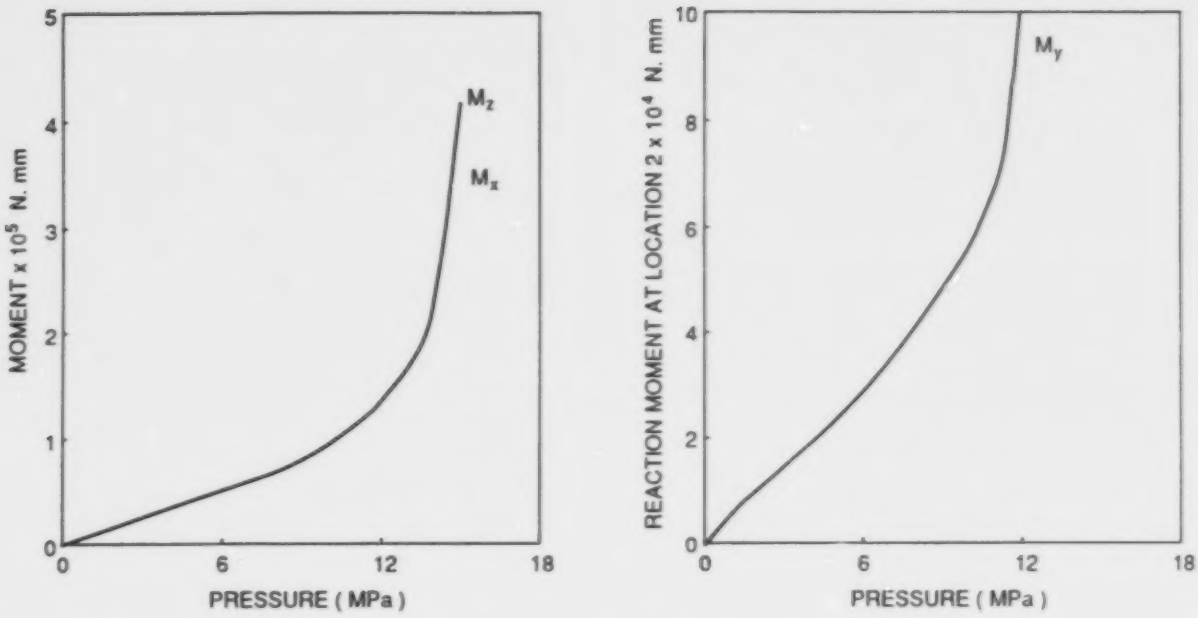

a) Location 1

b) Location 2

FIGURE E-8
BENDING MOMENT IN BUCKING WITH CREEP

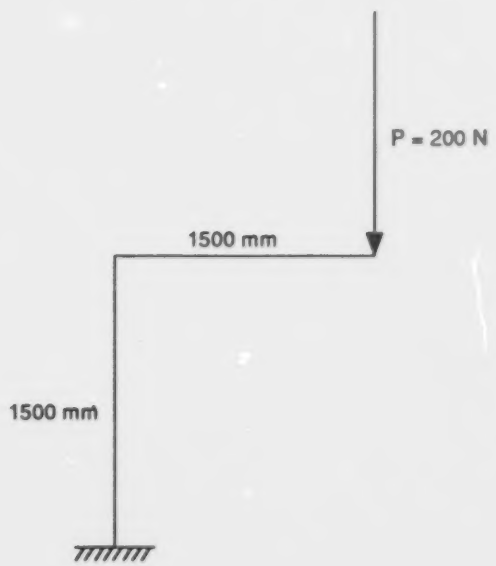

FIGURE E-9
FRAME USED IN VERIFICATION ANALYSIS

APPENDIX F

SELF-LOCKING CLOSURE

Table of Contents

F.1 Introduction

F.2 Closure Used in Tests and Analysis

F.2.1 Design Used in Tests and Analysis
F.2.2 Press-in Case
F.2.3 Pull-out Case
F.2.4 Internal Pressure
F.2.5 Friction Factor
F.2.6 Angle of Contact
F.2.7 Effect of Radius
F.2.8 Leak Test
F.2.9 Continuation of Test Program
F.2.10 Extrapolation of Results

F.3 Finite Element Analyses of Closure

F.3.1 Model Without Seal Weld
F.3.1.1 Results with No Weld
F.3.2 Model With Seal Weld
F.3.2.1 Analysis of Closure with Weld

F.1 Introduction

The closure consists of a flat, circular plate inserted into an end of a cylindrical shell. Their contacting surfaces are slanted at a small angle to allow for the self-locking effect, as shown in the following analysis. The analysis is conducted to assess the effect of various closure design parameters. The main parameters of interest are:

- force used to seal the closure (P),
- friction coefficient between the top plate and the steel shell (μ),
- taper angle of the two surfaces in contact (α),
- radius of the pipe.

Test results have been used extensively in the analysis to determine values of some parameters (e.g. friction factor) and to compare the analytical and experimental results. Since the test program was based largely on a 6-inch schedule 80 pipe with a 37 mm lid, this analysis will be based on these dimensions.

The analysis is approximate. It aims at evaluating the trend anticipated if one or more of the parameters are changed rather than to predict precise results. All deformations considered in the analysis are assumed to be linear-elastic, which was not true in the test program, where the lid was pressed until significant yielding occurred.

F.2 Closure Tests and Analysis

F.2.1 *Design Used in Tests and Analysis*

The dimensions of the pipe and top plate used in tests and analysis are shown in Figure F-1. The pipe is made of carbon steel. During the test, the lid was inserted with a force of 333 kN. The closure was opened using force of 100 kN and, in a subsequent test, by a pressure of 10 MPa.

F.2.2 *Press-in Case*

While the top plate is being pressed in, the balance of forces is as shown in Figure F-2. The pressing force P is balanced by a friction force (T) and a vertical component (G) of the force acting between the plate and the shell:

$$P = 2\pi r\,(T\cos\alpha + G)$$

where

$$G = F\tan\alpha \quad \text{and} \quad T = \mu\,F/\cos\alpha$$

F is the radial component of the force between the surfaces in contact (see Figure F-2) expressed in Newtons per unit (mm) of circumference.

$$P = 2\pi rF\,(\mu + \tan\alpha) = 2\pi rF\,(\mu + \alpha) \quad \text{(for a small angle)} \qquad (1)$$

Radial pressure on the steel shell is a function of a force F:

$$p = F/t^* \cos\alpha = F/t^* \quad \text{(for a small angle)} \qquad (2)$$

where

t'' - thickness of flat plate
t' - thickness of cylinder at the flat plate

The circumferential stress is:

$$Sc = pr/t' = Fr/t't'' \quad (3)$$

The radial stress is equal to:

$$Sr = F/t'' \quad (4)$$

The axial stress in the cylindrical shell, during pressing, is a function of the pressing force:

$$Sa = P/2\pi rt \quad (5)$$

F.2.3 *Pull-Out Case*

While pulling the lid out, the direction of the friction force reverses. Thus the pull-out force is equal to (based on the above derivation):

$$W = 2\pi rF\ (\mu - \alpha) \quad (6)$$

The closure is self-locking for angles (in radians) smaller than the friction factor.

Stresses are unchanged from the press-in case (see equations 3, 4 and 5).

The ratio of f=P/W is a convenient method for evaluating the significance of the angle of contact and the friction factor. From equations 1 and 6:

$$f = P/W = (\mu + \alpha)/(\mu - \alpha) \quad (7)$$

F.2.4 *Internal Pressure*

Internal hydraulic pressure was used in several tests to open the test container. The internal pressure (q) reduces the radial stress between the top plate and the pipe because of the radial deformation in the shell due to the pressure. The effective sealing force (Fe) is equal to:

$$Fe = F - qt''$$

The closure opens when force acting on the top plate is equal to the difference between the rim forces (see equation 1):

$$\pi r^2\ q = 2\pi r\ (T - G)$$

Replacing F with Fe in equations (1) for T and G, it can be shown that the lid will open under an internal pressure of

$$q = P\ (\mu - \alpha)/\pi r\alpha\ [r + 2t''(\mu - \alpha)] \quad (8)$$

The internal pressure required to open the container is proportional to the sealing force P.

To calculate the ratio f, we define the pull-out force as the difference between the forces at the contact surfaces:

$$W = 2\pi r\,(T - G) = 2\pi r\,(\mu - \alpha)(Fe - qt'') \qquad (9)$$

Then the ratio

$$f = P/W = (\mu + \alpha)/(\mu - \alpha) \qquad (10)$$

where $\beta = 1 - 2\pi r q t''\alpha/P$

F.2.5 *Friction Factor*

The self-locking closure works on friction. In general, the friction factor is a function of the materials in contact, their surface roughness, quality of lubrication and pressure between surfaces. For two steel surfaces, the friction factor can vary from 0.1 to 0.8 /7/.

The friction coefficient can be calculated using results, from equations 7 and 9, as a function of f:

$$\mu = \alpha(\beta f + 1)/(\beta f - 1)$$

where β is equal 1 for a pull-out case or is given by equation (10) for an internal pressure.

Table F-II shows the friction factors derived from several test results. Based on the results of our tests, we estimate the friction factor between 0.20 and 0.50 for a rough machined surfaces in as machined condition (machining oil not removed). As the friction factor is reduced, the ratio f increases, reducing the strength of the closure (see Table II). A system where the friction factor is below 0.3 is not recommended. On the other hand, increasing the friction factor above 0.6 will not improve the ratio significantly and it may result in very low contact stresses. Higher forces would be required for sealing such a connection and it could be more sensitive to any defects. The measured range of friction factors is considered the most suitable (see Table F.1 and Figure F-3).

F.2.6 *Angle of Contact*

In the test program, only a 6 degree angle was used. Based on the above analysis, the test results could be extrapolated to other angles using equations 7 and 9 (see Table F.1 and Figure F-4).

If α is increased above 6° the ratio f tends to increase, reducing the strength of the closure. As the angle is reduced, force W approaches P. This would result in too low contact stresses and high forces may be required to seal the closure.

F.2.7 *Effect of Radius*

Only 6-inch pipes were used in our test program so far. Equations 1, 6 and all stress equations suggest a straight line relationship between force, stress and radius. Equation 7 indicates that the ratio between closing and opening forces is independent of radius.

Several tests are planned using 12-inch pipes of various thicknesses. A single test using a 24-inch schedule XS pipe is being considered.

F.2.8 *Leak Test*

In all tests, leak rate was measured after the container was closed. A wide scatter of results was obtained which could not be related to sizes of tested components (lid thickness or pipe gauge). The results of the tests are shown in Table F.2. The scatter is caused by variety of manufacturing and assembly conditions which may require a very lengthy and detailed test program to identify. Such program may be of importance if a seal closure is essential to the container performance.

F.2.9 *Continuation of Test Program*

In the test program performed to-date only closures based on 6 inch pipes were evaluated. Further tests are considered to investigate:

- the effect of larger test specimens,
- the effect of a foil gasket on sealing,
- metallurgical evaluation of the seal, and
- further study into the effect of various closure parameters including friction factors, surface roughness, etc.

F.2.10 *Extrapolation of Results*

The results of the above calculations (in F.2.2 through F.2.4) can be used to predict the behavior of the 24-inch container closure. The dimensions of the container are shown in Figures 5 and 6. The friction coefficient is assumed to be equal to 0.35 and the angle of contact to 0.1 radian (6 degrees).

A force of 1.9 MN will be required to press the lid into the steel cask. This would produce sealing force F of 2 kN/mm. The force to open the closure is estimated at 1.1 MN. The internal pressure which would open the closure may exceed 8.4 MPa.

Stresses induced at the top of the cylindrical shell would be equal to:

$$Sc = 200 \text{ MPa} = 98\% \text{ Sy}$$

$$Sr = 29 \text{ MPa}$$

During pressing an axial stress would be produced in the steel shell equal to 40 MPa (20% yield).

F.3 Finite Element Analyses of Closure

F.3.1 *Model Without Seal Weld*

Stresses in the lid closure area were evaluated using an axisymmetric finite element model. Four-noded axisymmetric elements were used to model the shell-lid junction of the cask. Gap elements were defined between the lid and the wall to monitor contact conditions within the closure. Model geometry included the 6° lid taper, shown in Figure F-5.

The closure was analyzed in two steps. First, an interference was imposed between the lid and wall such that plastic strains reached 0.15%. Next, an external pressure of 10 MPa was applied.

F.3.1.1 *Results Without Weld*

Interference Fit

Results of the first run without the external pressure loading are shown in Figures F-6 and F-7. Figure F-6 shows the hoop stresses at the nodes in the closure. Compressive stresses reach 223 MPa indicating some yielding,as intended in the closure design. An interference fit of 0.7 mm caused material in the cylindrical wall to reach approximately 0.15% plastic strain in the hoop direction.

Axial stresses shown in Figure F-7 indicate bending in the lid. The center of the lid has deflected inwards approximately 0.3 mm.

10 MPa External Pressure

Before pressure is applied, the entire length of the closure is in contact. As external pressure increases, the center of the lid and wall are forced inwards which tends to open a gap at the outer surface of the closure. At 10 MPa, the closure has opened along approximately 67% of its length and has widened to 1.6×10^{-3} mm. at the top. Figure 18 shows schematically the separation of the closure as external pressure increased.

A plot of circumferential stresses, appears as Figure F-8. It shows no significant change in the peak stress value due to the external pressure. Axial stress shown in Figure F-9 indicates increased bending of the lid. The lid has deflected inwards approximately 0.7 mm.

F.3.2 *Model With Seal Weld*

The stress distribution in a weld depends on many factors including: weld preparation geometry, welding procedure, differential cooling rates and any post weld heat treatment. The many variables involved in defining the resultant stress field preclude a single definitive solution to the stress in this weld. The objective of this analysis was to determine if external pressure on the container would significantly increase stresses in the weld.

F.3.2.1 *Analyses of Closure with Weld*

Weld with Interference Fit

Model of the closure (see Figure F-10) with weld was created by refining the first closure model to include a finer mesh in the weld area. Gap elements existed along all but the top 15 mm (weld zone) of the closure. Weld elements were initially removed and an interference fit was applied across the closure. In step 2, weld elements were reinserted into the deformed mesh. Abaqus inserts elements in an unstrained condition and they must then deform to reach equilibrium. With the interference fit imposed adjacent to the weld, very large stresses were introduced in the weld elements. Although this method does not reproduce the weld stress field that would be caused by welding, it can be used to provide a baseline condition. Tresca's stresses in the weld appear in Figure F-11.

Welded Closure with 10 MPa

In the final step, external pressure was increased to 10 MPa.

When Figure G-11, (weld with no pressure), is compared to Figure F-12 (weld area at 10 MPa) very small changes in the stress field are apparent. This small variation indications that changes in the weld stress field due to this pressure are not significant.

In conclusion, it is unlikely that the 10 MPa external pressure would cause an increased risk of failure at the weld.

TABLE F.1

CLOSURE LOADS

Rraction Factor	Angle δ (°)	Force to Close P (kN)	Force to Open P (kN)	Sealing Force F (kN)
0.8	6	100	77	1.3
0.6	6	100	70	1.4
0.45	6	100	62	1.6
0.3	6	100	48	2.1
0.1	6	100	0	-
0.3	17	100	0	181.1
0.3	10	100	26	3.8
0.3	6	100	48	2.1
0.3	3	100	70	1.4
0.3	1	100	89	1.1

TABLE F.2

CLOSURE STRENGTH

Test No	Pipe Size (in)	Schedule	Top Plate Thickness (mm)	Surface Finish (RMS)	Closure Force (kN)	Load to Open		Friction Coefficient
						Force (kN)	Pressure MPa	
1.1	6	10	25	125	155	93.4	2.50	0.42
2.1	6	40	25	125	191	45.0	-	0.17
3.1	6	80	25	125	290	-	7.24	0.30
3.2	6	80	25	125	245	-	6.55	0.33
4.1	6	XX	64	125	614	-	20.70	0.49

89-214-K
177668 RD
GG7

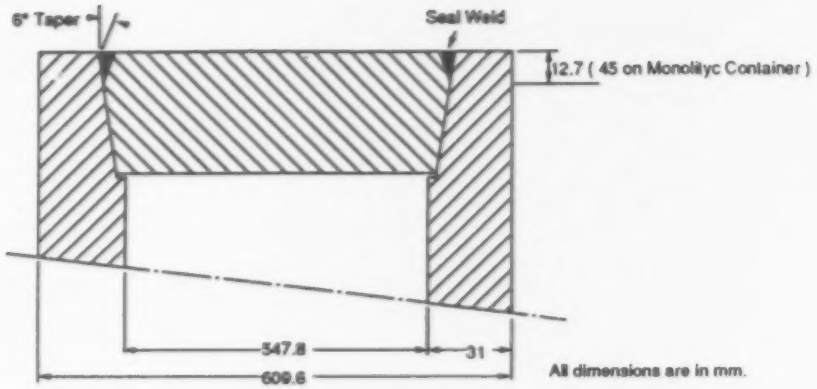

FIGURE F-1

CONTAINER FOR CLOSURE ANALYSIS

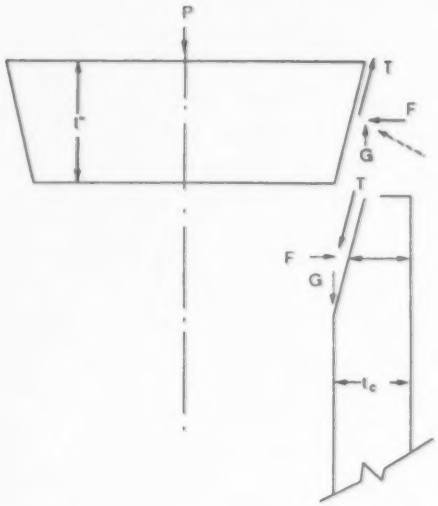

FIGURE F-2

FORCE DIAGRAM OF THE CLOSURE

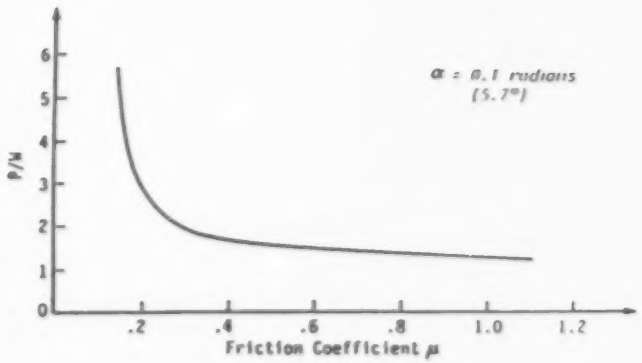

FIGURE F-3

EFFECT OF FRICTION COEFFICIENT

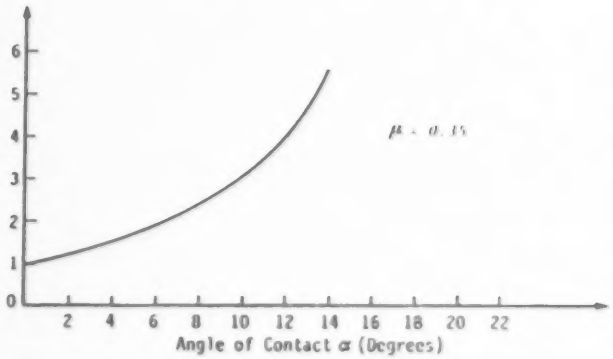

FIGURE F-4

EFFECT OF ANGLE OF CONTACT

89-214-K
160367-B11-RD

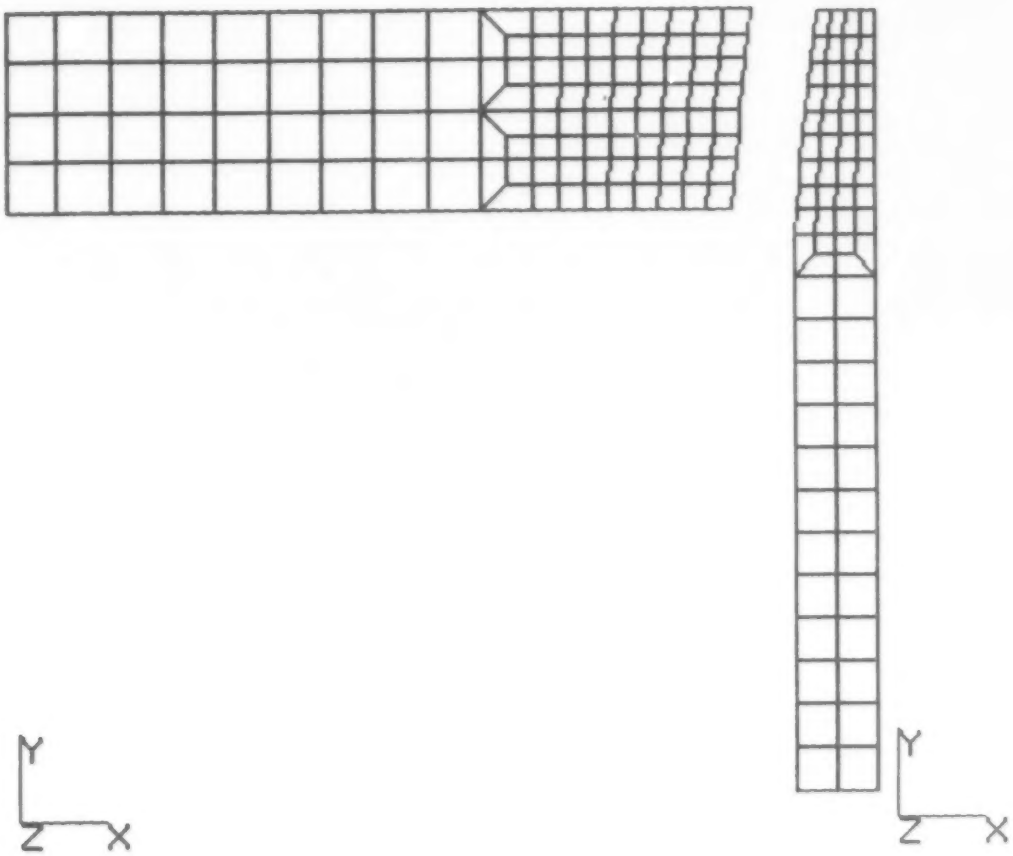

FIGURE F-5
LID CLOSURE MODEL, AXISYMMETRIC, LINEAR DISPLACEMENT ELEMENTS

89-214-K
177665 RD
QG 7

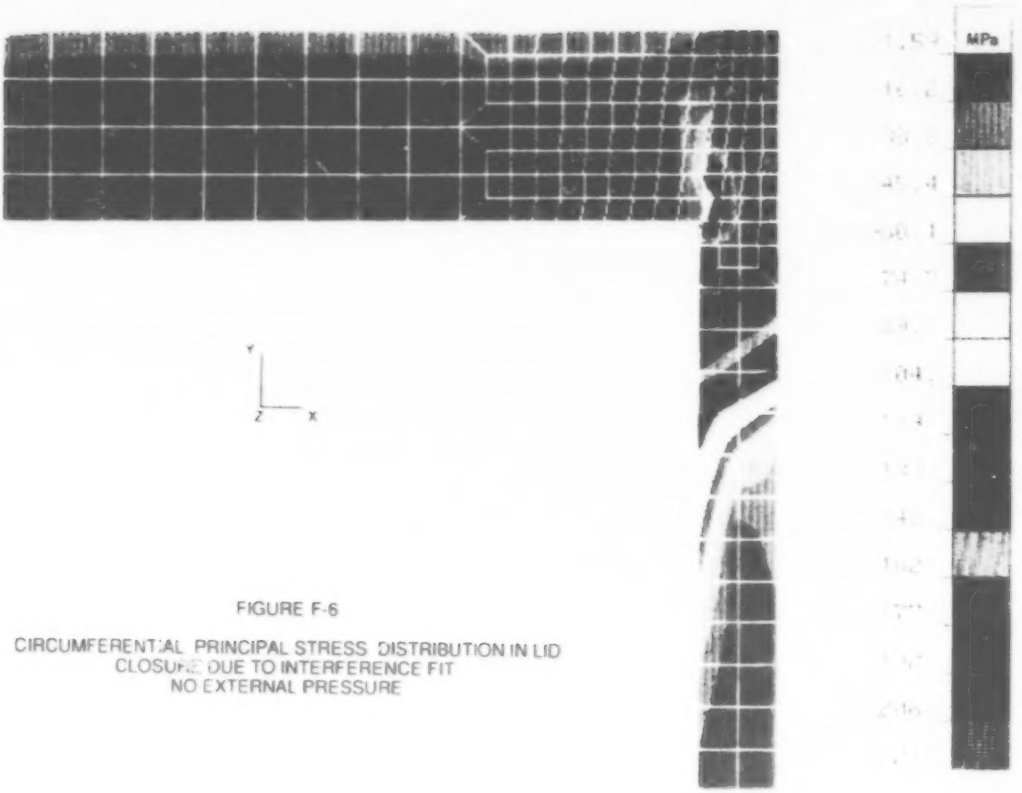

FIGURE F-6

CIRCUMFERENTIAL PRINCIPAL STRESS DISTRIBUTION IN LID CLOSURE DUE TO INTERFERENCE FIT NO EXTERNAL PRESSURE

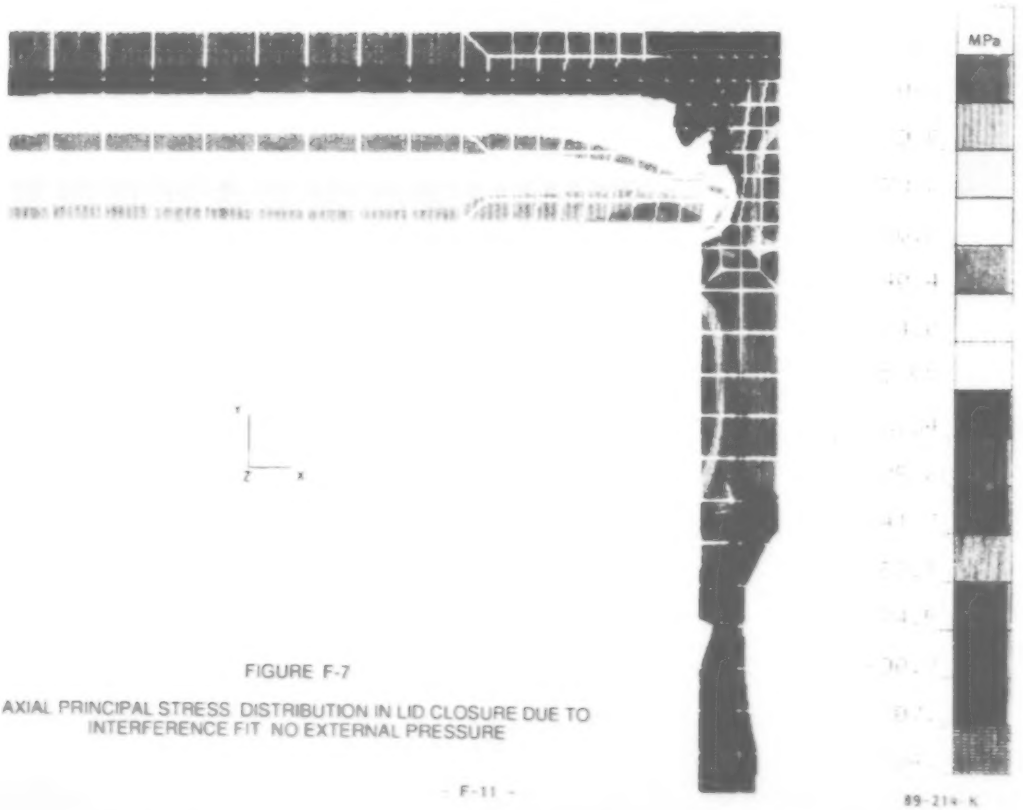

FIGURE F-7

AXIAL PRINCIPAL STRESS DISTRIBUTION IN LID CLOSURE DUE TO INTERFERENCE FIT NO EXTERNAL PRESSURE

89-214-K

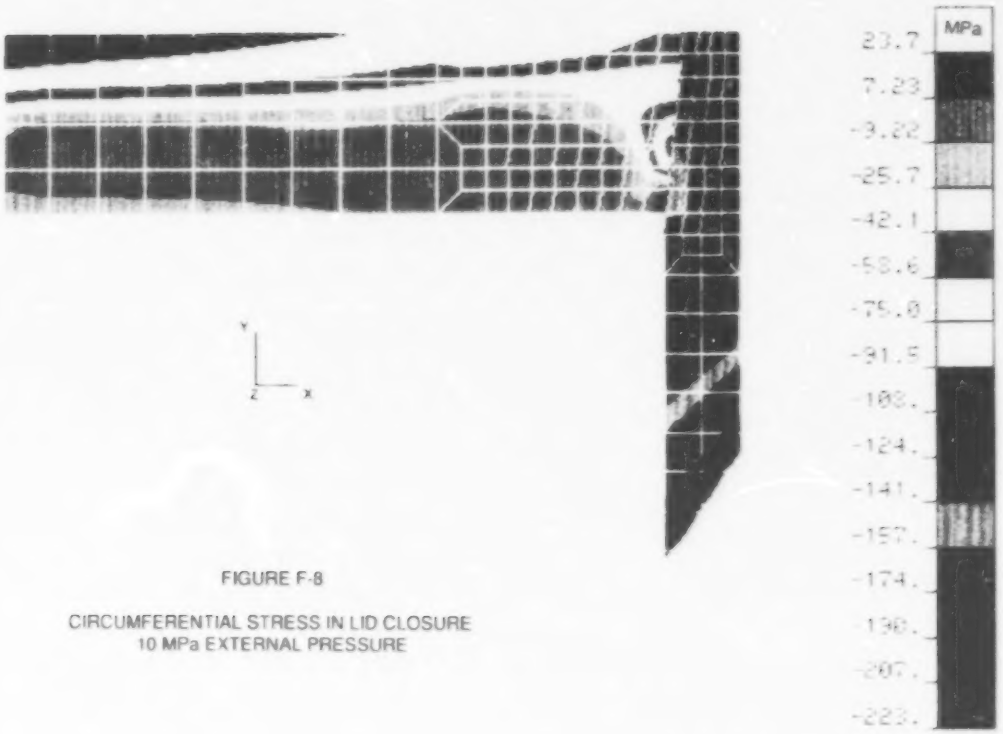

FIGURE F-8

CIRCUMFERENTIAL STRESS IN LID CLOSURE
10 MPa EXTERNAL PRESSURE

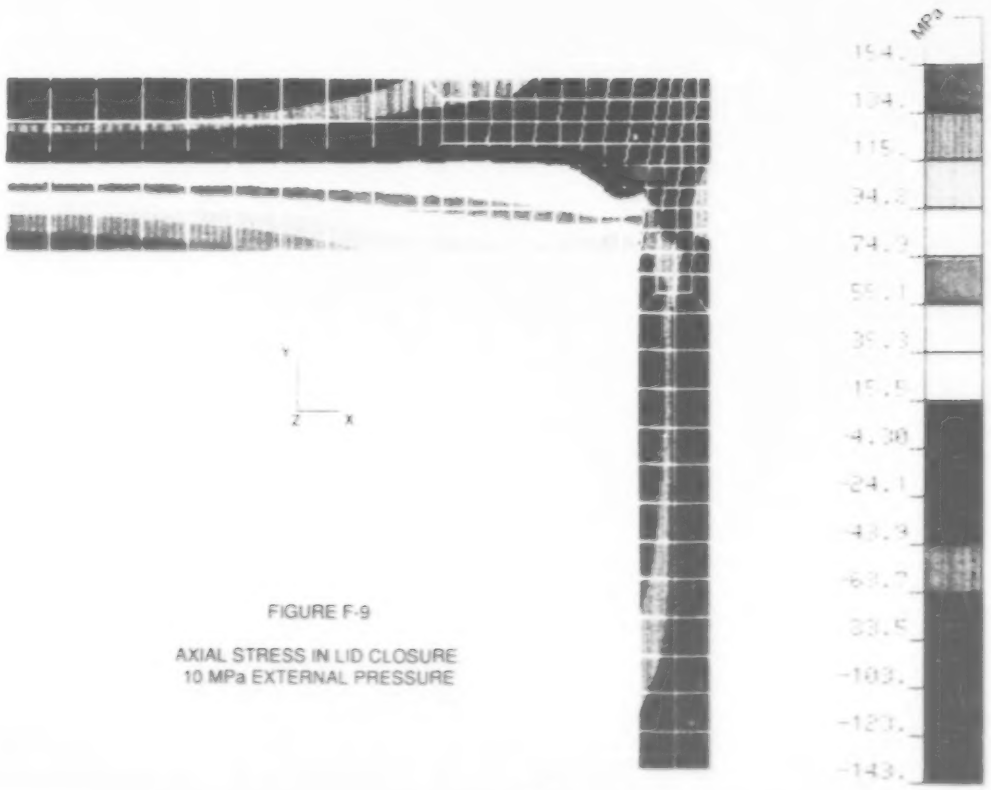

FIGURE F-9

AXIAL STRESS IN LID CLOSURE
10 MPa EXTERNAL PRESSURE

89-214-K

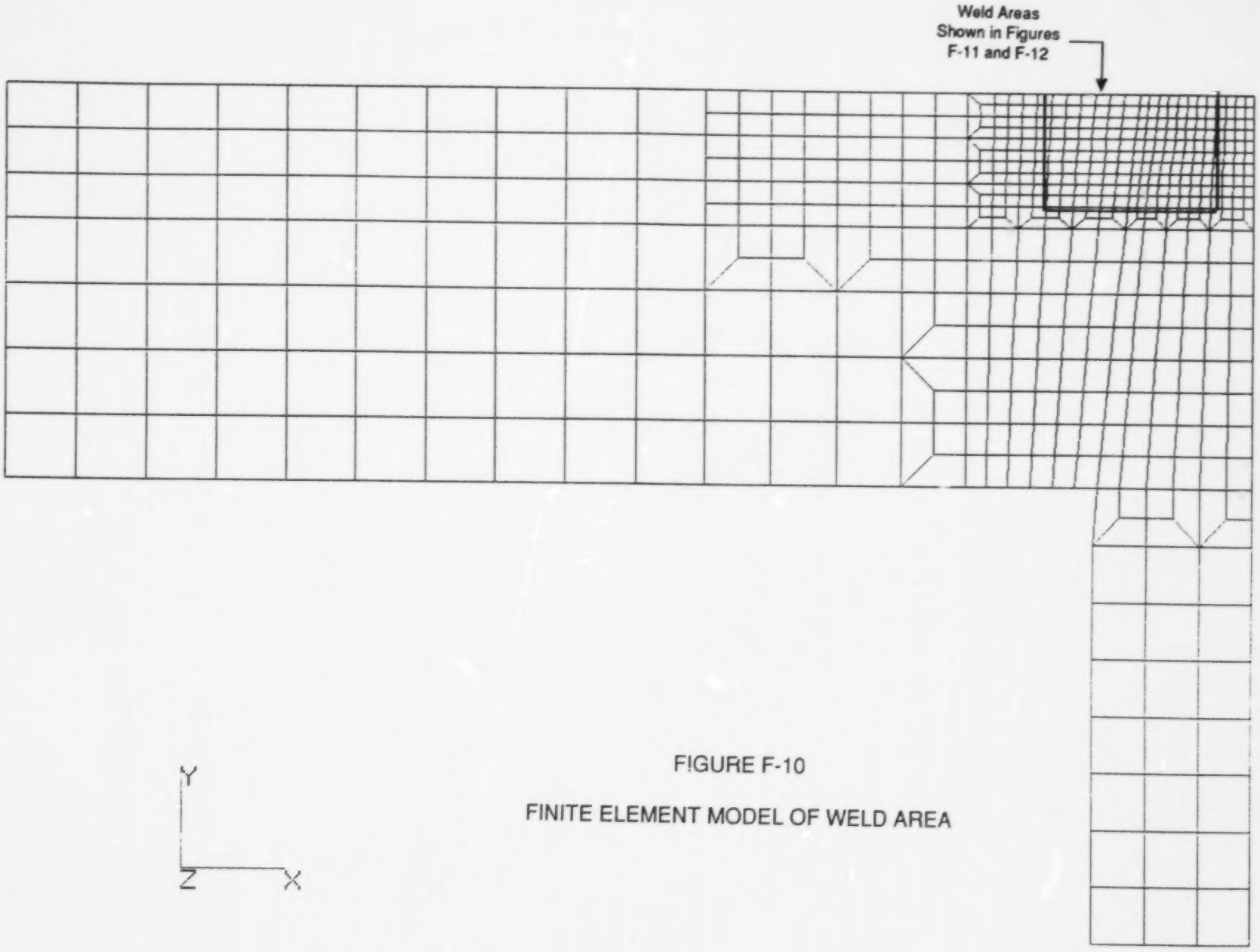

FIGURE F-10

FINITE ELEMENT MODEL OF WELD AREA

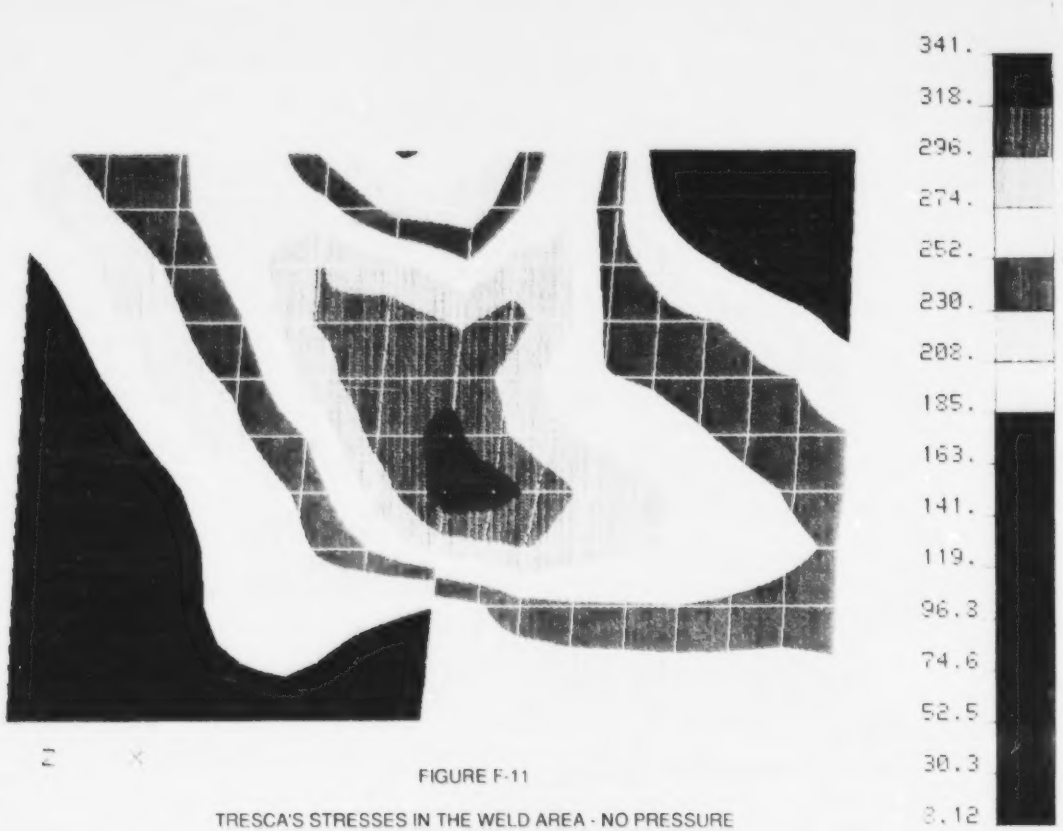

FIGURE F-11

TRESCA'S STRESSES IN THE WELD AREA - NO PRESSURE
Note: See Figure F-10 for Weld Location

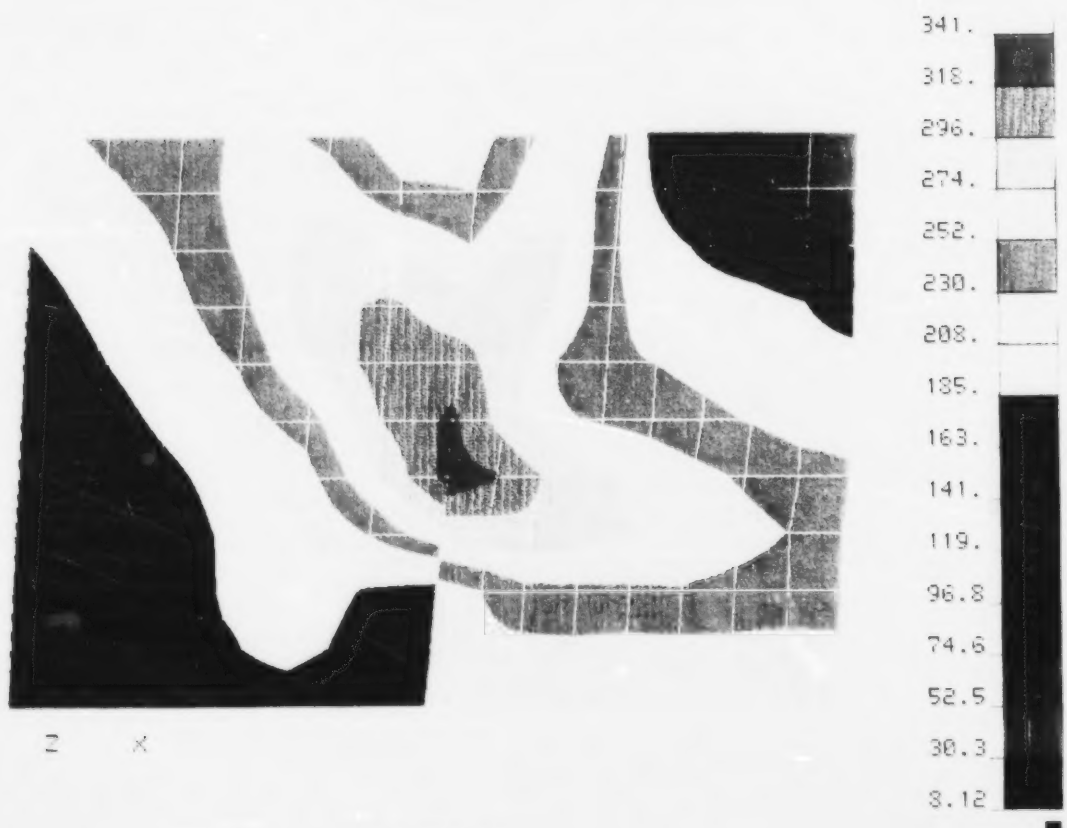

FIGURE F-12

TRESCA'S STRESSES IN THE WELD AREA WITH 10 MPa PRESSURE

89-214 K

APPENDIX G

TITANIUM SHELL ANALYSIS

Table of Contents

G.1 Introduction

G.2 Evaluation of Strain in Shell - Top Head Area

G.3 Results - Top Head Area

G.4 Evaluation of Strain in Shell - Bottom Head Area

G.5 Results - Bottom Head Area

G.6 Thin Titanium Shell

G.7 Evaluation of Strain in Thin Shell

G.8 Results

G.1 Introduction

A titanium overpack is included in the IBSS design as a corrosion resistant barrier. To ensure that failure of the overpack does not lead to premature perforation of the protective shell, an analysis of the stress, strain and deformation of the shell was performed.

G.2 Evaluation of Strain in Shell - Top Head Area

The current design of the titanium shell closure, shown in Figure G-1, leaves a small gap between the titanium and carbon-steel shells. Under high external pressure this unsupported area may collapse inward, allowing unacceptably high plastic strains (>= 5%) to develop in the titanium. Two analyses were performed to quantify deformation in this area with and without a steel support ring. This ring would have a triangular cross section. Strain in the titanium shell was evaluate using an axisymmetric finite element model. Material properties for titanium used in the analysis appear in Table G-1. Geometry of the titanium shell was developed using axisymmetric shell elements while the container body was modeled with linear displacement axisymmetric solid elements. The support ring was modeled as an extension to the rest of the cask body. Between the steel cask body and the shell, 1.0 mm gap elements were introduced to monitor contact between the titanium shell and the steel. These models were analysed using large displacement theory and isotropic material hardening. Figure G-2 shows the geometry of the top head models with and without the support ring.

G.3 Results - Top Head Area

4.76 mm Titanium Shell with Support Ring:

The gap between the titanium shell and the steel cask closed as the external pressure increased. At 10 MPa, the outer shell is supported by the cask everywhere except in the corner region of the lid. Figure G-3 (b) shows the deflection of the 4.76 mm thick shell onto the cask at the top edge. The titanium lid is in contact everywhere except for the outermost 50 mm.

Two regions of the titanium are highly stressed and consequently the most distorted. One is the wall immediately above the support ring, the second is at the bend in the lid. Neither of these regions has underlying support from the steel. Plastic strains here are summarized in Table G-2, and range from 0.00 to 0.31%. Plastic strains in the cylindrical shell wall are all below 0.2%. These values are well below the maximum allowable plastic strain defined in Section 3.0 (c).

4.76 mm Titanium Shell, No Support Ring:

Removal of the support ring from the model had no significant effect on the response of the titanium shell. Deflections of the titanium shell are shown in Figure G-4 (b). As found previously, the area most severely stressed is the unsupported corner. Plastic strains here range up to 0.31% while plastic strain in the cylindrical walls is less than 0.2%. Plastic strains and their location in the corner region are summarized in Table G-II.

G.4 Evaluation of Strain in Shell - Bottom Head Area

4.76 mm Thick Titanium Shell

Strain in the titanium shell in the bottom head region was evaluated with an axisymmetric finite element model (shown in Figure G-5 (a)) which incorporated the 40 mm bottom corner radius. Geometry of the titanium shell was developed using axisymmetric shell elements while the container body was modeled with linear displacement axisymmetric solid elements. Between the steel cask body and the shell, 1.0 mm gap elements were defined. The titanium shell elements were given a thickness of 4.76 mm.

G.5 Results - Bottom Head Area

4.76 mm Thick Titanium Shell

Figure G-5 shows the initial geometry of the bottom head region and the displacement of the titanium shell under 10 MPa. Under external pressure the titanium shell contacts the cask everywhere except at the extreme corner. Here plastic strains in the shell range up to 0.31%. In the cylindrical walls plastic strain is approximately 0.13%. Plastic strains and their locations are shown in Table G-IV.

G.6 Thin Titanium Shell

The titanium shell would initially be 4.76-mm thick. In the vault, uniform corrosion is postulated which may reduce the shell thickness. A minimum thickness of 2 mm is assumed here.

G.7 Evaluation of Stress in Thin Shell

The finite element model used to evaluate the stresses in the 4.76 mm thick titanium overpack was modified to represent a titanium thickness of 2 mm.

G.8 Results

Top Head - 2.0 mm Titanium Shell with Support Ring:

Figure G-6 (b) shows the deflection of the 2 mm shell with the support ring under 10 MPa external pressure. Plastic strains in the corner of the overpack are presented in Table G-3 and range in value from 0.13% to 0.55%. The reduction in thickness has caused a slight increase in plastic strain in the cylindrical wall, but values are still less than 0.2%.

Top Head - 2.0 mm Titanium Shell, No Support Ring:

The reduction in shell thickness and the resulting decrease in stiffness of the titanium wall causes a marked increase in the deformation. Figure G-7 shows the deformed shape of the unsupported corner area under 7 MPa pressure. The wall and lid have been pinched into contact. Plastic strains reach 2% in this highly deformed region. Analysis of this model was not continued past 7 MPa since strain values indicated plastic strain would exceed the maximum level proposed in Section 3.0 (c). A summary of plastic strains in 2 mm titanium at the top corner appears in Table G-III.

Bottom Head - 2.0 mm Titanium Shell

Figure F-8 (b) shows displacements in the 2 mm titanium overpack under 10 MPa pressure. The shell is supported everywhere by the underlying steel cask. Plastic strain in the titanium ranges from 0.15% in the cylindrical walls to 0.18% at the center of the bottom head. These values are well below the maximum levels of acceptable plastic strain proposed in Section 3.0 (c). A summary of plastic strain in the bottom head appears in Table G-IV.

TABLE G-I

TITANIUM MATERIAL PROPERTIES

Property	Value Assigned	% Plastic Strain
E	100,000.0 MPa	-
μ	0.29	-
S_y	216.0 MPa	0.0
S_1	325.0 MPa	0.02
S_2	345.0 MPa	0.20
S_3	300.0 MPa	7.19

NOTE: Mechanical properties are input to the program using a piece-wise linear formulation. S_y designates the largest strain where 'no' plastic strain occurs. S_n stress value at which the strain rate is given and where strain rate changes.

89-214-K
177660 RD
GG 7

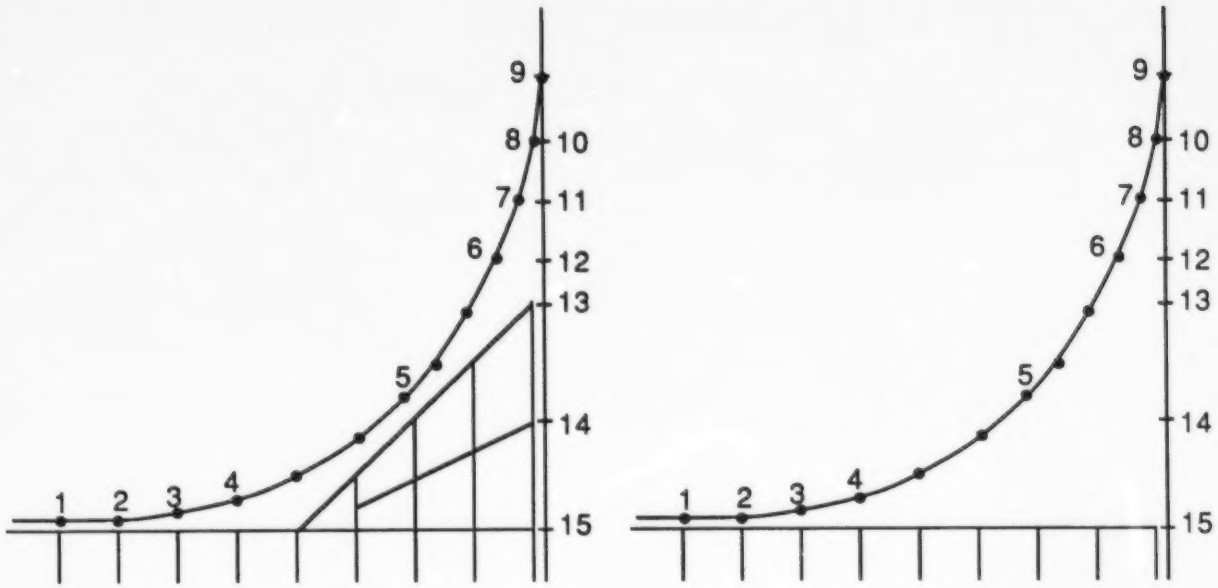

TABLE G-II

PLASTIC STRAIN IN TITANIUM SHELL AT THE TOP HEAD
4.76 mm SHELL THICKNESS

With Support Ring		Without Support Ring	
Node #	Plastic Strain Percent	Node #	Plastic Strain Percent
1	+0.20	1	+0.20
2	+0.05	2	+0.05
3	+0.01	3	+0.00
4	0.00	4	+0.00
5	-0.02	5	-0.02
6	-0.13	6	-0.13
7	-0.19	7	-0.20
8	-0.31	8	-0.31
9	-0.12	9	-0.12
10	-0.03	10	-0.03
11	-0.05	11	-0.04
12	-0.10	12	-0.09
13	-0.15	13	-0.15
14	-0.18	14	-0.18
15	-0.16	15	-0.16

177674 RD
GG 7

89-214-K

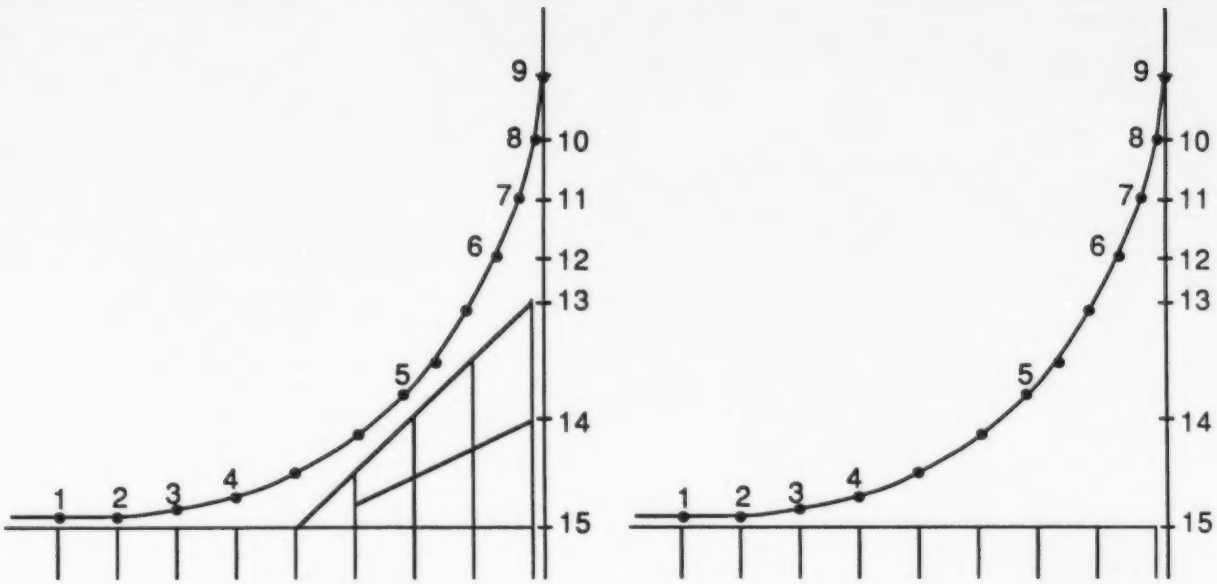

TABLE G-III

PLASTIC STRAIN IN TITANIUM SHELL AT THE TOP HEAD
2.0 mm SHELL THICKNESS

With Support Ring (10 MPa)		No Support Ring (7 MPa)	
Node #	Plastic Strain Percent	Node #	Plastic Strain Percent
1	+055	1	+0.52
2	+0.54	2	+0.52
3	+0.04	3	+0.04
4	+0.00	4	+0.00
5	+0.01	5	+0.00
6	-0.01	6	+0.00
7	-0.04	7	+0.04
8	-0.24	8	+0.44
9	-0.13	9	+0.05
10	-0.13	10	+.048
11	-0.28	11	-0.46
12	-0.29	12	-2.01
13	-0.18	13	-1.80
14	-0.14	14	-0.10
15	-0.13	15	+0.38

177673 RD
GG 7
89-214-K

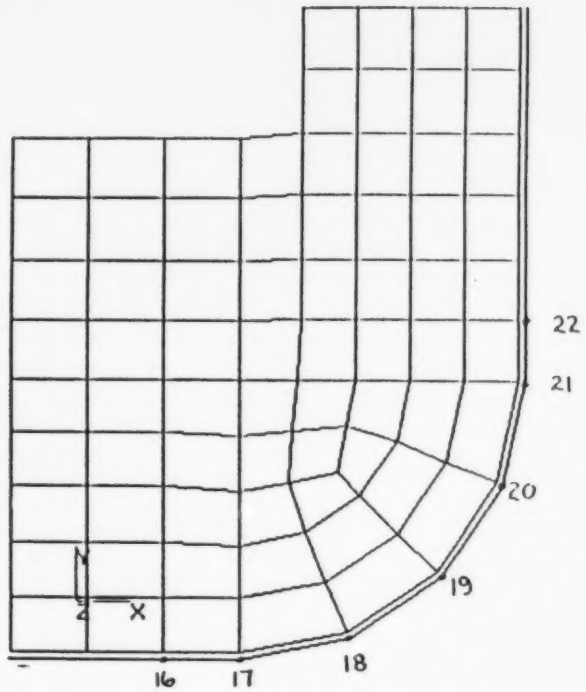

TABLE G-IV

PLASTIC STRAIN IN TITANIUM SHELL - BOTTOM HEAD

4.76 mm Shell Thickness		2.00 mm Shell Thickness	
Node #	Plastic Strain Percent	Node #	Plastic Strain Percent
16	-0.31	16	-0.21
17	-0.15	17	-0.20
18	-0.02	18	-0.04
19	+0.09	19	+0.02
20	+0.07	20	-0.01
21	-0.02	21	-0.17
22	-0.12	22	-0.19

89-214-K
177672 RD
GG 7

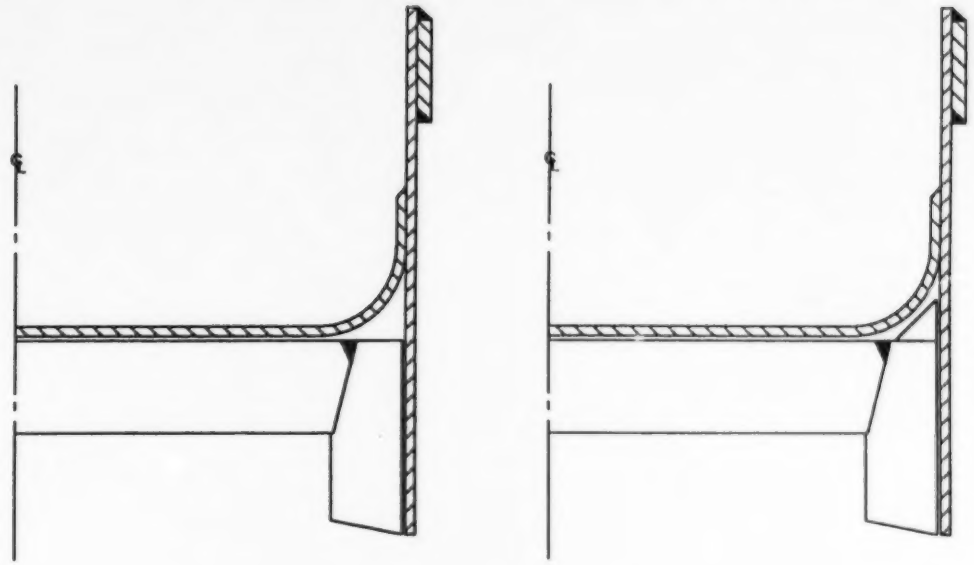

a) No Reinforcement

b) With Reinforcement

FIGURE G-1

GEOMETRY OF TITANIUM OVERPACK

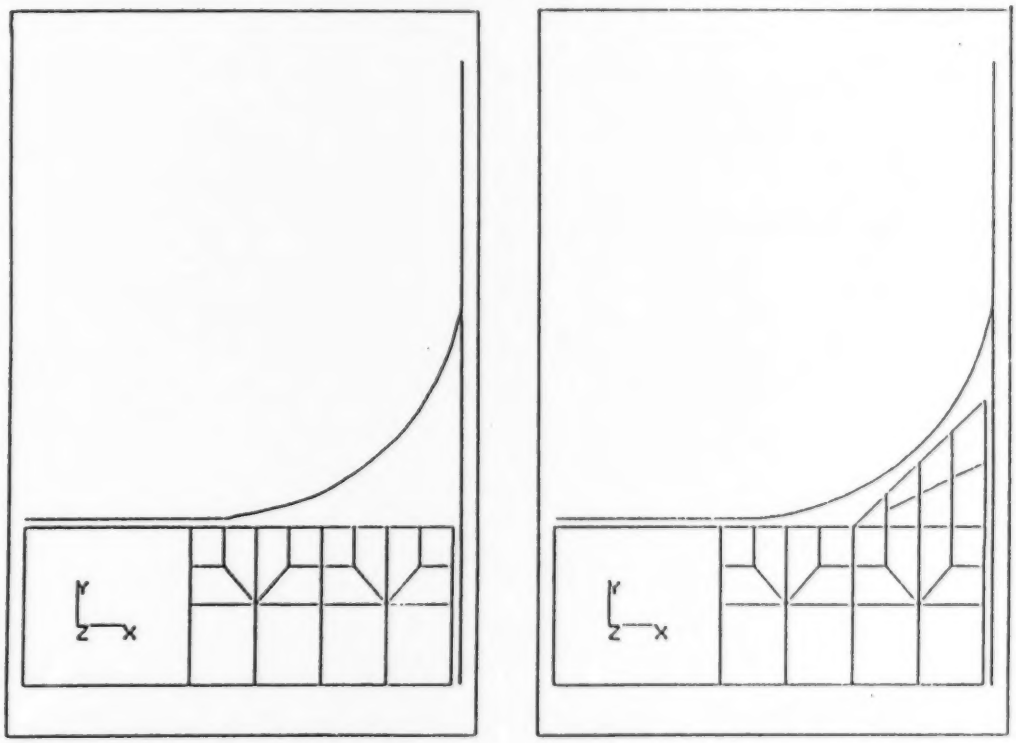

a) No Reinforcement

b) With Reinforcement

FIGURE G-2

FINITE ELEMENT MODEL, DETAIL OF TOP CORNER

89-241-K

177671 RD
0017

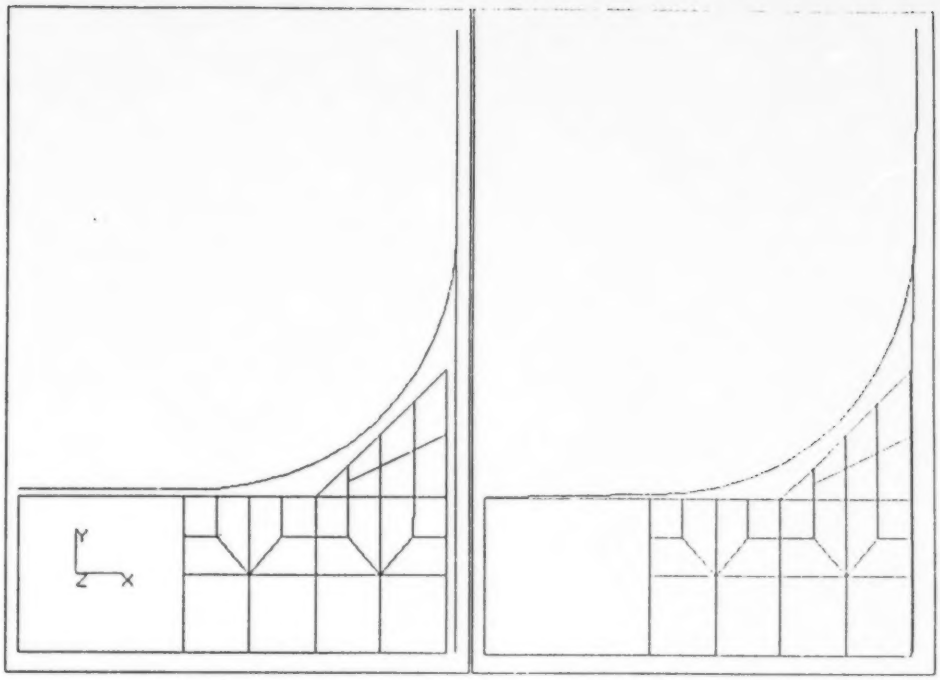

a) Undeformed b) Deformed

FIGURE G-3

4.76 mm THICK TITANIUM UNDER 10 MPa, WITH REINFORCING RING

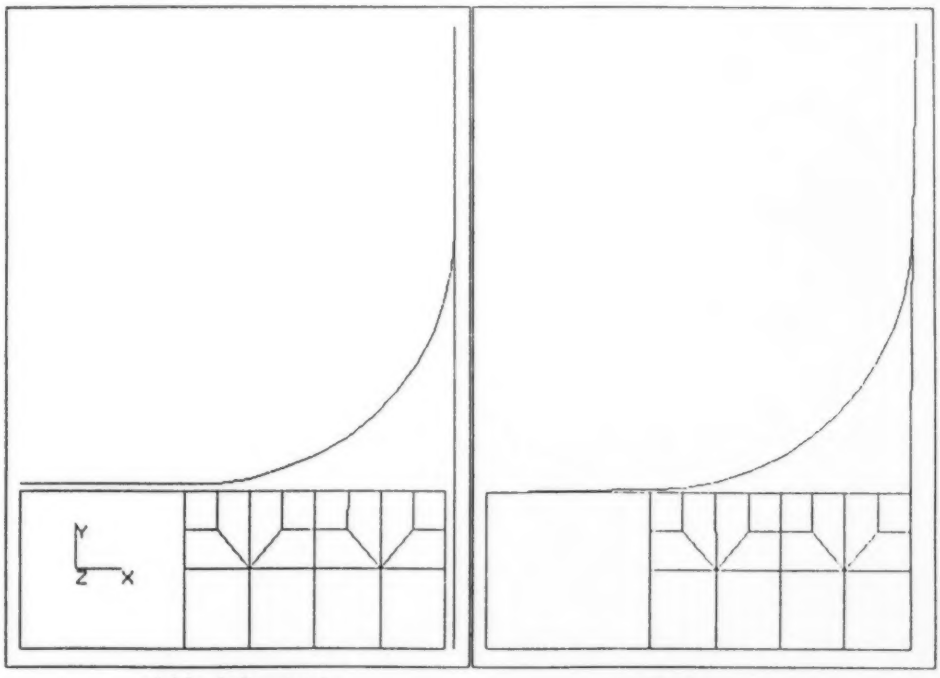

a) Undeformed b) Deformed

FIGURE G-4

4.76 mm THICK TITANIUM UNDER 7 MPa

89-214-K

177670 RD
GG7

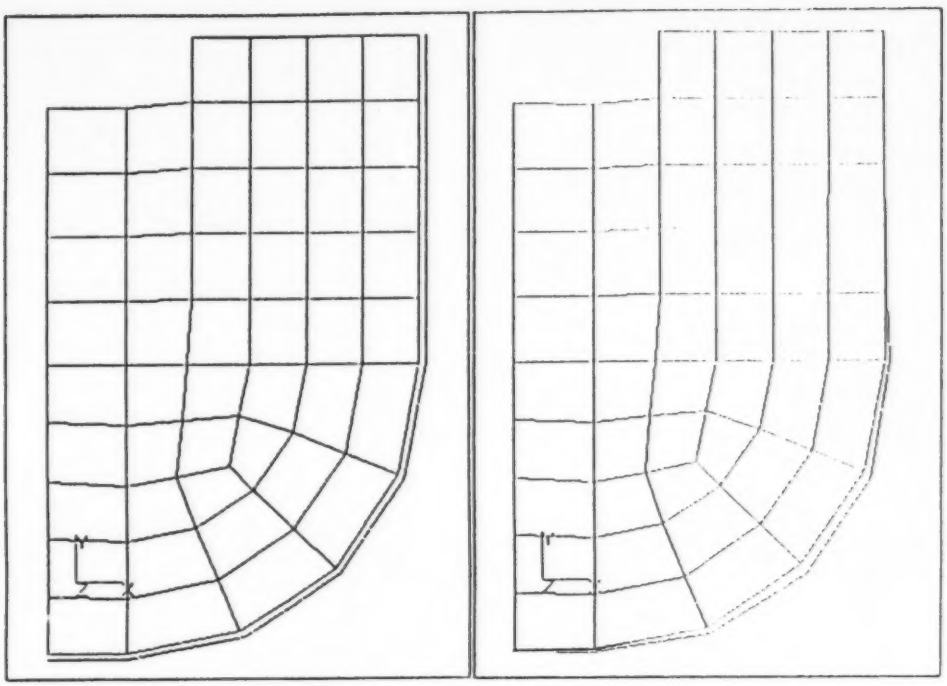

a) Undeformed b) Deformed

FIGURE G-5

4.76 mm THICK TITANIUM UNDER 10 MPa, BOTOM CORNER

89-214-K

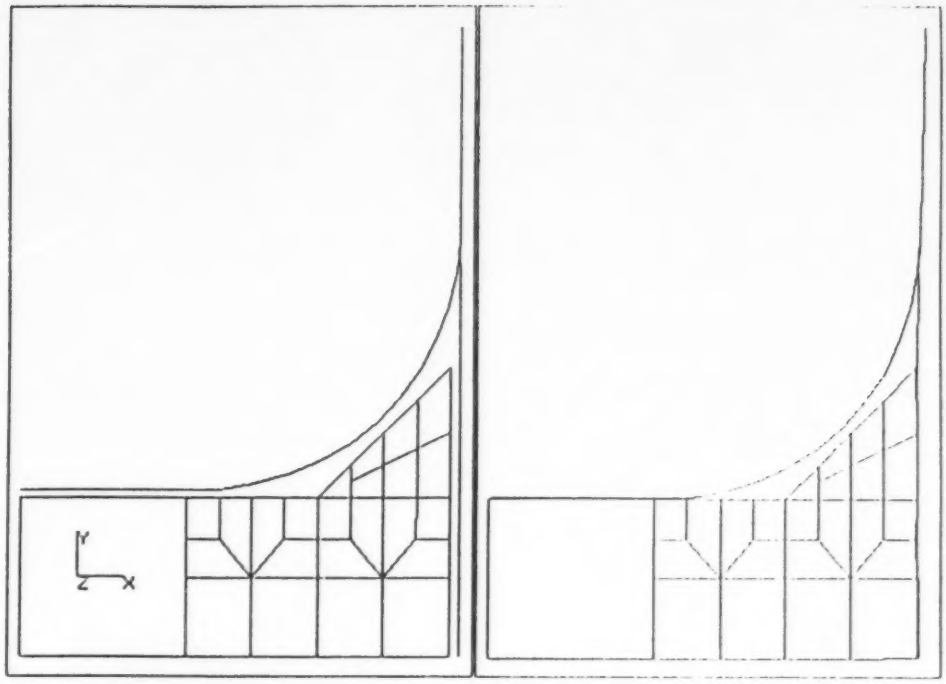

a) Undeformed b) Deformed

FIGURE G-6

2 mm THICK TITANIUM UNDER 10 MPa, WITH REINFORCING RING

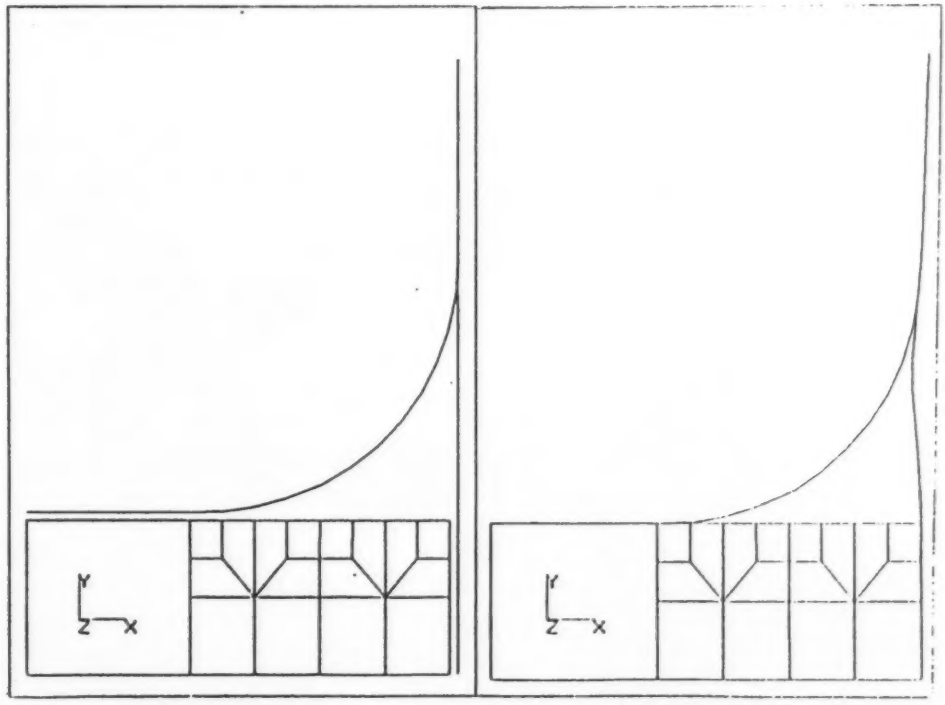

a) Undeformed b) Deformed

FIGURE G-7

2 mm THICK TITANIUM UNDER 7 MPa

89-214-K

177679/RD
GG7

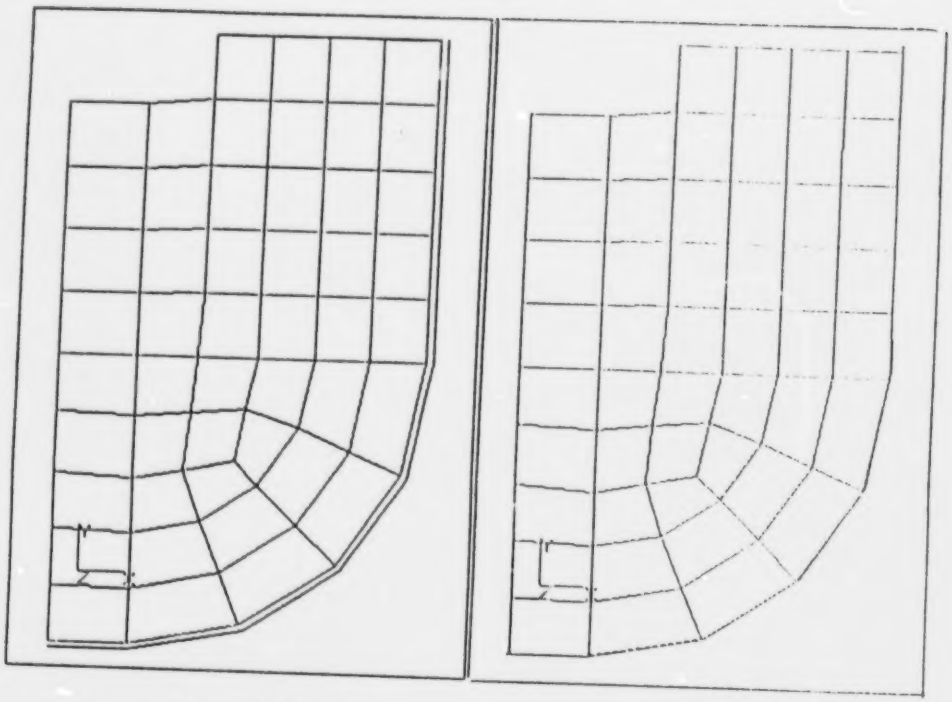

a) Undeformed

b) Deformed

FIGURE G-8

2.0 mm THICK TITANIUM AT 10 MPa, BOTOM CORNER

89-214-K

APPENDIX H

NON-UNIFORM LOADING

Table of Contents

H.1 Introduction

H.2 Effect of Compaction Loads

H.3 Effect of Backfill Swelling

H.1 Introduction

In the analyses described above, only hydrostatic pressure has been considered. Two non-uniform loading conditions are considered here as a part of the container qualification program:

- axial impact loading which will be applied during compaction of the backfill material above a container in a borehole
- non-uniform pressure which may form during slow and ununiform saturation of the repository with water.

The following finite element analyses show that the container can support these loads without exceeding the allowable stresses and strains. Accurate loads are not available from the repository design personnel. The analyses will be repeated when more detailed loads become available.

H.2 Effect of Compaction Loads

The container was assumed to be symmetric about its mid-height and axisymmetric. The 4.76 mm thick titanium shell was modeled with axisymmetric two-noded shell elements. The steel cask body was modeled with four-noded axisymmetric solid elements. This model was described in more detail in Section 9.2 of the report. Gap elements were defined between titanium and steel components allowing the unsupported titanium to respond initially in isolation. As the loading on the titanium shell increased, the shell contacted the underlying steel. The steel supported the titanium and took the compaction load.

A slight imperfection was introduced in the steel shell to initiate buckling at a realistic pressure. The compaction load was represented by an even pressure over the top head.

This analysis may not be conservative because radial forces at the top of the container were not included in the analysis where the compaction process might impose larger loads at the elevated rim (uniform load was applied).

Displacements increased linearly as pressure increased from 0 to 20 MPa. The largest calculated tensile strains in the titanium shell were acceptably low at 0.2% radial and 0.07% circumferential. The analysis was not continued beyond 20 MPa. Figure H-1 shows the progressive increase in displacement at the top rim as the load increased from 0 to 20 MPa in 2 MPa steps.

The container requires the reinforcing ring at the rim of the top lid to provide support for the titanium shell.

H.3 Effect of Backfill Swelling

The repository will saturate with ground water. If water saturates a borehole unevenly, the bentonite swelling pressure /4/ will not be uniform. Two load cases were evaluated.

In load case 1, we examine stresses and displacements in the cask when only a local swelling of the buffer material has occurred. This has been modeled as a variable pressure over a limited area of the cask (see Figure H-2a). Pressure is applied over 60° of the circumference and varies from 0 to 13 MPa.

$P(\Theta) = 13\cos(\Theta)$, where angle $0 < \Theta < 30$

In the second load case, the whole vault has been re-saturated in addition to the local swelling pressure. This results in a uniform pressure of 10 MPa about most of the circumference with an additional localized pressure that varies over 60° from 10 to 13 MPa (see Figure H-2b).

Maximum deflections of the cylindrical wall occurred at mid height of the cask, away from reinforcement provided by the top and bottom heads. Here the cask may be approximated by an infinitely long, axisymmetric cylinder. A 2-dimensional plane strain model was used to represent the cask behavior. Only steel cask was modeled, because titanium shell does not provide any reinforcement. Interface elements representing a small initial space (1 mm) were defined between cask and buffer around two thirds of the circumference. These elements allow for a continuous pressure distribution between contacting surfaces. Analysis considered the elastic-plastic properties of steel with strain-hardening.

Load case 1 (pressure varies from 0 to 13 MPa.) resulted in the higher stresses and deflections of the two cases analysed. Von Mises stresses at the center of the high pressure region reached 286 MPa (see Figure H-3a). This area was largely in bending.

Von Mises' stresses for load case 2 are shown in Figure H-3b. The reinforcing effect of the more even loading is apparent.
The resultant stresses are much lower and do not exceed 205MPa.

Displacements of the IBSS wall due to the two load cases reach a maximum of 4.5 mm under the concentrated load.

Stress levels are high enough in both cases to warrant a more complete investigation. A model incorporating pipe tolerances in wall thickness and out-of-roundness should be developed to determine the possibility of buckling. The effects of creep may also become important.

REFERENCE

H.1 Selvadurai, A.P.S., Dept. of Civil Eng. Carlton University: Theoretical Modeling of Container-Buffer-Rock Mass Interaction in a Nuclear Fuel Waste Disposal Vault During Water Uptake, AECL Technical Record 1985, TR-331.

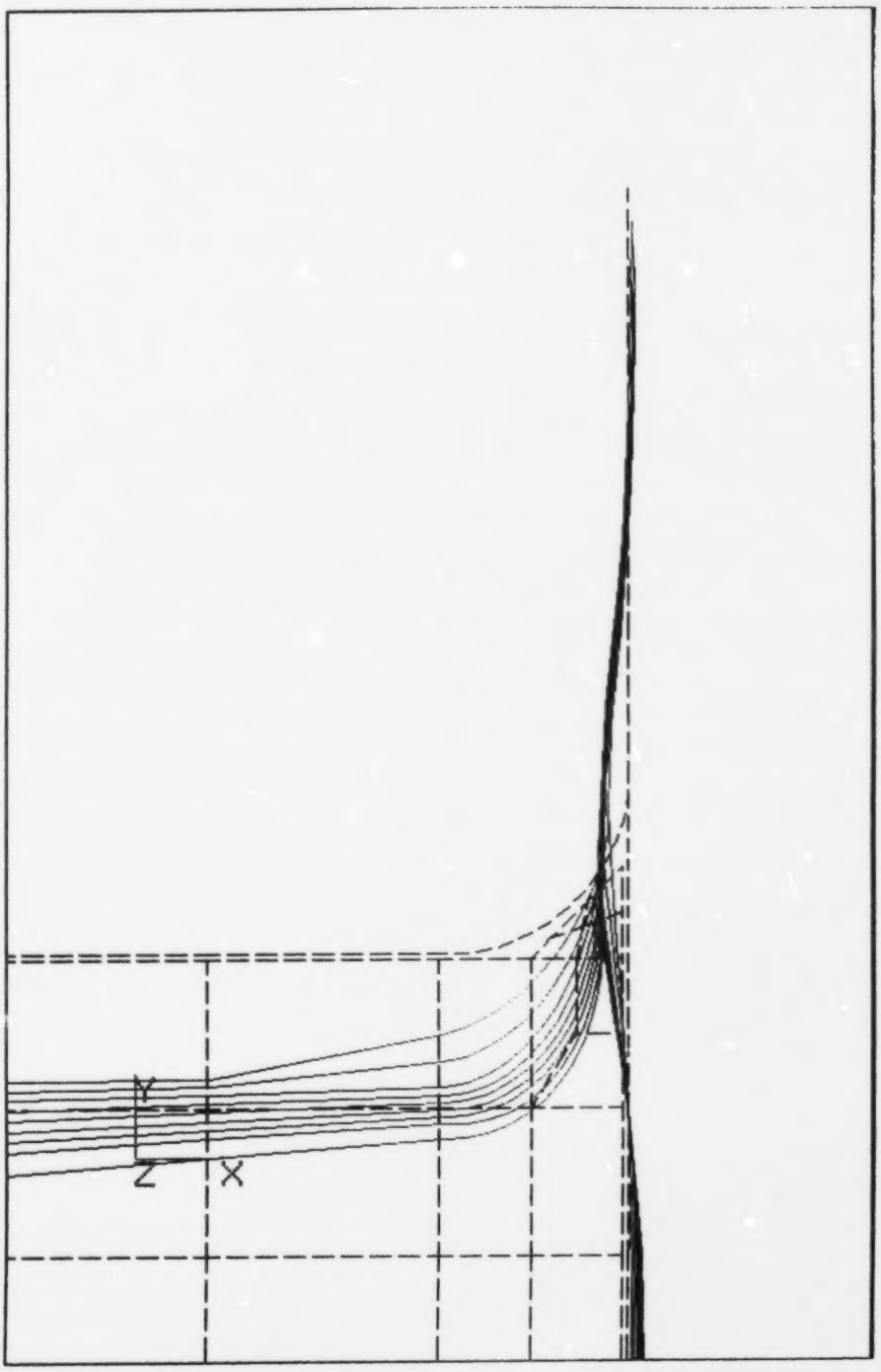

FIGURE H-1

**DEFLECTION AT THE RIM
AXIAL LOAD INCREASING FROM
0 TO 20 MPa IN 2 MPa STEPS**

89-214-K
180904-RD

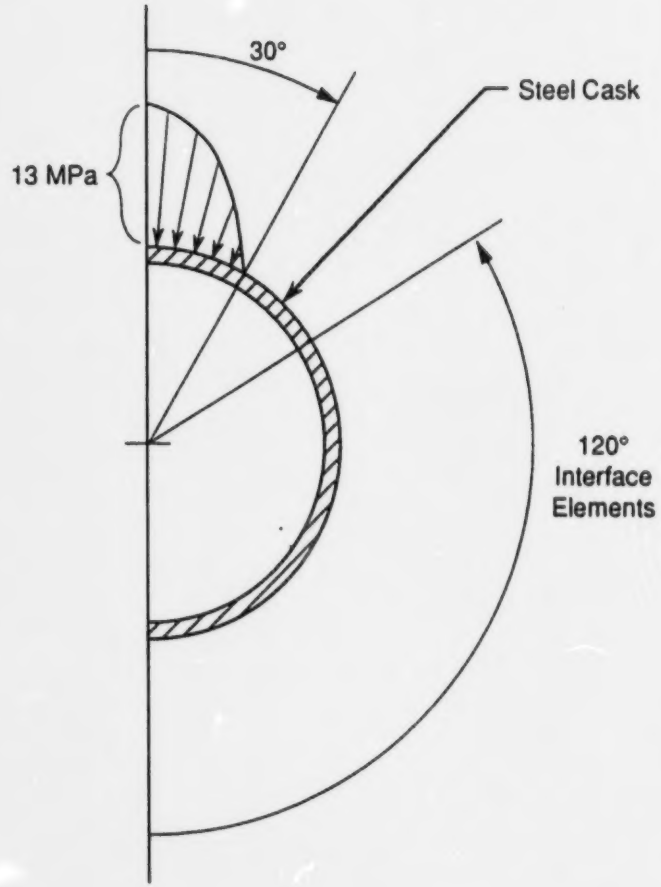

a) Load Case 1 - Local Pressure with 13 MPa Peak

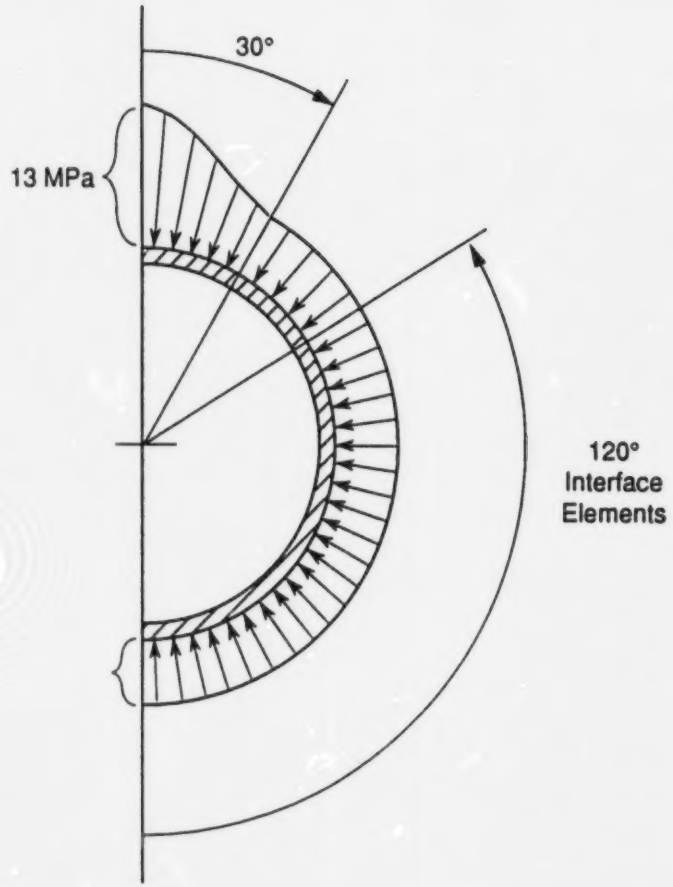

b) Load Case 2 - Uniform 10 MPa Pressure with 13 MPa Loçal Effect

FIGURE H-2

LOAD CASES CONSIDERED IN ANALYSES

a) Case 1 No Uniform Pressure

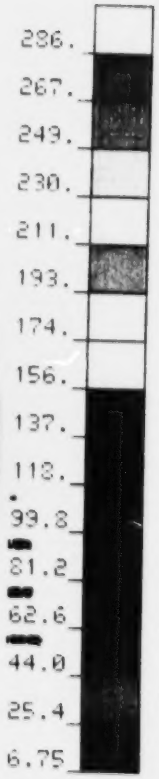

b) Case 2 - 10 MPa Uniform Pressure

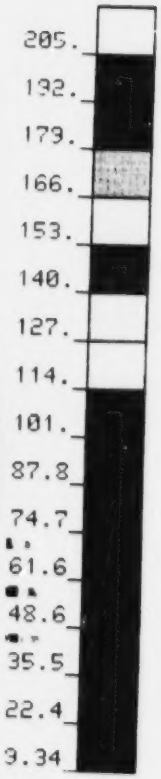

FIGURE H-3

STRESSES IN STEEL CASK UNDER NON-UNIFORM 13 MPa LOADING

83-218-K

APPENDIX I

ACCIDENTAL DROP OF 2.5 METERS

A preliminary analysis has been completed in a series designed to evaluate the ability of the IBSS container to withstand accidents that might occur during handling. The impact analyzed here simulates the effect of dropping a container 2.5 meters onto perfectly compacted (rigid) bentonite.

The analysis was performed using Ontario Hydro's DYNA3D computer code for non-linear explicit dynamics. A three dimensional model was used to perform this analysis.

One quarter of the cask, which included the rounded bottom corner detail, was modeled using eight-noded elements. The model included a 1% increase in the radius of the wall at mid height to facilitate initiation of buckling. Titanium shell was not included in this model since is not relied on to provide structural strength.

Bentonite can be modeled using orthotropic material properties in the software package. In the analysis, bentonite was assumed to be rigid. This is a very conservative assumption.

The internal basket and the the fuel bundles were not explicitly modeled. These parts of the container were represented as a solid cylinder which had a diameter equal to that of the baskets' bottom plate and a mass equivalent to that of the basket with fuel bundles. Figure I-1 shows the finite element mesh of the container and target.

In the analyses, bottom plate of the container impacted flat on the target. The container did not contact sides of borehole.

Because of the rigid base and large drop height, this impact resulted in excessively high stresses and deformations in the container model. Figure I-2 shows amplified deformations at the moment of contact when the largest stresses were recorded. The rebounding of the container from the rigid base and the associated deformations following the impact are shown in Figure I-3. The resulting stresses exceeded significantly the ultimate strength of steel. In order to obtain a more realistic effect of impact, material properties for the bentonite mixture must be refined.

The analysis shows our ability to perform complex dynamic analyses.

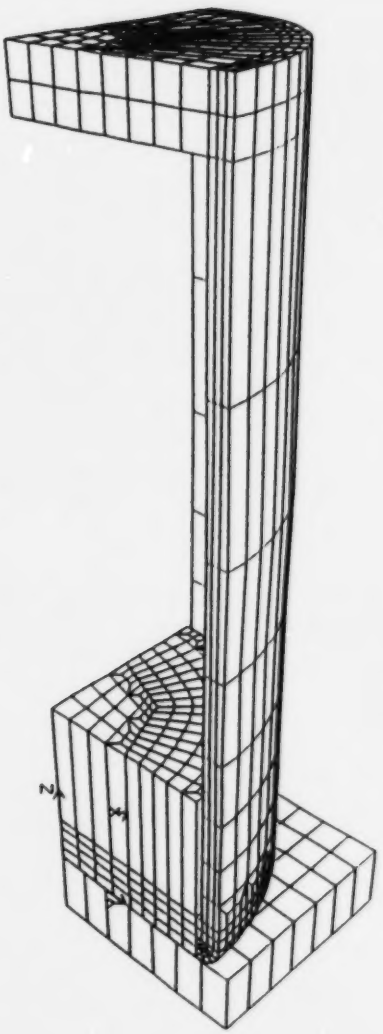

FIGURE I-1

FINITE ELEMENT MODEL
FOR IMPACT ANALYSIS

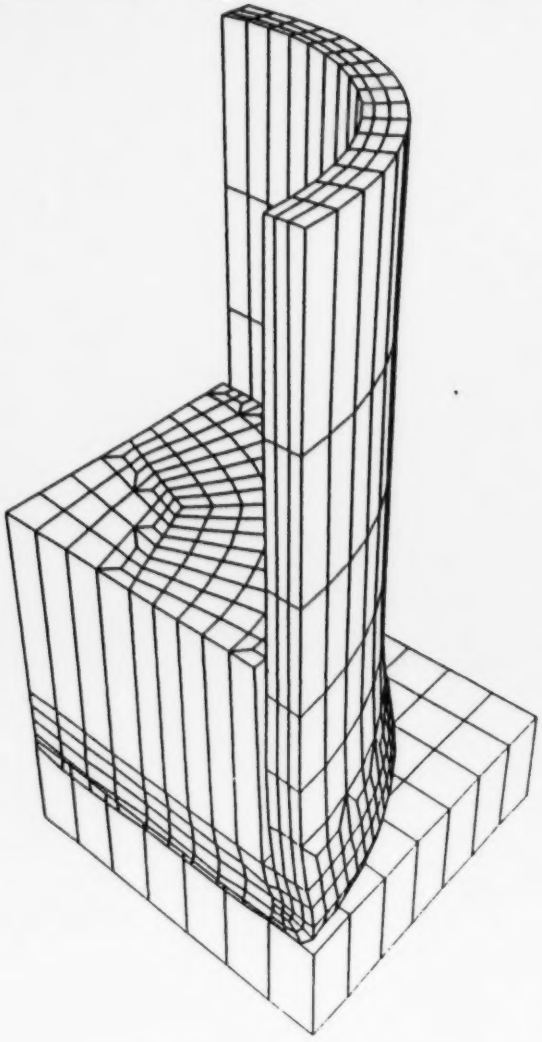

FIGURE I-2

DEFORMATION AT IMPACT

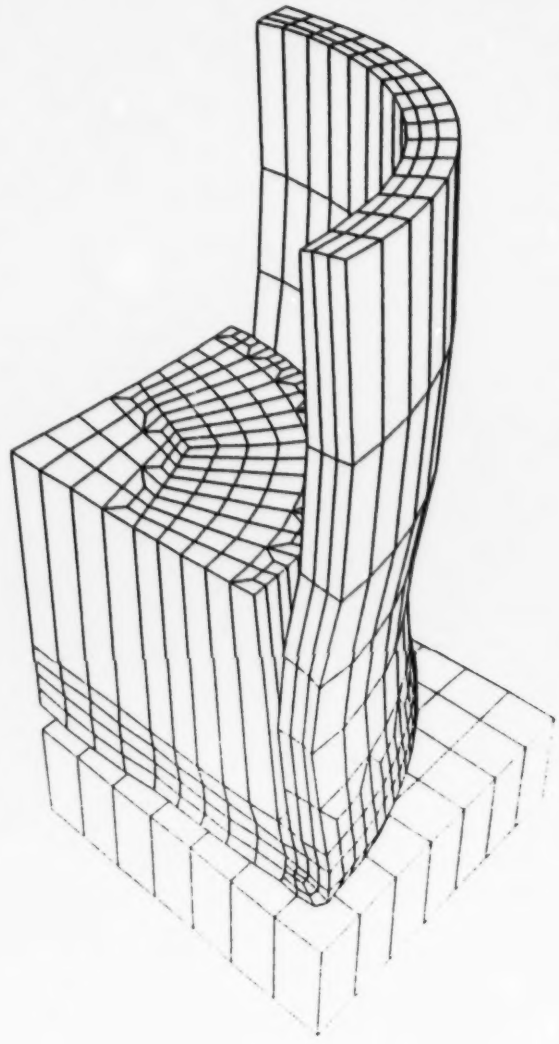

FIGURE I-3

CONTAINER REBOUNCING UP

APPENDIX J

ALTERNATIVE DESIGNS

Table of Contents

J.1 Introduction

J.2 Material Selection

J.3 Higher Strength Top Head

J.4 Corrosion Consideration

J.5 Bundle Capacity

J.1 Introduction

The two designs considered so far (bimetallic and monolithic) have been selected as the reference designs. Several alternative container designs are proposed within the IBSS project in consideration of:

- alternative bundle capacity - 72 or 96,
- alternative container diameters,
- corrosiveness of vault environment,
- preferred material: steel, cast iron stainless steel or other,
- higher strength top head.

Two basic types of containers are proposed: using a corrosion resistant overpack or, in case of a relatively benign vault environment, an adequate corrosion allowance which could make the container thicker with no titanium overpack (monolithic container).

Used fuel would be transferred to the container from modules containing 96 bundles. Disposal containers having capacity of 96 bundles were considered.

The dimensions and configurations of several alternative container designs are illustrated in Table III.

J.2 Material Selection

AISI 1020 L steel has been selected for the reference design, although this may not be the most suitable selection. A metallurgical evaluation should be conducted to determine if steel or cast iron would be more suitable. Steel offers several advantages: higher strength, higher ductility, easier welding, etc. Cast iron has lower cost, is easier to cast and it may have better corrosion resistance properties. Various types of steels and cast irons should be reviewed by metallurgists to ensure the best selection.

The creep rate in carbon steel at the postulated operating temperature of 100^{o} C is low enough that creep deformations will not pose problems (as shown in Appendix E). However, if higher temperatures are possible, an alloy with higher creep resistance (e.g. 1.25% chromium and 0.5% molybdenum) may be preferred.

J.3 Higher Strength Top Head

The design of the top corner area where the top head joins the cylindrical shell has several disadvantages characteristics:

- the area is subjected to the highest stresses and deformations
- it may be subject to fracture propagation because of the flaws introduced by welding and large shear forces between the head and the shell caused by external pressure
- the crevice above the weld can become an area of concentrated, localized corrosion

An alternative design of the top corner is proposed which may reduce some of these concerns. In this design the top head of the titanium shell has a similar geometry to the bottom head (see Figure A-5 of Appendix A). The top plate of the Steel cask is also redesigned, as shown in

Figure J-1. The recent developments in making and inspecting TIG welds in titanium/J.1/ make this new design attractive. Electromagnetic pickups could be used for handling of the container with the modified closure design.

The steel ring (see Subsection A.5 of appendix A) is not required in this alternative, making container assembly simpler.

J.4 Corrosion Consideration

In the titanium overpacked container, the overpack provides the corrosion protection. However, if the overpack is breached, the steel cask will provide some additional protection. The press-fit closure provides a crevice that would promote corrosion. A seal weld is required to reduce it. Slow and uniform corrosion could be expected elsewhere in titanium shell.

J.5 Bundle Capacity

Most container designs, currently being considered, have a 72-bundle capacity, arranged in four layers of 18 bundles per layer (see Figure 32a). This arrangement will allow for a convenient size container having a small diameter and acceptable height.

Bundles are stored at the stations in modules containing 96 bundles per module. It may be advantageous if the disposal container had the same capacity of 96 bundles. Two basket layouts having the capacity of 96 bundles are illustrated in Figure 32. Two alternative layouts are proposed: a six-layer arrangement containing 16 bundles per layer, or 24 bundles per layer in a four-layer configuration. The six-layer container has a smaller diameter than the 72 bundle containers, but its height is increased by about 1000 mm (see Table III). The four layer container has the same height as the 72-bundle container, but its external diameter increases to about 720 mm.

Wall thickness of the 96-bundle containers would likely increase to account for the larger container length or diameter. The required thickness was not determined.

REFERENCE

J.1 P. Maak, "Gas Tungsten Arc Welding of Titanium for Nuclear Fuel Waste Management", Ontario Hydro Research Report.

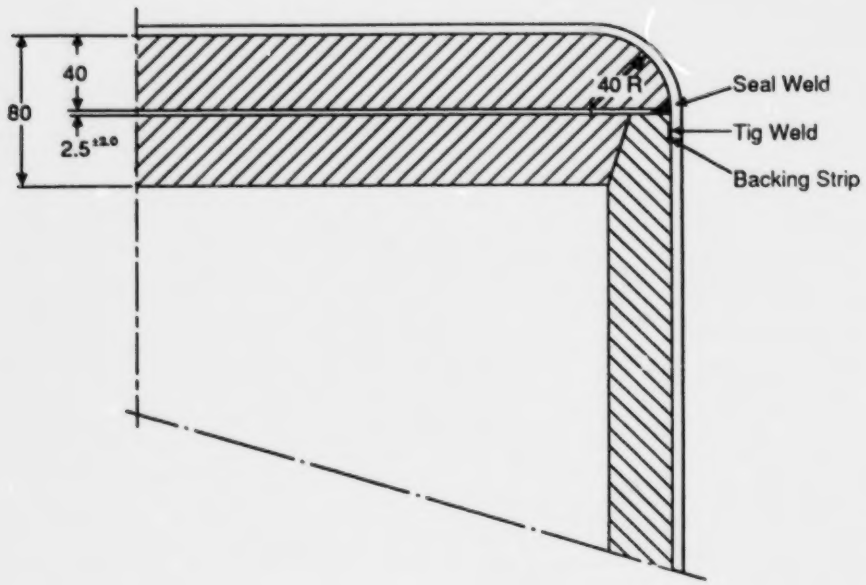

FIGURE J-1
MODIFIED TOP CLOSURE LAYOUT

89-214-K
177638 RD
0007